



Published in final edited form as:

Angew Chem Int Ed Engl. 2009 ; 48(1): 60–103. doi:10.1002/anie.200802248.

Shape-Controlled Synthesis of Metal Nanocrystals: Simple Chemistry Meets Complex Physics?

Prof. Younan Xia*,

Department of Biomedical Engineering, Washington University, St. Louis, Missouri 63130-4899 (USA)

Dr. Yujie Xiong,

Department of Chemistry, University of Washington, Seattle, Washington 98195-1700 (USA)

Dr. Byungkwon Lim, and

Department of Biomedical Engineering, Washington University, St. Louis, Missouri 63130-4899 (USA)

Dr. Sara E. Skrabalak

Department of Chemistry, University of Washington, Seattle, Washington 98195-1700 (USA)

Abstract

Nanocrystals are fundamental to modern science and technology. Mastery over the shape of a nanocrystal enables control of its properties and enhancement of its usefulness for a given application. The aim of this article is to present a comprehensive review of current research activities that center on the shape-controlled synthesis of metal nanocrystals. We begin with a brief introduction to nucleation and growth within the context of metal nanocrystal synthesis, followed by a discussion of the possible shapes that a metal nanocrystal might take under different conditions. We then focus on a variety of experimental parameters that have been explored to manipulate the nucleation and growth of metal nanocrystals in solution-phase syntheses in an effort to generate specific shapes. We then elaborate on these approaches by selecting examples in which there is already reasonable understanding for the observed shape control or at least the protocols have proven to be reproducible and controllable. Toward the end of this article, we highlight a number of applications that have been enabled and/or enhanced by the shape-controlled synthesis of metal nanocrystals. We conclude this article with personal perspectives on the directions toward which future research in this field might take.

Keywords

Metal; nanocrystal; shape control; nucleation; growth

1. Introduction

Nanocrystals are crystals with at least one dimension between 1 and 100 nm.[1] They also are characterized by a single-domain crystalline lattice, without the complicating presence of grain boundaries. Interest in nanocrystals has been growing steadily due to their unique position as a bridge between atoms and bulk solids as well as their fascinating properties and potential applications.[2] The ability to generate such minuscule crystals is central to advances in many areas of modern science and technology. In principle, the electron

* Fax: (+1) 314-935-7448, xia@biomed.wustl.edu.

confinement by a nanocrystal provides the most powerful means to manipulate the electronic, optical, and magnetic properties of a solid material. This notion explains why nanocrystals have been the primary source for discovering and studying quantum size effects, with examples of quantized excitation,[3] Coulomb blockade,[4] metal-insulator transition,[5] and superparamagnetism.[6] Among all kinds of inorganic solids, metals deserve our special attention because they represent more than two thirds of the elements in the period table. Most metals crystallize in the same cubic close-packed (*ccp*) structure, a face-centered cubic (*fcc*) lattice that allows for easy characterization. Metals also possess a range of wonderful properties, and many metals have found extensive use in applications that include catalysis,[7] electronics,[8] photography,[9] and information storage,[10] among others.[11] New applications for metals in areas such as photonics,[12] sensing,[13] imaging,[14] and medicine[15] are also being developed. Significantly, most of these applications require the use of metals in a finely divided state, preferably in the form of nanocrystals with precisely controlled properties.

The properties of a metal nanocrystal are determined by a set of physical parameters that may include its size, shape, composition, and structure (e.g., solid *versus* hollow). In principle, one can tailor and fine-tune the properties of a metal nanocrystal by controlling any one of these parameters, but the flexibility and scope of change are highly sensitive to the specific parameter. For example, in the case of localized surface plasmon resonance (LSPR) and surface-enhanced Raman scattering (SERS), both computational and experimental studies have demonstrated that the shape and structure of a Au or Ag nanocrystal play the most important role in determining the number, position, and intensity of LSPR modes, as well as the spectral region or polarization dependence for effective molecular detection via SERS.[16] In the case of catalysis, it is well-established that the activity of a metal nanocrystal can be enhanced by reducing its size.[17] The selectivity, however, is most sensitive to the packing of atoms on the surface or the exposed facets of a nanocrystal.[18] For example, Pt can selectively catalyze different types of chemical reactions, with the {100} and {210} facets being most active for reactions involving H₂ and CO, respectively.[19] Of course, the facets exposed on a nanocrystal have a strong correlation with the shape. These and many other examples clearly illustrate the importance of shape control to the efficient utilization of metal nanocrystals.

The last decade has witnessed the successful synthesis of metal nanocrystals in a variety of shapes. Examples include: sphere; spheroid; cube; cuboctahedron; octahedron; tetrahedron; right bipyramid; decahedron; icosahedron; thin plate with a triangular, hexagonal, or circular profile; and rod or wire with a circular, square, rectangular, pentagonal, or octagonal cross sections. As limited by space, we restrict ourselves to solution-phase methods of preparation in this review article. According to Wulff's theorem (or the Wulff construction),[20] a single crystal of an *fcc* metal assumes the so-called Wulff polyhedron (a truncated octahedron) as its equilibrium shape in an inert gas or vacuum (strictly speaking, this result is only valid at 0 K). This prediction has been experimentally validated for a number of metals.[21] In a solution phase, however, the product often adopts a shape drastically different from the Wulff polyhedron. This deviation can be attributed to a number of scenarios that may include: *i*) the equilibrium condition never being reached during synthesis; *ii*) the surface energies for various facets being different from those in a vacuum due to anisotropic interactions with a capping agent, impurity, or solvent; *iii*) twin defects being included during nucleation and growth to form shapes such as decahedron and icosahedron with a total free energy lower than that of the Wulff polyhedron; and *iv*) use of an elevated temperature for the synthesis. For these reasons, it is not hard to understand why solution-phase syntheses are inherently more powerful and versatile (at the same time, more complicated) than vapor-phase methods for generating metal nanocrystals of different shapes.

The first documented solution-phase synthesis of metal nanoparticles can be traced back to the 1850's when Michael Faraday prepared his now famous Au colloids by reducing gold chloride with phosphorus in water.[22] Over the past 150⁺ years, a myriad of solution-phase methods have been developed for preparing metal colloids; however, most of the samples were troubled by problems such as polydispersed sizes, poorly defined shapes, and limited morphologies. Only within the last decade have solution-phase methods blossomed and become a powerful approach toward preparing metal nanocrystals with the quality, quantity, and reproducibility suitable for a meaningful study of their shape-property relationships. As a result, most of the references cited in this review were published after 2000. For earlier work on metal nanoparticles, please refer to a number of nice review articles published in the 80's and 90's.[23] In addition, we focus only on those systems (see Table 1) where there is already some reasonable understanding for the observed shape control or at least the synthetic protocols have proven to be reproducible and controllable.

Compared to organic synthesis where endless molecules with complex structures and functions (e.g., fluorescent dyes or drugs) can be designed and synthesized, controlling the assembly of metal atoms into nanocrystals is still in a rudimentary stage. Interestingly, the chemical reactions involved in syntheses of metal nanocrystals often appear to be fairly simple, and most of them can be readily found in chemistry textbooks. It is the nucleation and growth mechanisms behind the simple chemistry that is extremely complicated. In fact, scientists have just begun to understand the complex physics that lead to the formation of nanocrystals with specific shapes. At the current stage of development, it is not an exaggeration to say that the chemical synthesis of metal nanocrystals (as well as for other solid materials) remains an art rather than a science. It must be emphasized that our current understanding of these syntheses is far from being able to present atomistic details for the evolution pathways that a precursor compound may take to form metal atoms, nuclei, and then well-defined nanocrystals. As a zero-order approach, we can divide a typical synthesis into three distinct stages: *nucleation*, *evolution of nuclei into seeds*, and *growth of seeds into nanocrystals*. Here, seeds are defined as something larger than nuclei, in which structure fluctuation is no longer an option. Electron microscopy can be used to analyze the internal structures of both seeds and nanocrystals, and from such analyses, it has been established – at least for Ag,[24] Au,[25] and Pd[26] – that the final shape of a nanocrystal is determined primarily by the internal structure of the corresponding seed (more specifically, the number of twin defects included) and the binding affinity of the capping agent. Searching for this kind of correlation has been the focus of research in this area. It is also the main theme of this review article, around which our discussion is organized.

2. Nucleation: The Birth of a New Phase

Nucleation represents the very first stage of any crystallization process. Despite the scientific and technological importance of this phenomenon and the tremendous efforts that have been devoted to studying the subject, attempts to examine, understand, and control this process have met with limited success.[27] One barrier to success is the lack of experimental tools capable of capturing, identifying, and monitoring the nuclei – that is, the minuscule clusters consisting of very few atoms and/or ions – formed in the earliest stage of a nanocrystal synthesis. It is also difficult (if not impossible) to directly observe the formation of nuclei in real space. By the time a crystal is visible to an electron microscopist, it has already grown beyond the nucleation stage.

There are a number of approaches being developed to address this technical challenge. The first approach relies on theoretical developments, where increasingly sophisticated theories have been formulated and refined to simulate and account for nucleation.[28] As a second approach, building blocks with much larger sizes (e.g., colloidal spheres) have been

employed as a model system to study nucleation and crystallization.[29] Although the relatively large sizes of colloidal spheres allow for the use of optical tools (such as a laser scanning confocal microscope) to monitor nucleation in real space, there are drastic differences between atoms and colloidal spheres in terms of size, surface properties, solvation, and interaction potential. As a third approach, efforts have been devoted to studying the nucleation of atoms on a flat surface.[30] With advancements in scanning probe microscopy (SPM), a nucleation process can now be followed in a vapor or liquid phase with remarkable spatial and temporal resolutions. The involvement of a solid substrate and a physical tip, however, introduce additional parameters (e.g., kinks, steps, or other types of defects on the solid substrate that can serve as nucleation sites, as well as tip-atom interactions) that are not present in solution-phase nucleation. As a fourth approach, organometallic chemists have been trying to prepare metal clusters consisting of a specific number of atoms through dedicated synthetic methods.[31] By crystallizing the clusters into larger crystals, the three-dimensional (3-D) structure of such clusters can be precisely determined by X-ray crystallography. This approach has been widely used to investigate the transition from discrete atoms to bulk solids by preparing ligand-stabilized clusters of different sizes.[32] The major drawback of this approach is that bulky ligands have to be introduced in order to cap and stabilize the metal clusters. There are likely significant differences between these synthetic clusters and the nascent nuclei formed in a crystallization process. In the next section, we only discuss nucleation in the context of metal nanocrystal synthesis.

2.1. The Molecular Mechanism of Nucleation

In a typical synthesis of metal nanocrystals, a precursor compound is either decomposed or reduced to generate zero-valent atoms – the building blocks of a metal nanocrystal. Yet, it is still unclear how nuclei and nanocrystals evolve exactly from a precursor. Depending on the explicit route to atoms, the nucleation process might take completely different pathways. For the decomposition route, nucleation is expected to follow the mechanism proposed by LaMer and coworkers in the early 50's (Figure 1).[33] This mechanism is based upon an extensive study of the solution-phase synthesis of monodisperse sulfur colloids. In the context of metal nanocrystal synthesis, the concentration of metal atoms steadily increases with time as the precursor is decomposed (typically from heat or sonication). Once the concentration of atoms reaches a point of supersaturation, the atoms start to aggregate into small clusters (i.e., nuclei) via self- (or homogeneous) nucleation. Once formed, these nuclei then grow in an accelerated manner causing the concentration of metal atoms to drop. If the concentration of atoms drops quickly below the level of minimum supersaturation, no additional nucleation events will occur. With a continuous supply of atoms via ongoing precursor decomposition, the nuclei will grow into nanocrystals of increasingly larger size until an equilibrium state is reached between the atoms on the surface of the nanocrystal and the atoms in the solution. Besides growth via atomic addition, the nuclei and nanocrystals can directly merge into larger objects via agglomeration.[34]

For the reduction route, the precursor compound is in a higher oxidation state than the atomic species. In this case, it is unclear if the precursor compound is reduced into zero-valent atoms first, which aggregate into nuclei and then grow into nanocrystals, or if the unreduced metal species begin forming nuclei prior to reduction. Simulations based on first-principles molecular dynamics have shed some light onto this question and indicate that precursor compounds can be directly converted into nuclei and add to other precursor-based nuclei or growing nanocrystals without going through a zero-valent state. For example, it has been shown that a Pt^{II}-Pt^I dimer stabilized with Cl⁻ can be formed directly from two dissolved PtCl₂(H₂O)₂ complexes through the introduction of one electron.[35] Here, the PtCl₂(H₂O)₂ complex is the hydrolysis product of PtCl₄²⁻, a precursor commonly used in the

synthesis of Pt nanocrystals. The Pt^I-Pt^{II} dimer can be transformed subsequently into a Pt^I-Pt^I dimer through the addition of another electron and the loss of Cl⁻. Interestingly, both the Pt^{II}-Pt^I and Pt^I-Pt^I dimers can react with a third PtCl₂(H₂O)₂ complex to form a trimer by coupling to a third reduction step. These partially reduced dimers and trimers likely represent early intermediates toward the formation of larger clusters or nuclei. Since dimers and trimers have higher electron affinities than the precursor (due to orbital delocalization), reduction is expected to occur preferentially via electron transfer from the reductant to these dimeric and trimeric units. This preference excludes the possibility for the monomeric precursor complexes being reduced directly into atoms and then adding to nuclei or growing seeds.

As mentioned, both the addition of Pt^{II} complexes to and the detachment of a ligand from a cluster can dramatically accelerate the growth of a metal nanocrystal. This acceleration is commonly referred to as *autocatalytic growth* and has been observed for a number of metal systems.[23a,36] It is worth pointing out that this reduction mechanism is only favorable under certain experimental conditions – for example, when a mild reducing agent and/or a high concentration of precursor are involved. Under these conditions, it is not necessary for the precursor to be reduced into atomic species before being added to the surface of a growing cluster (Figure 2). It is also not critical for the cluster (or a nanocrystal) to be fully reduced into the zero-valent state, suggesting that its surface is likely terminated by positively charged metal ions coordinated to ligands or solvated by solvent molecules. This unique structure at the interface might be related to the capping effect of some ionic species such as Cl⁻, Br⁻, and citrate, as well as polymeric species.

2.2. The Actual Starting Material of a Synthesis

Most of the solution-phase methods for preparing metal nanocrystals involve the use of a salt precursor dissolved in a solvent. It is generally assumed that metal ions exist as monomeric units through complexation with anions, ligands, or solvent molecules. Recently, in studying aqueous AgNO₃ solutions, we found that this is not always the case – metal ions may be complexed as larger units and their presence can influence reaction outcomes.[37] Specifically, using mass spectrometry, we found a surprisingly high abundance of trimeric Ag clusters in aqueous solutions prepared from commercially available AgNO₃ powders. Our data indicates that about 27% (molar) of the total Ag can be found in these trimeric clusters for a freshly prepared sample. Figure 3a shows a typical mass spectrum taken from an aqueous AgNO₃ solution immediately after preparation. In the mass/charge range of 80 to 600, there are four sets of peaks with distinct isotope patterns. According to the mass/charge (*m/z*) ratios in each pattern, the four peaks can be assigned to Ag⁺, [Ag₂(NO₃)]⁺, Ag₃⁺, and [Ag₃(NO₃)₂]⁺, respectively. The insets illustrate the well-defined doublet and quadruplet patterns characteristic of Ag⁺ and Ag₃⁺. Further studies revealed that the trimeric clusters decreased in concentration as the aqueous solution was aged in air under ambient conditions. As shown in Figure 3b, after 24 h only 13% of the total Ag content remained as trimeric clusters. The decrease in Ag atoms contained in these trimeric clusters essentially equaled the increase in newly formed Ag⁺ ions (including their complexes with NO₃⁻). This conservation of Ag implies that the trimeric clusters are directly transformed into Ag⁺ ions and their complexes with NO₃⁻ during the course of aging. We suspect that this transformation involves O₂ that is naturally present in the aqueous medium or later dissolved from air.

Regardless, changes in the concentration of trimeric clusters were shown to influence reaction outcomes. The observed trimeric clusters can be either positively charged (Ag₃⁺) or neutral (Ag₃) and are likely formed in the AgNO₃ solid through a photochemical reduction process much like in photography.[38] For the Ag₃⁺ cluster, its ground state has a triangular structure (¹A₁) with D_{3h} symmetry.[39] Its linear ¹Σ_g state is ~1 eV above the ¹A₁ state. The

Ag₃ cluster also has a triangular ground state, in this case (²E').[40] Both of these clusters have a stronger affinity for electrons than Ag⁺, making them more favorable sites for nucleation and growth once a reductant is introduced.[41] Electron microscopy studies show that the reduction of these AgNO₃ solutions with a mild reducing agent, poly(vinyl pyrrolidone) (PVP), yields triangular nanoplates. Interestingly, we found that the average edge lengths of the resulting Ag nanoplates increased with decreasing starting concentrations of trimeric Ag clusters. This observation supports our hypothesis that these trimeric clusters likely serve as nuclei for the addition and reduction of Ag⁺, with the triangular shape being largely retained during the growth process. The results from this study clearly illustrate the significance of fully characterizing the reagents and solutions used in nanocrystal syntheses. Such rigorous characterization of the solution species present under different conditions is critical to both understanding why nanocrystals of a particular shape form and ensuring reproducibility.

2.3. Capturing the Nuclei

Nuclei play the most important role in directing the assembly of atoms into nanocrystals. Due to their small sizes, very little is known about the nuclei present during a synthesis, not to mention a conclusive account of their explicit and likely dynamic roles. As discussed in Section 2.2, electrospray mass spectrometry can provide mass information about the small clusters present in a precursor solution.[42] It may also be a valuable tool for discerning the larger clusters formed in a nucleation process. Indeed, for metals such as Ag in which there are only a few isotopes, it is relatively easy to assign the mass/charge peaks to different-sized clusters because of their simple isotope patterns. Unfortunately, mass spectrometry only tells the size of a cluster. To determine the internal structure or geometric shape of a cluster, one has to rely on electrospray photoelectron spectroscopy in conjunction with accurate *ab initio* calculations.[43] Alternatively, collision-induced dissociation of a cluster coupled with mass spectrometry can provide some structural information. In a proof-of-concept experiment, Wang and coworkers used this method to confirm the tetrahedral shape of phenylphosphine-stabilized Au₂₀ clusters formed in a solution-phase reduction.[44] Still, this approach can only be applied to clusters with relatively good stability. It remains a great challenge to analyze transient clusters or nuclei by mass spectrometry methods.

In addition to mass spectrometry, both absorption and emission spectroscopic methods have been adopted for *in situ* characterization of certain metal clusters. As demonstrated by a number of groups, Ag clusters display distinct absorption and emission spectra depending on the number of Ag atoms contained in the cluster.[45] For example, when Ag⁺ ions were reduced in water by a pulse radiolysis method, Henglein and coworkers found that the most stable cluster was Ag₄²⁺. [46] This cluster exhibited a strong absorption peak at 275 nm, which was easily distinguished from both Ag atoms (360 nm) and Ag₂⁺ dimers (310 nm). Similarly, the emission spectra of Ag clusters can be used to identify their presence in a chemical synthesis.[47] With the use of specially designed glassware and procedures, it is feasible to sample the reaction solution and record the spectra without disturbing the nucleation and growth processes.[48] By combining mass spectrometry with other analytical techniques, it should be possible to analyze the evolution pathway from metal ions to atoms and clusters of various sizes under different experimental conditions.

So far, Au₁₃, Au₂₀, Pt₃₈, M₅₅ (M=Au, Pt, and Rh), Pt₃₀₉, Pd₅₆₁, Pd₁₄₁₅, and Pd₂₀₅₇ clusters have been reported in the literature.[44,49] With the exceptions of Au₂₀ and Pt₃₈, these clusters can be referred to as “full-shell clusters” in which their constituent atoms assume a closed geometry with the densest sphere packing possible. For example, starting with a central atom, 12 and 42 atoms can be placed around it to form a second and third shell, respectively, and thus M₁₃ and M₅₅ clusters. In general, 10n²+2 atoms need to be incorporated into the *n*th shell to form a cluster with the densest packing of atoms. As shown

in Figure 4, these full-shell clusters display shapes remarkably similar to those that typify the stable and observable seeds from which metal nanocrystals are known to grow. It is thus reasonable to speculate that similar types of clusters are also involved as the intermediates (e.g., nuclei) during the formation of metal seeds from precursor molecules. However, it remains a critical technological challenge to capture, identify, and monitor such clusters with the necessary temporal resolution. Such information would be invaluable in correlating synthetic parameters with nuclei assembly and eventual seed structure (i.e., single-crystal or twinned).

3. Evolution from Nuclei to Seeds

Once a cluster has grown past a critical size, structural fluctuations become so energetically costly that the cluster becomes locked into a well-defined structure. This critical point marks the birth of a seed. As illustrated in Figure 5, these seeds hold an important position in bridging the nuclei and the nanocrystals.[24-26] In general, the seeds may take a single-crystal, singly twinned, or multiply twinned structure, and all of these may co-exist in a typical synthesis. The key to obtaining only one nanocrystal shape to the exclusion of others is to ensure tight control over the population of seeds with different internal structures. How can the population of seeds be controlled and manipulated during a synthesis? This question needs to be addressed from a number of different angles as structures, in general, are history dependent and their formation is determined by both thermodynamic and kinetic factors. In essence, the population of differently structured seeds is determined by the statistical thermodynamics of the free energies of different species in combination with kinetic effects regarding the generation and addition of metal atoms to a nucleus. This picture can be complicated by the introduction of other processes such as oxidative etching. In the following sections, we elaborate on the roles these factors play in determining the internal structure of a seed.

3.1. Thermodynamic Control

When a reaction is under thermodynamic control, the greatest proportion of the most stable product will be produced. To approximate the most stable product, the formation of single-crystal seeds can be considered in the context of Wulff's theorem, which attempts to minimize the total interfacial free energy of a system within a given volume. The interfacial free energy, γ , can be defined as the energy required for creating a unit area of "new" surface:

$$\gamma = \left(\frac{\partial G}{\partial A} \right)_{n_i, T, P} \quad (1)$$

where G is free energy and A is surface area. For a newly formed seed, crystal symmetry is broken due to missing bonds at the surface causing the surface atoms to be attracted toward the interior. A restoring force is needed to pull the surface atoms back to their original positions. Using this simple model (i.e., an ideal surface), the interfacial free energy is given by:[50]

$$\gamma = \frac{1}{2} N_b \epsilon \rho_a \quad (2)$$

where N_b is the number of broken bonds, ϵ is the bond strength, and ρ_a is the density of surface atoms. For an *fcc* structure with a lattice constant of a , the surface energies of the low-index crystallographic facets that typically encase nanocrystals can be estimated as: $\gamma_{\{100\}} = 4(\epsilon/a^2)$, $\gamma_{\{110\}} = 4.24(\epsilon/a^2)$, and $\gamma_{\{111\}} = 3.36(\epsilon/a^2)$, resulting in the energetic sequence of $\gamma_{\{111\}} < \gamma_{\{100\}} < \gamma_{\{110\}}$. This sequence implies that a single-crystal seed should take an octahedral or tetrahedral shape in order to maximize the expression of $\{111\}$ facets and minimize the total surface energy. Both shapes, however, have larger surface areas than a cube of the same volume. As a result, single-crystal seeds are expected to exist as truncated octahedrons (or Wulff polyhedrons) enclosed by a mix of $\{111\}$ and $\{100\}$ facets. This shape has a nearly spherical profile and thus the smallest surface area to minimize the total interfacial free energy. Such seeds have been observed experimentally in the syntheses of a number of metal nanocrystals.

In addition to these single-crystal seeds, singly and multiply twinned seeds containing at least one twin defect – a single atomic layer in the form of a $\{111\}$ mirror plane – have been observed under the same reaction conditions.[51] As discussed in the introduction, there are a number of factors that can contribute to this observation. Similar to a single crystal, the surface of a singly twinned seed tends to be enclosed by a mix of $\{111\}$ and $\{100\}$ facets to lower the total interfacial free energy. For a multiply twinned seed, the strain energy caused by twin defects will greatly increase as the seed grows in size. For example, a five-fold twinned, decahedral seed can be considered as an assembly of five single-crystal, tetrahedral units sharing a common edge (Figure 6a).[51] Each tetrahedron has two sides in contact with a neighbor through $\{111\}$ twin planes. Since the theoretical angle between two $\{111\}$ planes of a tetrahedron is 70.53° , five tetrahedrons joined with $\{111\}$ twin planes will leave a gap of 7.35° , which must be compensated for by increasing the separation between adjacent atoms. Such an elongation of bond length will cause internal lattice strain, as well as a disordered region at the boundary (see Figure 6, b and c).[52,53] Due to the fan-out configuration, the defected region will keep increasing in area as the decahedral seed is enlarged laterally, making the total free energy of the system go up. As a result, multiply twinned seeds are only favored by thermodynamics at relatively small sizes. With this in mind, it is not hard to appreciate the simulation results by Ferrando and coworkers, in which icosahedrons were found to be stable at small sizes, decahedrons at medium sizes, and Wulff polyhedrons at large sizes for an *fcc* metal.[54] Of course, the crossover points are highly dependent on the metal (see Table 2). This critical dependence on size suggests that the population of different seeds is not controlled by thermodynamics alone – it is also sensitive to reaction kinetics, a parameter that can be experimentally manipulated!

3.2. Kinetic Control

When multiply twinned seeds are relatively small, the extra strain energy caused by twinning can be compensated by maximizing the surface coverage with $\{111\}$ facets and thus achieving the lowest total free energy.[55] If these seeds expand in size rapidly, however, theoretical analysis indicates that the low surface energy of $\{111\}$ facets can no longer remedy the excessive strain energy, resulting in their transformation into single crystals.[54-56] This analysis indicates that multiply twinned seeds need to be confined to relatively small sizes in order to increase their yields. Experimentally, this condition can be achieved by keeping the rates of atomic generation and/or addition sufficiently slow. When the generation of metal atoms is slow, multiply twinned seeds will prevail over single-crystal counterparts because they can be kept at small sizes for a long period of time. Under the same reduction kinetics, singly twinned seeds may also appear, albeit in lower quantities than the multiply twinned ones due to the presence of $\{100\}$ facets with a higher energy. Taken together, it is possible to control the population of seeds containing different numbers

of twin defects by varying the reduction or decomposition rate of a precursor, which is the essence of kinetic control.

If the decomposition or reduction becomes considerably slow, the atoms tend to form nuclei and seeds through random hexagonal close packing (rhcp), together with the inclusion of stacking faults.[57] This type of synthesis has been known as *kinetically controlled* and the seed typically takes a shape deviated from those favored by thermodynamics (i.e, a higher energy structure). In one case, inclusion of stacking faults and/or twin planes can lead to the formation of a plate-like seed (Figure 6d). Completely different from the polyhedral seeds, a plate-like seed is covered by {111} facets at the top and bottom surfaces, together with stacking faults and/or twin defects along the vertical direction (Figure 6, e and f). Due to a relatively large surface area (as compared to a polyhedral seed of the same volume) and the lattice strain energy caused by defects, the total free energy of a plate-like seed is extremely high regardless of its coverage with {111} planes. As a result, formation of plate-like seeds can never be favored in terms of thermodynamics. To obtain plate-like seeds in solution, both nucleation and growth must deviate from a thermodynamically controlled pathway. In practice, structures characteristic of kinetically controlled syntheses can be achieved by: *i*) substantially slowing down precursor decomposition or reduction,[58] *ii*) using a weak reducing agent,[59] *iii*) coupling the reduction to an oxidation process,[60] or *iv*) taking advantage of Ostwald ripening.[61] The key is to ensure an extremely low concentration of metal atoms in solution so the nuclei will not be able to grow autocatalytically into polyhedral structures. Instead, the atoms will add to the edges of a planar cluster to generate a plate-like seed.

3.3. Oxidative Etching

The distribution of single-crystal versus twinned seeds can be further manipulated through the use of oxidative etching, in which zero-valent metal atoms are oxidized back to ions.[62] Since most syntheses are conducted in air, O₂ is present in the reaction solution throughout the entire process. If a ligand for the metal ion is also present in the same solution, a combination of the ligand and O₂ can result in a powerful etchant for both the nuclei and seeds. As shown in Figure 6(a-c), the defect zones in twinned seeds are much higher in energy relative to the single-crystal regions and thus are most susceptible to an oxidative environment, with their atoms being attacked by the etchant, oxidized, and dissolved into the solution. In contrast, single-crystal seeds are more resistant to oxidative etching as there are no twin boundary defects on the surface. By taking advantage of this selectivity, the population of different seed types in the reaction solution can be manipulated controllably. For example, in the polyol synthesis of Ag nanocrystals, all twinned seeds can be removed from the solution by adding a trace amount of Cl⁻ to the reaction (Figure 7).[62] As a result, single-crystal seeds and nanocrystals will prevail. By replacing Cl⁻ with a less corrosive anion, Br⁻, it is possible to selectively eliminate only the multiply twinned seeds, leaving behind a mixture of single-crystal and singly twinned seeds in the solution.[63] As will be illustrated in Section 4, these seeds can grow into nanocrystals with drastically different shapes.

Oxidative etching has already been validated for a number of noble metals, including Ag, Pd, and Rh.[62-64] In these examples, both O₂ and a ligand are required in order to observe oxidative etching. For example, when a polyol synthesis for Ag nanocrystals is performed under argon, the multiply twinned seeds formed in the early stage of the reaction will grow quickly to form pentagonal nanowires (see Section 5.2). Likewise, if no Cl⁻ is added, multiply twinned seeds will be formed which quickly evolve into quasi-spherical particles within 1 h. Only when both O₂ and Cl⁻ (or another ligand) are present, will single-crystal seeds be obtained in high yields. Based upon the same mechanism, multiply twinned seeds can be saved by *i*) removing O₂ from the reaction system by bubbling an inert gas through,

[64a,65] *ii*) blocking oxygen adsorption to the seeds through the selection of suitable capping agents (e.g., citrate),[66] or *iii*) diminishing the role of oxidative etching by scavenging oxygen in the solution with a redox pair (e.g., Fe(^{III}/^{II}) or Cu(^{II}/^I) salts).[65,67]

It is worth pointing out that in many cases the counter ions of metal precursors or the miniscule amounts of ionic impurities present in the chemical reagents can facilitate oxidative etching and have a profound impact on the population of different types of seeds. For example, Na₂PdCl₄, a commonly used precursor for synthesizing Pd nanocrystals, contains the Cl⁻ needed for oxidative etching.[64a] Also, in polyol syntheses based on ethylene glycol, Cl⁻ may be present at sufficiently high concentrations (typically on the ppm level) to facilitate oxidative etching.[65] Additionally, due to its synthesis and storage in steel vessels, ethylene glycol can be contaminated with trace Fe-containing species. Both Fe^{II} and Fe^{III} ions have been shown to influence oxidative etching by coupling to O₂ and the reductant. Knowledge of such impurities and their effects is essential to the reproducibility and scale-up of shape-controlled syntheses of metal nanocrystals.

4. Evolution from Seeds to Nanocrystals

Once a seed is formed, it can grow in size through the addition of metal atoms; however, observation of crystal growth on the atomic level is not easy (or even possible), especially when the crystal growth occurs in solution. From chemical deposition studies, it is known that when atoms add to a surface, the adatoms diffuse around on the surface until they meet a step site where they can be incorporated. The overall growth of a crystal is controlled by the competition between a decrease in bulk energy (which favors growth) and an increase in surface energy (which favors dissolution). It is this dynamic interplay of growth and dissolution that dictates the evolution of seeds into nanocrystals. Thanks to developments in electron microscopy, it is now possible to resolve the internal structures and shapes of seeds and nanocrystals produced at different stages of a synthesis. As a result, a one-to-one correlation between the initial seeds and final nanocrystals has been established for a number of noble metals.[24-26] Since this kind of study can only be performed *ex situ* for a very limited set of samples, it is still hard to fully reveal the details involved in a typical growth process.

The right half of Figure 5 summarizes the correlation that has been established between different types of seeds and the final nanocrystals of an *fcc* metal. In general, from single-crystal seeds, octahedrons, cuboctahedrons, or cubes will be produced depending on the relative growth rates along the <111> and <100> directions.[50a] If uniaxial growth is somehow induced, the cuboctahedral and cubic seeds will grow into octagonal rods and rectangular bars, respectively.[26] From singly twinned seeds, right bipyramids enclosed by {100} facets,[63a,68] a nanocrystal consisting of two right tetrahedrons symmetrically placed base-to-base, will be produced. Interestingly, these seeds also can evolve into nanobeams when uniaxial growth is initiated.[69] From multiply twinned seeds, icosahedrons, decahedrons, and pentagonal nanorods (or nanowires) can be produced, [24-26] depending on whether the {100} planes on the side surface are stabilized or not.[70] Finally, when the seeds contain stacking faults, they will grow into thin plates with the top and bottom faces being {111} facets and the side surfaces being enclosed by a mix of {100} and {111} facets.[57-61] Because of the six-fold symmetry of an *fcc* system, these seeds typically become thin plates with a hexagonal cross section. As the growth is continued, the final products can also take a triangular shape by eliminating the {111} facets from the side surfaces.[59b,60]

Nature seldom stops short on possibilities! It should be emphasized that Figure 5 illustrates only the generic shapes that are observed from seeds produced under typical experimental

conditions. As will be discussed in the following sections, it is quite possible that the final product adopt a shape very different from these generic ones due to surface capping effects, defect structures, crystal overgrowth, and the presence of exotic seeds.

4.1. Surface Capping

One way in which the final nanocrystal may be driven to adopt a shape different from those in Figure 5 is through the introduction of a selective capping agent. It is well-documented in catalysis literature that the chemisorption of atomic or molecular species from the gas phase onto a metal nanoparticle can cause dramatic morphological changes.[71] For example, in a paper published in 1986, Harris reported that quasi-spherical Pt nanocrystals evolved into nanocubes when exposed to H₂ gas contaminated with a trace amount of H₂S.[72] It was proposed that {100} facets were formed preferentially over {111} facets in the H₂S-rich environment because the former surface interacted more strongly with sulfur. In solution, this kind of chemisorption or surface capping can have a profound impact on the shape displayed by a nanocrystal. Generally speaking, the binding affinity of a capping agent can vary from one crystal facet to another. Such preferential capping can effectively hinder the growth of a particular facet, thus providing a means for controlling the relative surface areas of different facets.

The capping agent may simply be a byproduct liberated during a synthesis. For example, decomposition of metal carbonyl compounds during a synthesis liberates CO, which can bind strongly to many metal surfaces.[73] Such adsorbed CO can effectively inhibit or block metal addition, resulting in a synthetic “dead zone”, a regime with low supersaturation in which crystal growth essentially ceases.[74] Such hindered growth induced by an adsorbate is analogous to “surface poisoning” in catalysis, and as CO often preferentially adsorbs onto specific facets, those facets become selectively poisoned. It is also worth pointing out that many nanocrystal surfaces can catalyze the oxidation of CO to CO₂ in the presence of O₂ and that the generated CO₂ can easily desorb from such surfaces. During this catalytic process, the surface atoms might migrate across the surface causing additional morphological changes.[75] On the other hand, the catalytic oxidation of CO can be poisoned with the addition of sulfur, and the adsorption of sulfur (or even O₂) on the metal surface might have an effect similar to CO on nanocrystal growth.[76] Gold is an exceptional case in which site poisoning is unlikely.[77] Yet, in general, the final shape of a metal nanocrystal is determined by the interplay of all these possible interactions.

The capping agent can also be added purposely to a solution-phase synthesis to control the shape of a nanocrystal. Through its chemical interaction with a metal surface, the presence of a capping agent can change the order of free energies for different crystallographic planes, and thus their relative growth rates. The plane with a slower addition rate will be exposed more on the nanocrystal surface. For example, PVP is a polymeric capping agent whose oxygen atoms bind most strongly to the {100} facets of Ag and Pd.[70] This preferential capping can drive the addition of metal atoms to the other crystal facets when crystal seeds are suitably large. Thus, for single-crystal seeds terminated with only {111} and {100} facets, metal atoms will add preferentially to the poorly passivated {111} facets; these adatoms then migrate to the face edges, resulting in an elongation of the {100} facets and the formation of nanocubes with sizes >25 nm.[78] Bromide can have a similar effect as an ionic capping agent; however, owing to its much smaller size, it is capable of selectively adsorbing onto the {100} facets of Ag, Au, Pd, and Pt nanocrystals with edge lengths <25 nm to induce the formation of smaller nanocubes, rectangular nanobars, and octagonal nanorods.[26] In a manner similar to that of single-crystal seeds, for multiply twinned seeds with a decahedral profile, nanorods or nanowires with a pentagonal cross section will form if their side {100} surfaces can be stabilized by Br⁻ or PVP.[68,70] Likewise, from singly twinned seeds, right bipyramids or nanobeams will form if their {100} surfaces can be

stabilized by Br⁻ or PVP.[63a,68] It is worth pointing out that, in addition to being added intentionally, the Br⁻ can come as an impurity in many chemical reagents or a counter ion in many commonly used ionic surfactants such as cetyltrimethylammonium bromide (CH₃(CH₂)₁₅N⁺(CH₃)₃Br⁻ or CTAB).[79] In contrast to PVP and Br⁻, citrate ions have been found to bind most strongly to {111} facets, at least for Pd, thus favoring the formation of octahedrons, icosahedrons, and decahedrons.[66,80]

The use of a capping agent to dictate the shape of a nanocrystal should be considered a thermodynamic means of controlling shape as it makes some facets thermodynamically more favorable by reducing their interfacial free energies through chemisorption. Despite the importance of surface capping in controlling the shape of a nanocrystal, its explicit role(s) and mechanism(s) are poorly defined and a full understanding is still elusive. One technical barrier is the lack of experimental tools capable of resolving the molecular structure of a capping agent (especially, a polymeric one) on a nanocrystal surface. Although a number of spectroscopic methods -- e.g., X-ray photoelectron spectroscopy (XPS), energy dispersive X-ray spectroscopy (EDXS), FTIR, and Raman -- have been employed to confirm the presence of a capping layer on the surface of nanocrystals,[81,82] none of them are capable of resolving the configuration and packing of the capping molecules. This situation is expected to change in the near future as new tools such as SPM and second harmonic generation (or SHG)-based methods are applied to addressing this problem.[83] Computational studies also can greatly enhance our understanding of surface capping. For example, it was recently found that the binding of citric acid to a Ag(111) surface releases 13.8 kcal/mol binding energy compared to 3.7 kcal/mol for a Ag(100) surface.[84] This huge difference in binding energy was attributed to citric acid adopting different molecular symmetries on the Ag(100) and Ag(111) surfaces. The roughly three-fold symmetry of citric acid matches that of the Ag(111) surface and results in four Ag-O bonds. Also, migration of a hydrogen atom within citric acid bound to the Ag(111) surface activates the electrons of the methylene-carboxyl oxygens, providing additional binding affinity towards the (111) surface. In contrast, citric acid forms only two Ag-O bonds with the Ag(100) surface because of a geometry mismatch. Similar analyses could help identify capping agents suitable for stabilizing other crystal facets; however, due to the involvement of polyvalency, [85] it is believed that polymeric capping agents work differently than small molecules with only a few binding sites.

4.2. Twin Defects and Stacking Faults

Since *fcc* metals have a cubic crystal structure, there is no intrinsic driving force for them to grow into one-dimensional (1-D) or two-dimensional (2-D) nanocrystals. Obviously, these two classes of highly anisotropic shapes will be obtained only when the cubic symmetry of the lattice is somehow broken. One way to accomplish this break in symmetry is to incorporate twin defects or stacking faults into the nanocrystals. For metals, two major types of such nanocrystals have been reported: five-fold twinned nanorods or nanowires (1-D system)[68,70,79] and nanoplates (2-D system).[57-61] It has been proposed that capping agents play an important role in directing the anisotropic growth either via preferential adsorption on specific crystal facets (e.g., PVP on {100} and citrate on {111})[70] or through reaction confinement within micelles assembled from surfactants.[25,86] Although these two mechanisms can explain how capping agents assist the formation of anisotropic nanocrystals, they fail to address some other experimental observations. For example, both nanorods and nanoplates can also be obtained by thermal evaporation in vacuum where no capping agent is present.[87] Consequently, one needs to consider alternative growth mechanisms. As both of these anisotropic nanocrystals include twin defects or stacking faults, they provide a break to cubic symmetry naturally.

Stacking faults commonly occur in close-packed lattices, which consist of hexagonally packed atomic planes with six-fold symmetry. For a *ccp* lattice, the stacking sequence of these layers should be ABCABCABC; however, stacking faults can be introduced, disrupting the stacking sequence for one or two layers (e.g., ABCABABC). A twin defect is a special case in which the stacking faults create a mirror image.[88] Among the *fcc* metals, Ag and Au have the lowest energy barriers for incorporating stacking faults, so planar defects can be readily included in their crystals. Simulations suggest that the presence of such planar defects introduce self-propagating ledges which can serve as active sites for crystal growth.[89]

When a single planar defect (e.g., a twin or a stacking fault) is involved, hexagonal plates can form in the early stage of growth due to the six-fold symmetry of an *fcc* lattice. As proposed by Lofton and Sigmund, the presence of a planar defect can cause the six side faces, where the defect plane ends, to form alternating concave- and convex-type surfaces (see Figure 8a).[52b] Because each atomic site only has three nearest atomic neighbors on the convex-type surface, the stabilization energy for attaching atoms to this surface is relatively low. As a result, the atoms on this surface tend to be dissolved into solution again, creating a high-energy barrier for the addition of atoms. In contrast, the concave-type surface creates a reentrant groove, a self-perpetuating ledge that increases the number of nearest neighbors for an adatom and thus the stabilization energy. In this case, atomic addition becomes favorable. Taken together, in a crystal with a single planar defect, the fast addition of metal to the concave sides can cause those very faces to grow out of existence, leading to a triangular plate whose side faces are bounded by three convex sides that favor atomic addition.

The preference of atomic addition on the concave structure can also be understood using the concept of “chemical potential” which is defined as the Gibbs free energy per atom. The chemical potential of an atom on any curved surface can be expressed by the Gibbs-Thomson formula:

$$\Delta\mu = \gamma\Omega(1/R_1 + 1/R_2) \quad (3)$$

where R_1 and R_2 are two principal radii of curvature, $\Delta\mu$ is the change in chemical potential, and Ω is the atomic volume. For a convex surface, the curvature is positive, thus the chemical potential of an atom on such a surface is higher than that on a flat surface. In contrast, the chemical potential is quite low on a concave surface. As atoms prefer the site with the lowest chemical potential, atomic addition will only occur on concave-type sides.

For the growth of five-fold twinned nanorods, multiple twin defects are involved. It has been proposed that the nanorods grow from decahedral seeds along the axis parallel to the twin planes (Figure 8b).[52a] If a decahedron is viewed as an assembly of five tetrahedrons joined together by twin planes, each vertex is equal to a point where a concave-type face grows out, leaving five edges and two axial points as convex-type faces. In this case, a decahedral seed should grow into a large decahedron instead of a five-fold twinned nanorod, but this case is not observed in a typical synthesis. Therefore, another factor must be responsible for the anisotropic growth. In principle, when atoms in a decahedron are located far from the central axis, the lattice strain will become extremely high. This strain energy will be greatly increased when a decahedral seed grows laterally. In contrast, elongation of the decahedron along the axis parallel to the twin planes does not cause any increase in strain energy. As a result, decahedral seeds preferentially grow along the axial direction into five-fold twinned nanorods and then nanowires. As another requirement for this type of

growth, there must be a capping agent in the solution that can stabilize the newly formed {100} side faces through chemisorption.

4.3. Shape Evolution during Crystal Growth

Crystallographers call the characteristic shape of a crystal (or the relative area of its faces) its "habit".[90] A primary factor determining the habit of a crystal is the relative rates at which different crystal planes grow. Consequently, during crystal growth, the habit of a crystal can change if there is a mix of different facets on the surface. In fact, crystal growth is a very dynamic process! For example, consider an imaginary 2-D octagonal crystal with alternating fast and slow growing edges. As Figure 9 illustrates, continued crystal growth will result in an elongation of the slow growing edges at the expense of the faster growing ones, producing a square, faceted with the slow growing edges. In 3-D, if the fast growing edges correspond to the corners of a truncated cube, the final crystal shape will then be a cube faceted by the slow growing planes. In contrast, if in 3-D the fast growing edges correspond to the faces of a truncated cube, the final crystal shape will be an octahedron faceted by those slow growing planes. Such a dynamic evolution can occur to selectively enlarge one set of crystallographic facets at the expense of others on a nanocrystal, yielding new shapes. For example, Yang and coworkers have shown that an *fcc* single crystal can evolve from a cube to a cuboctahedron and then to an octahedron, with an increasing ratio of {111} to {100} facet areas.[91] As Figure 10 shows, when metal atoms add to the {100} faces of a nanocube, they migrate to the edges of the face resulting in the elongation of the {111} facets. As this process continues, the cubes will be transformed into cuboctahedrons and eventually octahedrons. This shape evolution process has also been known as overgrowth. Interestingly, as discussed in Section 4.1, the introduction of a capping agent to a synthesis can alter the growth rates of the different facets, thus dramatically altering the final nanocrystal shape.

4.4. Seeded Growth: Epitaxial vs. Non-Epitaxial

With regards to nanocrystal growth, pre-formed nanocrystals with well-defined facets can be added to a synthesis and serve as primary sites for nucleation (in this case, heterogeneous) and crystal growth. If, during crystal growth, the added metal atoms continue with the same crystal structure as the seed, then it is an epitaxial process. This condition is achieved when the seeds have the same chemical identity as the growth atoms, and this approach has been used most commonly to grow Au nanorods from Au seeds (see Section 5.3).[92] Amazingly, the twin structure of the seed is transferred to the entire nanocrystal via epitaxial growth, although the final nanocrystal shape may deviate from that of the initial seed due to the factors outlined in Sections 4.1 and 4.3.

Epitaxial growth also can be achieved when the seeds and added atoms are chemically different; however, in this case, it is more accurately referred to as heteroepitaxial growth. Heteroepitaxy has long been used in gas-phase deposition to prepare functional heterostructures or junctions but had not been explored in the solution phase until recently.[93] As a prerequisite for heteroepitaxial growth, there must be a close lattice match between the seed and the deposited atoms (e.g., Pd and Pt have a lattice mismatch of only 0.77%). As discussed in more detail in Sections 5.1 and 5.4, this approach can be used to prepare bimetallic core-shell nanocrystals (Figures 11 and 12), in which the core consists of the initial seed used for heteroepitaxial deposition.[94] When there is a large lattice mismatch between the seed and the deposited atoms (e.g., Au and Pt have a lattice mismatch of 4.08%), heteroepitaxial growth is unfavorable due to high strain energy. As a result, non-conformal growth ensues, giving rise to shapes not necessarily predicted from the structure of the seed (see Section 5.3). Very recently, Xie and coworkers considered this approach more fully and found that even with large lattice mismatches, conformal growth was

possible, with Au/Pd core-shell cubes (lattice mismatch 4.71%) being produced; they suggested that, in addition to minimal lattice mismatch (<5%), the metal bond energies of the two components were important for conformal growth.[94b]

5. Case Studies of Different Metals

The first example of the shape-controlled synthesis of metal nanocrystals was demonstrated by El-Sayed and coworkers with the preparation of Pt nanocubes and tetrahedrons.[95] Shortly thereafter, Au nanorods,[96] FePt nanocubes,[97] Ag nanoplates,[98] and Ag nanocubes[78a] were demonstrated. Since these early examples, there have been many reports of other metals being prepared as shape-controlled nanocrystals and of other shapes. Here, we survey this work so to highlight the principles outlined in Sections 1-4, beginning our discussion with Pd because the largest number of shapes has been generated for this noble metal. As we hope to convey, Pd is an ideal model system for understanding the synthesis of metal nanocrystals with well-controlled shapes, and the principles that direct Pd nanocrystal growth can be easily extended to other *fcc* metals and alloys.

5.1. Pd

Palladium is most interesting for its extraordinary capability to absorb H₂. Incredibly, it can absorb up to 900 times its own volume of H₂ at room temperature and atmospheric pressure, making it an efficient and safe storage medium for H₂. When it is finely divided, Pd also can serve as a good catalyst for hydrogenation and dehydrogenation reactions as well as petroleum cracking. In organic chemistry, a large number of carbon-carbon bond forming reactions such as Heck or Suzuki coupling are facilitated by catalysts based on Pd(0) or its compounds.[99] The largest use of Pd today is probably in catalytic converters, which convert up to 90% of the harmful gases (including hydrocarbons, CO, and NO) from auto exhaust into less harmful substances such as CO₂ and H₂O. All of these applications could be greatly enhanced with the use of Pd nanocrystals enclosed by the same appropriate facet. [100]

The predominant shape of Pd nanocrystals is the Wulff polyhedron when the sample is prepared by relatively fast reduction or decomposition. Experimentally, Na₂PdCl₄ is the most commonly used precursor for the reduction route because of its stability in air and good solubility in a variety of solvents. In this case, no additional Cl⁻ is needed to initiate oxidative etching as this anion will be released from the salt precursor during reduction. Pd(NO₃)₂ is also commercially available and could be used as a precursor to Pd; however, it is hygroscopic and tends to hydrolyze to Pd(OH)₂. [101] In general, alcohols, glycols, and hydrazine can all serve as the reductant source to ensure fast reduction of various Pd precursors.[60,102] Among these options, ethylene glycol offers a unique example as it serves as both the solvent and primary reductant at the temperatures commonly used for Pd nanocrystal synthesis. For a typical synthesis conducted in air at 110 °C with Na₂PdCl₄ as a precursor, the product sampled after 5 min contained 90% Wulff polyhedrons (~8 nm in size) and 10% multiply twinned particles (MTPs, including decahedrons and icosahedrons). [60] When the reaction was prolonged to 3 h, all the MTPs were eliminated due to oxidative etching, leaving behind only Wulff polyhedrons (Figure 13a),[63a] and if allowed to continue beyond 3 h, even these single-crystal structures were subjected to oxidative etching. As a result, it is difficult to grow Pd nanocrystals larger than 10 nm using this method. Additionally, because PVP is too big to have a significant capping effect on very small nanocrystals, these Pd nanocrystals <10 nm in size cannot evolve into perfect cubes, but rather maintain their Wulff polyhedral structure.

While the above work illustrates the power that oxidative etching can have in controlling the population of twinned structures in solution, the preparation of single-crystal Pd

nanocrystals encased with only one type of facet (e.g., cubes as compared to Wulff polyhedrons) is desirable, particularly for applications in catalysis. To achieve this goal, two approaches have been explored: *i*) modulation of reduction/oxidation conditions during the polyol synthesis and *ii*) use of a capping agent much smaller than PVP. In the first approach, Pd nanocubes with edge lengths up to 50 nm were prepared by adding Fe^{III} species to a polyol synthesis at 90 °C. In this case, the addition of such species was found to enhance the oxidation of Pd(0), thus effectively reducing the number of seeds formed during the nucleation stage.[78b] At the same concentration of precursor, the presence of fewer seeds means a larger size for the final product. Using this approach, the final size of the Pd nanocrystals could be controllably increased simply by increasing the concentration of the Fe^{III} species. Due to the capping effect of PVP, these larger single-crystalline nanocrystals adopted a cubic shape and, as expected, with some slight corner truncation (Figure 13b).

Considering the second approach, Br⁻ was added as a smaller capping agent and found to promote the development of {100} facets, allowing for the generation of Pd nanocubes 8 nm in edge length (Figure 13c).[64d] This synthesis was carried out in water with PVP as a reductant, and both XPS and EDX analyses suggest that Br⁻ is capable of chemisorbing onto the {100} facets of very tiny Pd nanocrystals. In this way, the selective chemisorption of Br⁻ alters the order of surface energies for different facets, allowing for nanocubes, not Wulff polyhedrons, to be produced at small sizes.

During the course of this work with Br⁻, it was also found that this anion could initiate anisotropic growth for cubic nanocrystals if the reduction rate was accelerated by introducing ethylene glycol as a reductant.[64d] In one example, Pd nanobars enclosed by {100} facets and with a square cross section were synthesized from a reaction containing ethylene glycol, water, PVP, and KBr (see Figure 13, d and e). The aspect ratio of the nanobars was observed to increase with an increase in the concentration of ethylene glycol. In a second example, Pd nanoneedles with a rectangular cross section of decreasing area were prepared in water with ascorbic acid and sodium citrate as co-reductants and CTAB as a capping agent.[103] How and why such anisotropic growth occurs are yet to be fully understood; however, localized oxidative etching in the presence of Br⁻ appears to be involved. As the chemisorbed Br⁻ layer prevents the further addition of Pd atoms to the Pd nanocrystal, the surface has to be activated in some way to continue the growth process. For a cubic nanocrystal, localized oxidative etching could selectively activate only one of its six faces for atomic addition. Then, if enough Pd atoms can be supplied to the etched site by accelerated reduction, atomic addition will surpass the removal of atoms caused by etching at that face, breaking cubic symmetry and eventually leading to the formation of a nanobar. In this case, a relatively fast reduction rate, achieved by having a high concentration of ethylene glycol in water, is needed to provide sufficient Pd atoms for continuous growth. For a Wulff polyhedral nanocrystal, selective activation of an octagonal face by localized oxidative etching leads to a nanorod whose side surfaces are a mix of both {100} and {110} facets. As for the formation of Pd nanoneedles, the exact mechanism still needs to be resolved. We believe that the Br⁻ from CTAB may play a critical role, in addition to the capping effect of the surfactant.

In addition to single-crystal seeds, the Pd system is rich in twinned structures.[104] As discussed in the beginning of this section, the retention of twinned seeds produced during polyol reduction is difficult to achieve due to the intrinsically corrosive environment. Yet, in a recent study, we found that citric acid or citrate ions could protect such seeds from oxidative etching.[66,80] There are two possible mechanisms for explaining this observation: *i*) they can compete with oxygen adsorption and thus reduce the amount of oxygen immobilized on the Pd surfaces or *ii*) they can react with and exhaust the adsorbed oxygen. Regardless of the mechanism, it becomes possible to stabilize twinned Pd

nanocrystals enclosed by {111} facets – decahedrons and icosahedrons – and even single-crystal octahedrons, presumably due to the strong binding of citrate to the {111} facets.

The key to producing one of these nanocrystal shapes to the exclusion of the others is to control the population of the various seed types in a synthesis. Amazingly, using a simple water-based system in which only Na_2PdCl_4 , PVP, and citric acid were added, we were able to achieve these various seeds and tune their yields simply by controlling the concentration and reduction rate of the precursor.[66,80] It has been shown by simulation that icosahedral, decahedral, and Wulff polyhedral clusters are favored for Pd at small ($N < 100$), medium ($100 < N < 6500$), and large sizes ($N > 6500$), respectively.[54] Thus, to generate Wulff polyhedral seeds, and eventually octahedrons, a high atomic concentration is required because the number of Pd atoms in a seed is highly dependent on the atomic concentration in the solution. Two factors affect the atomic concentration: *i*) the reduction rate and *ii*) the concentration of precursor. As citric acid is a mild reducing agent, the Pd precursor concentration has to be kept relatively high in this synthesis. When this condition is met, Pd octahedrons are produced in 90% yields (Figure 13f). The same protocol can be used to generate Pd decahedrons in high yields. In this case, the concentration of citric acid or citrate ions has to be increased to ensure sufficient capping of the {111} facets, thus reducing the surface energy of the {111} facets and compensating for the extra strain energy caused by twinning. For these reasons, decahedral seeds can be stabilized effectively and grow into large decahedrons (Figure 14a) even though the number of atoms might be above the favorable medium range for decahedral seed generation. Finally, when the atomic concentration is significantly lowered by reducing the Pd precursor concentration, icosahedral seeds become favorable due to the slow addition of Pd atoms. As a result, Pd icosahedrons become the major product (Figure 14b).[66,80]

Besides citric acid, ascorbic acid may be used as a reducing agent. When it was used at 80 °C in the presence of Br^- , anisotropic growth of decahedral seeds was induced, resulting in pentagonal nanorods with their side {100} faces presumably stabilized by Br^- . [68] Although there is modest oxidative etching in this system, these five-fold twinned nanorods can be stable for a long period of time. In the same synthesis, right bipyramids were also formed from singly twinned seeds, with their {100} facets being stabilized with Br^- . In general, the product typically consisted of 30% five-fold twinned nanorods with length up to 150 nm, 17% MTPs, 18% singly twinned right bipyramids, and 35% nanocubes (Figure 14c). When the reaction temperature was increased to 100 °C, oxidative etching was greatly enhanced in this system. Thus, multiply twinned structures were rarely found in the final product, although right bipyramids were still present up to 30% in the final product distribution (Figure 14d).

When the reduction of the Pd precursor is greatly slowed down, Pd nanoplates will be produced in high yields, indicating a kinetically controlled reaction. Such nanoplates can have a triangular or hexagonal cross section, and as was observed in some of these syntheses, hexagonal plates can evolve into triangular plates as their sizes are increased. Such a transformation likely occurs by the mechanism proposed by Lofton and Sigmund (see Section 4.2).[52b] Many different approaches have been developed to slow down the generation rate of Pd atoms.[58-60,105] In polyol syntheses, the net reduction can be slowed through the introduction of Fe^{III} species and the O_2/Cl^- pair, both oxidative etchants for Pd(0).[60] For the O_2/Cl^- pair, etching can be enhanced by adding an acid. For Fe^{III} species, adjusting their concentration allowed the reduction rate to be precisely controlled so to generate triangular or hexagonal Pd nanoplates (see Figure 14e for triangular nanoplates). As a second approach, the reduction rate can be kept slow by using a mild reducing agent (e.g., PVP, formate, methanol, or glycolate) at low temperatures. For example, the ends of commercially available PVP have been found to be terminated with a hydroxyl group

using ^{13}C NMR spectroscopy.[59a] Such a polymer, just as with long-chain alcohols, can serve as a mild reducing agent for kinetically controlled syntheses including those of Pd nanoplates (Figure 14f).[59b] In practice, controlling the ratio of PVP to precursor as well as the molecular weight of PVP can provide further control of the reduction rate. As a third approach, Pd atoms can be slowly generated through decomposition of a Pd-octanedionate complex in the presence of various tetraalkylammonium salts to form hexagonal Pd nanoplates in high yields.[58a] Finally, a RNA-mediated synthesis of Pd nanoplates has been reported.[105] In this case, the RNA sequence was found to be critical to the formation of plate-like morphology, and it was suggested that the RNA provided a critical folding motif for interaction with the precursor complex that directed the formation of nanoplates. Interestingly, by changing the RNA sequence, Pd nanocubes could be obtained through a similar reaction. It is worth pointing out that the sugar unit in RNA contains hydroxyl groups, which might also be involved in reducing the Pd precursor.

Recently, it has been shown that polyhedral Pd nanocrystals with edge lengths >30 nm could be obtained by heteroepitaxial seeded growth, in which preformed Pt nanocubes (such as those discussed later in Section 5.4) were added to a synthesis and served as sites for nucleation and the controlled overgrowth of Pd nanocrystals.[94a] The final products exhibited a well-defined core-shell Pt/Pd structure made possible by the minimal lattice mismatch between Pt and Pd. By controlling the concentration of NO_2 present during the synthesis, the growth rates along the $\langle 100 \rangle$ and $\langle 111 \rangle$ directions could be varied to produce octahedrons, cuboctahedrons, and cubes (Figure 11). In these cases, the NO_2 was generated in situ from the decomposition of HNO_3 in the presence of HCl. The generated NO_2 can then dissociate on the Pd surface, giving NO and atomic oxygen; the NO will desorb while the atomic oxygen should remain on the surface and modulate the growth rates of different facets.

5.2. Ag

Historically, silver has most widely been used in jewelry/metal-craft and photography (where photosensitive Ag halides are reduced).[9] More recently, Ag, particularly in nanoparticle form, has been finding use as a catalyst in various oxidation and oxidative coupling reactions (e.g., formaldehyde production from methanol and air).[106] In fact, Ag nanoparticles are the only practical catalyst available today for converting ethylene to ethylene oxide, an important industrial precursor. Silver nanostructures also have been the source of extensive research for their widespread use as substrates for SERS, optical labeling, and near-field optical probing.[15] Experimentally, AgNO_3 is the most commonly used precursor when preparing Ag nanocrystals via the reduction route because of its good solubility in polar solvents. This compound, however, is highly sensitive to light, and as discussed in Section 2.2, this sensitivity can have a significant effect on the nature of Ag species in solution. As a result, cautions must be taken in the storing and handling of this precursor.

Like other *fcc* metals, icosahedral, decahedral, and Wulff polyhedral seeds and their corresponding nanocrystals are the thermodynamically favored products. Yet, according to simulations, the size window that favors both Ag icosahedrons and decahedrons is much broader than with other metals (Table 2).[54] As a result, multiply twinned seeds typically predominate under most reaction conditions. Of course, the multiply twinned seeds can be selectively removed via oxidative etching just as in the Pd system (see Figure 7).[62] In practice, however, oxidative etching with the Cl^-/O_2 pair is a slow process for the Ag system, with single-crystal products only being produced after a couple days of reaction. This oxidative etching process can be enhanced by the introduction of a protonic acid (either by directly adding HCl or through the transformation from H_2).[107] In these cases, single-crystal Ag nanocubes could be produced in less than half day. It should be pointed out that

Ag cuboctahedrons (Figure 15a) and perfect nanocubes (Figure 15b) are only observed once the Ag nanocrystals have grown past 20 nm, at which point PVP as a capping polymer can promote the formation of {100} facets. At smaller sizes, the single crystals adopt a Wulff polyhedral (or spherical) profile so to minimize their overall surface area. While oxidative etching has proven to be an extremely powerful tool for controlling the population of twinned seeds in solution, the slowness of this process in the Ag system inhibits large-scale synthesis.

Recently, we reported a very rapid route to Ag nanocubes in which oxidative etching was not necessarily involved.[108] In this case, sulfide or hydrosulfide is added to ethylene glycol at a ppm level prior to the introduction of PVP and AgNO₃. Upon AgNO₃ addition, Ag₂S clusters or nanocrystallites are formed, which can serve as primary sites for nucleation by catalyzing the reduction of Ag⁺. [109] In a related study, Yang and coworkers also produced single-crystal Ag nanocubes in a matter of minutes, in this case by adding trace CuCl₂ to a 1,5-pentanediol-based polyol synthesis.[67a] While the role of the Cu salt was not discussed in their publication, it presumably facilitates single-crystal seed formation via a similar mechanism. Interestingly, they also showed that their Ag nanocubes could grow in size to become truncated octahedrons (Figure 15c) and then octahedrons (Figure 15d). Although PVP was used in this synthesis, it seems unable to reduce the surface energy of {100} facets below that of the {111} facets and could be due to not enough PVP being present during synthesis.

Besides PVP, the addition of Br⁻ to a polyol synthesis can also promote the formation of {100} facets and thus Ag nanocubes (Figure 15e).[110] Under the right conditions, Br⁻ can even induce anisotropic growth to transform Ag nanocubes into nanobars with rectangular cross sections (Figure 15f).[63b] While the mechanism for such growth is not fully understood, it is believed to be analogous to the case of Pd nanobars in which Br⁻ chemisorption and localized oxidative etching are involved. The function of Br⁻ in the synthesis of Ag nanocrystals, however, is much more complicated than that of Pd because Ag is much more chemically active. For example, it has been observed that the addition of Br⁻ to a polyol synthesis of Ag can induce oxidative etching even though Br⁻ is less corrosive than Cl⁻. At high Br⁻ concentrations (60 μM, Ag:Br 1700), all twinned seeds are removed; however, decreasing the concentration of Br⁻ by 50% removes only the most reactive multiply twinned seeds from the solution. As a result, a mixture of single-crystal and singly twinned seeds remain, which can grow into Ag nanocubes and right bipyramids, respectively (Figure 16a).[63a] Interestingly, the singly twinned seed can also be induced into anisotropic growth by doubling the AgNO₃ concentration and reducing the reaction temperature, producing a 1-D Ag nanocrystal with a single twin plane running down the long axis. These unique Ag nanocrystals have been referred to as nanobeams (Figure 16b). [69]

As with the singly twinned seeds, anisotropic growth of decahedral Ag seeds can be induced to facilitate the formation of 1-D nanocrystals such as nanorods and nanowires – in these cases, however, the resulting crystal will have a pentagonal cross section (Figure 16c). [111-113] Although early work indicated that small nanoparticles of Pt or Ag were needed to promote anisotropic growth,[111] recent studies have shown that such seeds are not necessary at all. Only AgNO₃, ethylene glycol, and PVP are needed! [70] PVP stabilizes the {100} side faces of nanowires, and the internal twin defects of the initial seeds induce the 1-D growth. In order to obtain multiply twinned seeds (and thus nanowires) in high yields, oxidative etching has to be blocked during the synthesis. This requirement has been achieved in the Ag system by simply bubbling an inert gas through the reaction solution [62] or through the addition of redox active metal salts – for example, Fe^{II}/Fe^{III} or Cu^I/Cu^{II} – which increases the rate of Ag deposition relative to oxidation.[65,114]

Besides those structures built upon thermodynamically favored Wulff polyhedrons, it is possible to switch to kinetically favored structures. This condition can be met by slowing down the generation of Ag atoms, just as in the Pd system.[115-117] The resulting Ag crystals are plate-like, similar to those prepared by Mirkin and coworkers in 2001 in which Ag nanoparticles were photo- or thermally transformed into nanoplates (Figure 16d) over a long period of time via an Ostwald ripening mechanism.[98] To prepare Ag nanoplates by slowing down reduction, a mild reducing agent such as HO-terminated PVP, ascorbic acid, or glycylglycine is often used (Figure 16e).[59] Alternatively, the precursor reduction rate can be slowed down by complexing the Ag⁺ ions with a strongly coordinating polymer such as polyacrylamide (PAM) whose amino groups could form complexes with Ag⁺ ions.[58b] According to the Nernst equation, the redox potential of the Ag⁺/Ag pair should be greatly reduced due to formation of such a complex, which can in turn greatly reduce the reduction rate and favor the formation of nanoplates through kinetically controlled growth.

Finally, Ag nanobelts (Figure 16f) have been observed, being prepared through a thermal transformation in a manner similar to the early nanoplate work.[61b] The growth mechanism responsible for this class of nanostructures remains unresolved; however, the total free energy of a nanobelt should be as high as that of a nanoplate due to the internal strain caused by twinning and their generally large surface areas. These properties imply that the nanobelts are kinetically controlled products. It would be interesting to develop a kinetically-controlled reduction route to such structures in high yields.

5.3. Au

The synthesis of Au nanocrystals with well-defined shapes appears to be one of the most popular subjects of research over the past decade, as judged from the total number of publications per year on this subject. This trend, in large part, is due to the unique and often tunable properties of Au nanocrystals that include LSPR, biocompatibility, and easy surface modification. When combined together, Au nanocrystals represent an ideal platform for chemical and biological sensing as well as applications in nanomedicine. For example, Au nanoparticles can readily adsorb protein molecules onto their surfaces, causing a shift in the LSPR of the nanoparticles.[13] When coated with specific antibodies, these immuno-Au nanocrystals can be used to probe the presence and position of antigens on cell surfaces as well as to potentially deliver therapeutic agents selectively.[14] Most recently, Au nanoparticles were discovered to display unique catalytic properties for a variety of oxidation reactions; however, the performance of these Au catalysts is highly dependent on the size of the nanocrystal.[118]

There have been many demonstrated methods for controlling the shape of Au nanocrystals, and as with the Pd and Ag systems, the selection of reductant, reaction conditions, and stabilizer are all critical to forming a particular shape. As expected, strong reducing agents, as typified by polyol reduction, facilitate the synthesis of thermodynamically favored polyhedral Au nanocrystals.[119] There are, however, notable differences. For example, in contrast to the Ag and Pd systems, the binding of PVP to Au does not appear sufficiently strong to promote the formation of {100} facets and is probably due to differences in surface reactivity. As a result, single-crystal and multiply twinned Au nanocrystals enclosed by {111} facets – octahedrons (Figure 17a), truncated tetrahedrons (Figure 17b), icosahedrons (Figure 17c), and decahedrons (Figure 17d) – predominate as compared to {100} encased crystals that typify the Pd and Ag systems.[91,120] Interestingly, when Ag⁺ or Br⁻ ions are present during reaction, truncated (Figure 17e) or perfect Au nanocubes (Figure 17f) result.[91,121]

As observed in the Pd and Ag systems, when the reduction rate is substantially slowed, Au nanoplates will be produced, and this kinetic control can be achieved by using a mild

reductant such as phenylenediamine, an extract from the plant lemongrass (*Cymbopogon flexuosus*), PVP, or glucose. Such kinetic control can also be achieved by performing the syntheses at room temperature. The nanoplates usually have hexagonal or triangular profiles (Figure 18, a and b).[59b, 122] Au nanoplates may also be prepared by reducing the concentration of Au precursor in a synthesis. In this case, the concentration of the generated metal atoms is never high enough to facilitate seeds favored by thermodynamics. Instead, the Au atoms appear to aggregate into small clusters, which then can agglomerate into larger nanocrystals.[123] As a result of this aggregate assembly, twin defects or stacking faults are introduced, which favor Au nanoplate formation. Finally, as in the Ag case, photo-induced Ostwald ripening of Au nanoparticles results in Au nanoplates.[124] Yet, no matter which method is used, the resulting Au nanoplates have a hexagonal or triangular cross section depending on the reaction rate and/or time.[125] As a special case of plate-like morphology, Au nanobelts have also been prepared. In one example, HAuCl_4 was reduced with ascorbic acid in a mixed surfactant system containing sodium dodecylsulfonate (SDS) and CTAB.[126] The reaction was performed below room temperature to ensure sufficiently slow reduction, while the belt-like morphology was attributed to a cooperative effect between the mixed surfactants (Figure 18c). With glucose as a reductant, Au nanobelts have also been prepared under sonication.[127]

While the preceding paragraphs reiterate the importance of reduction kinetics and shape control, seeded growth, as pioneered by the Murphy group, has proven to be extremely powerful in the Au system.[79,128] In this method, small Au nanoparticles are first prepared via fast reduction with a strong reducing agent. These seeds are then used to initiate further nanocrystal growth when additional precursor is added and then slowly reduced in the presence of a surfactant or polymeric stabilizer. Most commonly, HAuCl_4 is reduced with ascorbic acid in the presence of citrate-capped twinned Au seeds and CTAB to produce anisotropic Au nanorods and nanowires. These 1-D nanostructures have a pentagonal cross section with end surfaces being terminated by $\{111\}$ facets; the side surfaces are poorly defined but are enclosed by either $\{100\}$ or $\{110\}$ facets, or both (Figure 18d).[129] Interestingly, when CTAB-capped single-crystal seeds are used and Ag^+ ions are added to the synthesis, 1-D single-crystal nanorods enclosed by $\{110\}$ side facets and $\{100\}$ end facets were observed (Figure 19a).[128,130] In this case, the Ag^+ is thought to be reduced preferentially on the $\{110\}$ facets due to an underpotential deposition process. Strong CTAB binding to the deposited Ag via Br^- can then prevent Au deposition to the $\{110\}$ faces, resulting in anisotropic growth. Besides Br^- and Ag^+ ions, the concentrations of Au seeds and Au precursor can be manipulated to tune the nanocrystal shape. For example, when the concentration of seeds relative to Au atoms is low, overgrowth of Au nanocrystals is possible.[121,131] For Au nanocrystals with truncated cubic or octahedral shape, such overgrowth can lead to the formation of branched structures, including monopods, multipods (Figure 19b), and flower-like structures.[131a,b,f] For Au nanorods, such overgrowth leads to dog bone (Figure 19c), dumbbell (Figure 19d), and bipyramid nanostructures.[131c-e]

As a variant of these seeded growth methods, Yang and coworkers extended their heteroepitaxial method to prepare Au nanorods.[94a] In this example, single-crystal Pt nanocubes were used to seed Au nanocrystal growth. In contrast to their Pt/Pd work discussed in Section 5.1, the lattice mismatch between Pt and Au is much greater (4.08% mismatch versus 0.77% for Pt/Pd), giving rise to non-conformal growth. As a result, Au nanorods with incorporated Pt nanocubes are produced in high yield.[94a]

Besides these seeding methods, single-crystal Au nanorods and nanowires can be synthesized by electrochemical[96] and photochemical[132] methods. Interestingly, in both cases, Br^- is necessary. In the seeded growth of Au nanorods, Br^- is also present, originating from the CTAB. It has been speculated that CTAB might form micelles to induce and direct

1-D growth; however, a recent study revealed that the organic tail of CTAB was not necessary for Au nanorod formation.[63b] These observations, in combination with the examples of 1-D growth in the Pd and Ag systems, suggest that Br⁻ might be more critical to 1-D growth than the alkyl chain of CTAB. Besides Au rods and wires, polyhedral Au nanocrystals including decahedrons, cubes, and octahedrons have been prepared using seeded growth processes.[133]

As an interesting example of 1-D Au nanocrystal growth, very recently, we and others reported the synthesis of ultrathin Au nanowires with diameters <2 nm.[134] These structures formed through a unique growth process in which a polymeric strand of oleylamine-AuCl complex is first formed via aurophilic interaction when mixing AuCl and oleylamine in hexane.[134a] The resulting complex can best be described as a linear chain composed of a Au^I...Au^I backbone that is surrounded by oleylamines (Figure 20a). By slowly reducing the strands, with the aid of Ag nanoparticles, ultrathin Au nanowires are produced (Figure 20b). Interestingly, high-resolution transmission electron microscopy (HRTEM) study reveals that these wires grow along the <111> direction, which is likely due to their unique growth mechanism (Figure 20c).

5.4. Pt

Platinum is an extremely valuable metal due to its exceptional and unique properties as a catalyst for CO oxidation in catalytic converters, the H₂/O₂ reaction in fuel cells, sulfuric acid production, and petroleum cracking, among others.[7c] It can also be used as a stable electrode material. As Pt is particularly expensive, there is a real incentive to reduce the amount of Pt required in processes where it is essential. To this goal, much research has emphasized the size reduction of Pt catalysts so to maximize the surface area. Researchers also have emphasized the improved selectivity of Pt nanocatalysts to which the exposure of crystal facets more intrinsically active for a particular process would be beneficial. In these ways, the shape-controlled synthesis of Pt nanocatalysts would be very beneficial.

In contrast to the Pd, Ag, and Au cases, twinned structures of Pt rarely form.[135] This observation probably arises from the high internal strain energy associated with Pt twinned crystals.[136] Since the first publication of Pt cubes, tetrahedrons, and truncated octahedrons by the El-Sayed group in 1996, much effort has been devoted to this synthesis, which involves the reduction of K₂PtCl₄ by H₂ in the presence of sodium polyacrylate as a capping agent.[95,137] It was observed that the Pt tetrahedrons produced initially evolved into truncated octahedrons and eventually cubes through the deposition of Pt atoms on the exposed {111} facets.[58b] This selective atomic addition to {111} facets seems to be related to the different capping abilities at various facets.[58b] The concentration of the capping agent has also been shown to influence this evolution in shape.[95] In related work, Pt nanocubes (Figure 21a) and cuboctahedrons (Figure 21b) were prepared by reducing K₂PtCl₄ with H₂ generated *in situ* from NaBH₄ decomposition. In these studies, tetradecyltrimethylammonium bromide (TTAB) was used as a surfactant. Interestingly, switching to a milder reducing agent, ascorbic acid, led to the formation of Pt nanodendrites (Figure 21c).

More recently, the polyol reduction method was used to synthesize Pt nanocrystals in the presence of PVP and Ag⁺ as an ionic mediator.[138] In these studies, it was found that, just as in the seeded growth of Au nanorods, the addition of Ag⁺ can affect the final nanocrystal shape. Again, Ag⁺ enhances crystal growth along the <100> axis, but in this case facilitating the formation of Pt octahedrons. Like the case of Au, overgrowth on truncated octahedrons of Pt can lead to the formation of branched structures. This phenomenon has only been observed at a low concentration of seeds and high concentration of Pt atoms. To meet these criteria, two strategies have been employed. In the first system, oxidative etching by Fe^{III}

species was coupled to a polyol reduction process to keep the initial concentration of Pt seeds extremely low.[135b] Then, by continuously bubbling N_2 through the reaction, oxidative etching was blocked so that a high concentration of Pt atoms could be generated and persist. In this way, Pt cuboctahedral seeds could grow into tetrapods through the overgrowth on their $\{111\}$ corners (Figure 21d). The second system was built upon H_2 reduction, to which a high concentration of Pt precursor was used to ensure the necessary overgrowth.[139] Since these initial reports, a number of related methods have been used to synthesize branched Pt nanostructures, including the very recent demonstration by El-Sayed and coworkers in which tetrahedral Pt seeds were used to grow single-crystal star-like Pt nanostructures with up to 30 arms.[140]

Single-crystal Pt nanowires can be obtained under the same conditions as in the aforementioned polyol synthesis for Pt tetrapods; however, the reaction has to be allowed to proceed in air, not N_2 (Figure 21e).[135a] In this case, precursor reduction is kept slow for the entire reaction. A high-resolution TEM study of these Pt nanowires revealed that they grow along the $\langle 111 \rangle$ axis, just like the ultrathin Au nanowires formed by reduction of oleylamine-AuCl complexes. The mechanism for Pt nanowire growth along the $\langle 111 \rangle$ axis remains mysterious, although autocatalytic nucleation might be involved.[35] Mainly, with such slow reduction, the concentration of Pt atoms in the solution could be too low to form nuclei. Instead, two Pt precursor complexes (i.e., $[PtCl_4]^{2-}$ or its water-substituted form $[PtCl_2(H_2O)_2]$) might form a dimer as described in Section 2.1, on which more Pt complexes could be attached to form a long-chain complex. After reduction, this long chain would be converted into a Pt nanowire. Due to this unique mechanism, the growth direction might be different from that of Au and Pd nanorods. Interestingly, Pt nanorods and nanowires with this same structure have been grown on a number of different supports including silica/polymer beads, metal gauzes, ceramic nanofibers, and silicon wafers, which should facilitate their application in catalysis.[141] In addition, Pt nanorods and nanowires have been synthesized using a γ -irradiation method[142] and a Pd-seeding process, [141a] respectively. Finally, in related work, interconnected Pt nanowires were synthesized in a two-phase water-chloroform system containing CTAB. Pt precursor reduction and nanocrystal growth were confined within a worm-like micellular network formed within droplets of chloroform, and this confinement was thought to contribute to the unique shape (see Figure 21f).[143, 144]

Besides the conventional nanocrystals, a number of unconventional Pt nanocrystals covered by high-index facets have been prepared. Examples include: tetrahexahedron covered by $\{hk0\}$, trapezohedron by $\{hkk\}$, trisoctahedron by $\{hhl\}$, and hexoctahedron by $\{hkl\}$ ($h > k > l$). For example, the tetrahexahedron (THH) with O_h symmetry is bound by 24 high-index planes of $\{hk0\}$, which can be considered as a cube with each face capped by a square-based pyramid. In general, it has been a grand challenge to synthesize these types of nanocrystals because of their high surface energies. Recently, a breakthrough in the synthesis of such nanocrystals was achieved by putting a square wave potential (a pulse sequence that alternates between reducing and oxidizing potentials at a rate of 10 Hz) on 750-nm polycrystalline Pt spheres (deposited on a substrate of glassy carbon) in the presence of ascorbic acid and sulfuric acid (Figure 22).[145] The resulting THH nanocrystals were enclosed by $\{730\}$, $\{210\}$, and/or $\{520\}$ facets, as revealed by HRTEM. In this system, the adsorption and desorption of oxygen on Pt induced by the square wave potential was responsible for this unconventional shape, emphasizing the significance surface capping by gaseous species may play in directing or controlling the shape of a nanocrystal. As high-index facets contain many dangling bonds and atomic steps, surface Pt atoms can easily form Pt-O bonds so to protect such facets. In contrast, $\{111\}$ and $\{100\}$ facets are so compact that oxygen has to diffuse into and out of the lattice. As a result, these ordered surface structures would be destroyed.[146]

While many Pt nanocrystals of controlled-shapes have been demonstrated, as the previous examples illustrate, there is a general preference for Pt to adopt shapes based on single-crystal seeds. In fact, it has proven extremely difficult to achieve Pt plate-like structures through the strategy based upon kinetic control. For example, when we employed PVP as a mild reducing agent just as in the Ag and Pd nanoplate syntheses, only 15% of the product consisted of plate structures and they all were quite small (edges <10 nm).[59b] This observation was attributed to the higher internal strain expected for Pt twinned structures. Very recently, however, we have demonstrated that Pt nanoplates with large lateral dimensions (edges >50 nm) could be obtained by using Pd nanoplates as seeds for heteroepitaxial deposition of Pt (Figure 12).[94c] In this approach, the Pd nanoplates were synthesized by reducing a Na_2PdCl_4 precursor with PVP as a reductant (as discussed in Section 5.1) and then served as seeds for the nucleation of Pt atoms formed by reducing H_2PtCl_6 with citric acid. The product consists of the core being a hexagonal or triangular Pd nanoplate and the shell being made of a thin, uniform Pt shell, demonstrating the layer-by-layer epitaxial growth of Pt on Pd surface. The close lattice match between Pd and Pt and the slow reduction rate associated with the mild reducing power of citric acid are instrumental in achieving the conformal epitaxial growth of Pt shells on Pd nanoplates.

As an interesting variant of the plate-like morphology, Yang and coworkers reported the synthesis of planar Pt tripods (Figure 23) from Pt seeds containing a single twin in the (111) plane (the same defect structure that characterizes the Ag and Pd nanoplates).[147-149] In this work, $\text{Pt}(\text{acac})_2$ was reduced in the presence of adamantanecarboxylic acid, hexadecylamine, and various 1,2-alkanediols. A detailed electron microscopy study revealed preferential nucleation and growth from activated trough sites present on the twinned seed. In addition to the planar tripod structures, mono-, bi- and various 3-D multipods of Pt could be formed, with their structures being attributed to the twin structures of the various seed crystals (Figure 23).

5.5. Cu

Similar to Ag and Au, Cu nanocrystals can take most of the shapes that have been observed for Pd.[150-158] Due to its high reactivity, however, a strong reducing agent such as N_2H_4 needs to be used in combination with an elevated reaction temperature to reduce a typical precursor (e.g., cupric sulfate, nitrate, or acetate) to Cu atoms. In addition, the synthesis has to be performed under the protection of an inert gas such as Ar or N_2 to avoid oxidation of the Cu nanocrystals by the O_2 in air. These complications are probably the primary reasons why solution-phase syntheses of Cu nanocrystals have not been widely explored despite the technological advances (e.g., as catalysts for water-gas shift[159] and gas detoxification reactions[160]) that could potentially benefit from Cu nanocrystals having controllable shapes.

In addition to the less interesting, irregular shapes, Cu nanocrystals may adopt nanocube or five-fold twinned nanorod structures. For example, Cu nanocubes of 100 ± 25 nm in edge length have been reported from a modified polyol process, in which CuSO_4 was reduced with ascorbic acid in the presence of PVP as a capping agent.[151a] In this synthesis, the authors propose that the PVP was responsible for the termination of Cu nanocubes with {100} facets; however, it is worth pointing out that we recently tried this synthesis and only obtained Cu_2O nanocubes, not Cu nanocubes.[151b] Alternatively, hydrazine has been used to reduce CuCl_2 dispersed in aqueous media containing dodecyl benzene sulfonic acid sodium (DBS) as a capping agent.[151c] In this case, Cu nanocubes of 50 ± 6 nm in edge length were reported. Strange enough, the authors provide an electron diffraction pattern taken along the <111> direction, rather than the most convenient <100> direction. The yellow color described in this paper is also indicative of Cu_2O , rather than Cu. In a third report, Cu nanocubes of 75-250 nm in size were prepared using a seed-mediated growth

process in which no capping agent was involved.[151d] Again, the results described in this report need to be double checked and confirmed. We have a strong feeling that the synthesis of Cu nanocubes has yet to be achieved in spite of the claims in the literature.

Regarding the synthesis of five-fold twinned nanorods, three solution-phase methods have been reported so far. In the first method, Pileni and coworkers used hydrazine to reduce copper(II) bis(2-ethylhexyl)sulfosuccinate, $\text{Cu}(\text{AOT})_2$, in a mixture of isooctane and water. [152a] By adjusting the percentage of water to achieve an interconnected network of cylinders, the yield of Cu nanorods could reach 38%, while other particles were MTPs (Figure 24a). The second system used octyl ether as the solvent while 1,2-hexadecanediol was used to reduce $\text{Cu}(\text{acac})_2$ at temperatures greater than 190 °C. Oleic acid and oleyl amine served as capping agents.[152b] The growth of rod structures was attributed to an interplay between the two capping agents; however, tight control over the product shape distribution was never achieved with this system. Finally, the third method was based upon polyol reduction in which ethylene glycol served as both the solvent and source of reductant. PVP was used as a capping agent, just as in the synthesis of Ag nanowires.[152c] Although no detailed mechanism was proposed for the growth of these nanorods, they should evolve from multiple twinned seeds, just like the cases of other noble metals.[153] This hypothesis is supported by mechanistic studies conducted in the vapor phase, where pentagonal Cu nanowires were grown on solid supports using an MOCVD method.[154]

In addition to cubic and rod-like nanocrystals, Cu nanoplates have also been reported.[155] As with the previously discussed metals, the formation of Cu nanoplates requires extremely slow reduction. In one case, $\text{Cu}(\text{CH}_3\text{CO}_2)_2$ was reduced by hydrazine in acetonitrile at 80 °C under an inert atmosphere.[155a] The hexagonal plates were ~27 nm in dimension (from edge to edge) and displayed an LSPR peak around 575 nm. In another demonstration, an aqueous solution of $\text{Cu}(\text{CN})_2^-$ was exposed to γ -irradiation to produce Cu nanoplates encased by the expected {111} top and bottom facets.[155b] It should be pointed out that there are many publications reporting the synthesis of Cu nanocrystals; however, most of these studies do not provide detailed structural characterization of the products so it is difficult to address mechanistic issues.[156] Many of them also seem to be limited in value in terms of shape control. However, we did come across a remarkably simple procedure for generating Cu nanowires with an unusual, circular cross section.[157] In a typical synthesis, aqueous $\text{Cu}(\text{NO}_3)_2$ and NaOH solutions were mixed to form $\text{Cu}(\text{OH})_2$ precipitates, followed by the addition of ethylenediamine (EDA, a coordination ligand for Cu^{2+}) and hydrazine (a reductant). After heating in a water bath at 60 °C for 15 min, Cu nanowires of 90-120 nm in diameter were formed in high yields. We have been able to reproduce this work in our own laboratory (Figure 24b).[158] These Cu nanowires could be further employed as a sacrificial template to generate Au, Pd, and Pt nanotubes through a galvanic replacement reaction.

5.6. Rh, Ir, and Ru

These three metals are prominent catalysts for a broad range of industrial applications that include petroleum refining processes and the Monsanto acetic acid process.[161] They are also commonly used as catalysts for the hydrogenation of unsaturated compounds.[162] It is expected that controlling the shape of their nanocrystals will provide a great opportunity to maximize their performances in these applications. However, attempts to synthetically and systematically control their shapes have met with limited success.[64c,163-166] So far, Rh is the most successful among these three metals, with nanocubes, tetrahedrons, nanobars, and multipods having been obtained, in addition to other irregular shapes. Of these shapes, Rh nanocubes and multipods are probably the most well-known, being first prepared by Tilley and coworkers using a polyol process to reduce RhCl_3 in the presence of PVP.[164a] As shown in Figure 25 (a and b), Rh nanocubes and multipods could be selectively obtained at 190 °C and 140 °C, respectively. Intermediate structures were obtained in between those

temperatures. Similar to the synthesis of other metal multipods, it is believed that these Rh multipods also arise from the overgrowth of cubic or octahedral seeds. By keeping the reaction temperature low, the number of seeds formed in solution could be kept extremely low, while simultaneously allowing the concentration of Rh atoms to increase with time. These conditions appear ideal for overgrowth along the $\langle 111 \rangle$ direction and therefore multipods are produced. Increasing the temperature limits overgrowth as more seeds are formed in the nucleation stage. As a result, single-crystal Rh nanocubes are produced, as facilitated by PVP capping. In a recent study, it was demonstrated that Rh nanocrystals of different shapes could be obtained at the same temperature (120 °C) by varying the rate at which the RhCl_3 precursor was added to a seeded growth process.[164b,164c] Son and coworkers have considered a thermal decomposition route to Rh nanocrystals in which various Rh-containing organometallic compounds were decomposed in oleylamine.[164d] Interestingly, different shapes evolved from different precursors. For example, Rh tetrahedrons (Figure 25c) were produced from $\text{Rh}_2(\text{CO})_4\text{Cl}_2$ at 190 °C. Yet, Rh nanorods (Figure 25d) were obtained when $\text{Rh}(\text{C}_5\text{H}_8\text{O}_2)_3$ was used as the precursor. While the mechanistic details from these systems still need to be elucidated, it is believed that both the decomposition rate and capping properties of the released organic byproducts play important roles in determining the final shape of the nanocrystals.

In contrast to Rh, the shape-controlled synthesis of Ir and Ru nanocrystals remains a grand challenge. To date, the most uniform and best-defined shape for Ir is single-crystal quasi-nanospheres, prepared by reducing Ir(methylcyclopentadienyl)(1,5-cyclooctadiene) with hexadecanediol in dioctyl ether in the presence of oleic acid and oleylamine as capping agents.[165e] For Ru, the products prepared from both polyol reduction and aqueous systems do not have well-defined shapes.[166] It is anticipated that shape control can be achieved for these metals by taking advantage of the mechanistic understanding and protocols established for the Pd, Ag, Au, and Pt systems.

5.7. Fe, Co, and Ni

Iron, cobalt, and nickel are best known for their ferromagnetic properties.[167] Much effort has been devoted to the synthesis of their nanocrystals so that the magnetic moment of the entire nanocrystal can be made to align when a magnetic field is applied. Their synthesis is also of interest because of their potential superparamagnetism.[6] Various precursors either have been decomposed or reduced in aqueous or organic media so to prepare nanocrystals of these metals. As with the previously discussed metals, the shape of the resultant nanocrystals can be controlled by adjusting precursor concentration and reduction/decomposition rates as well as through the selection of specific capping agents. Often, however, the solvents and precursors used for these systems differ dramatically from those used to prepared Pd, Ag, Pt, and Au nanocrystals, making direct comparisons difficult. It is also worth noting that the resultant nanocrystals tend to be covered by their native oxides because Fe, Co, and Ni are easily oxidized even in well-controlled inert environments.

For the synthesis of Fe nanocrystals, iron pentacarbonyl, $\text{Fe}(\text{CO})_5$, is commonly used as a precursor,[168] with simple Fe nanoparticles being reported as early as 1979 from the thermal decomposition of $\text{Fe}(\text{CO})_5$. Since this initial report, a number of similar approaches have been developed to produce Fe nanocrystals with sizes in the range of 2-20 nm (Figure 26a).[168f] In a special case, 2-nm body-centered cubic (*bcc*) α -Fe nanoparticles were transformed into nanorods. This transformation was achieved by refluxing the particles in pyridine with the assistance of didodecylmethylammonium bromide (DDAB). While the exact mechanism responsible for this transformation remains elusive, the irreversible binding of DDAB to the central region of growing nanoparticles is believed to play a vital role. Besides $\text{Fe}(\text{CO})_5$, $\text{Fe}[\text{N}(\text{SiMe}_3)_2]_2$ (where $\text{Me}=\text{CH}_3$) has proven to be a good precursor for generating Fe nanoparticles.[169a] Iron nanocubes of ~7 nm in size have been prepared

through the decomposition of $\text{Fe}[\text{N}(\text{SiMe}_3)_2]_2$ with hexadecylamine (HDA) and oleic acid or hexadecylammonium chloride (HDAC) as capping agents in mesitylene at 150 °C (Figure 26b). Most recently, an Fe^{II} -oleate complex has been used as a precursor toward Fe nanocubes with edge lengths of ~20 nm.[169b] In addition to the thermal decomposition of organometallic compounds, Fe nanocrystals can be prepared by reduction of Fe-containing salts, although extreme care must be taken to exclude oxygen.[170] Using this approach, the synthesis of Fe nanowires was also reported, where the anisotropic growth was attributed to the introduction of 1,0-phenanthroline as a coordinating ligand.

Unlike Fe, Co can crystallize in hexagonal close packed (*hcp*)-, *fcc*-, or ϵ - phase.[171] As a result, initial work on preparing Co nanocrystals emphasized phase control, not shape control. In particular, the ϵ -phase is a cubic phase with the space group of $p4_132$, which appears to be metastable under normal conditions but very sensitive to the reaction conditions.[171c] It can be completely transformed into the *fcc*-phase when heated to 500 °C. For example, Sun and Murray developed a solution-based route to ϵ -Co nanoparticles in which superhydride (LiBEt_3H) solution is injected into an octyl ether solution containing CoCl_2 at 200 °C with oleic acid and trialkylphosphine as the capping agents (Figure 26c). [171b] Raising the reaction temperature to 300 °C facilitated the formation of *hcp*-Co nanoparticles. Besides the reduction of CoCl_2 , monodispersed Co nanoparticles in the ϵ -phase were synthesized through the rapid pyrolysis of $\text{Co}_2(\text{CO})_8$ in the presence of a mixture of surfactants that consisted of oleic acid, lauric acid, and TOP.[172]

From this early work, it became apparent that the reaction temperature was the critical parameter to controlling the phase of Co nanoparticles produced. In the literature, however, all the examples of non-spherical Co nanocrystals involve *hcp*-Co as the major product. For example, Alivisatos and coworkers prepared *hcp*-Co nanodisks through the rapid decomposition of $\text{Co}_2(\text{CO})_8$ in the presence of linear alkylamines (Figure 26d).[171h] In this case, the observed plate-like morphology cannot be attributed to kinetically controlled synthetic conditions. Rather, the amino group of the alkylamine is thought to inhibit the growth of {001} faces on Co nanocrystals, thus facilitating the disc-like shape. Decomposition of $\text{Co}(\eta^3\text{-C}_8\text{H}_{13})(\eta^4\text{-C}_8\text{H}_{12})$ under H_2 in anisole has been used to generate *hcp*-Co nanorods (Figure 26e).[173] Interestingly, this reaction was performed in the presence of oleic acid and a number of different long chain alkyl amines and simply changing the length of the alkyl chain was found to affect the dimensions of the final nanorods. Finally, Wang and coworkers generated polyhedral Co nanocrystals by modifying the method pioneered by Sun and Murray.[171d] From their synthesis, a mixture of shapes – cubic-like, hexagonal-like, and cubic – were observed. Detailed high resolution TEM analysis revealed that these polyhedron had {221} and {310} facets.

Ni nanocrystals with an *fcc*-phase also have received much attention for their magnetic properties.[174-177] A typical procedure for synthesizing Ni nanocrystals is to use $\text{Ni}(\text{COD})_2$ (COD=1,5-cyclo-octadiene) as a precursor, which decomposes at temperatures as low as 60 °C. A number of different capping agents (e.g., HAD or TOPO) and solvent systems have been considered.[174] Usually such products need to be protected from oxidation by purging the reaction solution with H_2 . From this work, a high-yield synthesis of Ni nanorods has been reported, with growth along the <111> direction. Nanoparticles can also be prepared by the reduction of Ni-containing salts in the presence of capping agents, although so far there are few examples of non-spherical shapes.[175] As an exception, hexagonal and triangular Ni nanoplates (Figure 26f) were recently prepared.[176] In this synthesis, $\text{Fe}(\text{CO})_5$ was added and found to slow down the reduction rate of Ni-formate. Since Ni is an *fcc* metal, it is believed that this slow reduction process is responsible for the plate-like morphology that typifies kinetically controlled syntheses.

5.8. Metals with Low Melting Points

For metals (e.g., Bi, Cd, In, Pb, Sb, and Sn) with melting points below 400 °C, they tend to form nanocrystals with a spherical shape if the syntheses are performed at temperatures close to their melting points.[178,179] When the reaction temperatures are kept significantly below their melting points, the nanocrystals can also take a variety of non-spherical shapes. It is worth pointing out that the strategies or mechanisms discussed in Sections 2-4 for shape control may not be applicable to these metals because, with the exception of Pb, none of them crystallizes in the *fcc* lattice: Bi (rhombohedral), Cd (hexagonal), In (tetragonal), Sb (rhombohedral), and Sn (tetragonal).

Among these metals, Bi and Pb are the most widely studied due to their thermoelectric and superconducting properties, respectively. Similar to the noble metals, a typical synthesis begins with the decomposition or reduction of a precursor compound, forming nuclei, which then grow into nanocrystals. For those nanocrystals prepared by a thermal decomposition method, often the reaction temperature has to be kept above the melting point of the metal. Consequently, the “nanocrystals” remain in a liquid state throughout the entire synthesis and assume a spherical shape so to minimize their surface area and thus the total interfacial free energy. When the reaction is quenched (typically by pouring the hot mixture into a cold bath), the liquid “nanocrystals” solidify into nanospheres with smooth surfaces. Figure 27a shows a typical sample of Bi nanospheres synthesized using this approach.[178d]

In addition to the decomposition of a compound or reduction of a salt precursor, nanocrystals of low-melting metals can be prepared by directly breaking large droplets of the molten metals under a shear force.[178a] In general, when a liquid filament is dispersed in another liquid, it may experience Rayleigh instability and become undulated with a finite wavelength.[180] The fastest-growing wavelength of the undulation is dependent on the diameter of the filament, the viscosities of the two liquids, and their interfacial energies.[181] As the instability proceeds, the amplitude of the wave will increase, and the filament will break into small droplets. By this mechanism, large drops of a molten metal can be elongated and broken into small, uniform droplets. These small liquid droplets can then be transformed into nanocrystals with a spherical shape when the sample is quenched.

Non-spherical nanocrystals of Bi have been prepared by a number of methods including hydrothermal reactions, γ -irradiation, and microwave treatments.[182-185] Among these methods, the hydrothermal route seems to be the most productive as it has generated Bi nanocubes, triangular nanoplates, and nanowires (Figure 27, b-d). From this work, it was found that adjusting the concentration of capping agent during a synthesis can change the shape of the Bi nanocrystals; however, the hydrothermal process itself is inherently complex and a systematic study of the mechanisms behind the various shapes is difficult due to the use of an autoclave.

At temperatures below the melting point, Pb nanowires with rectangular cross sections have been synthesized by decomposing lead acetate in ethylene glycol in the presence of PVP (Figure 28a).[186] Although Pb has an *fcc* crystal structure, the growth of Pb nanowires occurs through a mechanism different from other *fcc* metals, probably owing to its low melting point. The growth mechanism for Pb nanowires is more or less similar to the solution-liquid-solid (SLS) model which was originally developed for generating single-crystal semiconductor nanowires in the solution phase (Figure 28b).[187] As shown in Figure 28c, each Pb nanowire is composed of three segments: root, stem, and tip. In the initial stage of reaction, Pb atoms produced from the decomposition of lead acetate condense into nanoscale droplets, after which some grow and evolve into micrometer-sized crystals. The micrometer-sized crystal can function as the root to initiate the nucleation and growth of a nanowire. Because of its low melting point, atomic addition to the reactive root (usually at

the sharp corners or thin ends) may form a small droplet at the tip. Once the size of the droplet at the tip has reached a critical value, Pb atoms start to crystallize at the interface between the tip and the root to form a stem. As more Pb atoms are driven to the tip, the stem continues to grow into a uniform nanowire until all of the Pb source droplets are depleted. This growth occurs at the expense of nanoscale Pb droplets remaining in the solution phase and can be thought of as an Ostwald ripening process. Both TEM and electron diffraction studies reveal that the root has a plate-like morphology (Figure 28c), and by increasing the concentration of PVP, Pb nanoplates are obtained instead of nanowires (see Figure 28d). [186]

In the case of In, InCp ($\text{Cp} = \text{C}_5\text{H}_5^-$) has been explored as a precursor to synthesize In nanospheres and nanowires in THF through UV exposure in the presence of a long-chain amine.[188] There is no explicit discussion of the mechanism, but it was suggested that both the planar structure of InCp and a templating effect from the long-chain amine were instrumental to nanowire formation. The introduction of $[\text{Sn}(\text{NMe}_2)_2]_2$ to the reaction facilitated the growth of $\beta\text{-In}_3\text{Sn}$ nanowires. Most recently, Schaak and coworkers reported the room temperature synthesis of In nanoparticles with well-defined shapes.[189] By controlling the addition rate of NaBH_4 /tetraethylene glycol to a solution containing isopropyl alcohol, InCl_3 and PVP, the shape of In nanoparticles could be tuned from high aspect ratio nanowires to octahedrons and truncated octahedrons.

In the case of Sb, nanowires and fractal nanostructures have been obtained by reducing Sb^{3+} with Zn powder or NaBH_4 at room temperature.[190] Sb nanowires have also been prepared by aging a mixture of Sb nanoparticles and a precursor compound.[191] As a unique feature of this system, fractal growth was frequently observed due to the involvement of non-equilibrium growth.[191,192]

5.9. Alloys

Transition metals can form various alloys and intermetallic compounds. Often these multi-metal materials have very unique properties that make them attractive for use in magnetic, catalytic, optical, and electronic applications. With so many examples of these materials being prepared as nanocrystals, it is difficult to include all cases in this review article. As a result, we will take FePt alloys as a representative example. FePt alloys have received a great deal of attention in recent years, partly due to their high magnetocrystalline anisotropy. [97,193-195] FePt alloys are known to have either a chemically disordered *fcc*-structure or a chemically ordered face-centered tetragonal (*ftc*) structure, as shown in Figure 29a.[194] The fully ordered *ftc*-FePt can be considered as alternating atomic layers of Fe and Pt stacked along the *c* axis and has a higher magnetocrystalline anisotropy than *fcc*-FePt. Also, it has a high coercivity, a thin domain wall of 2.8-3.3 nm, and a small minimal grain size of 2.9-3.5 nm.[97] FePt alloys also are much less sensitive to oxidation than either pure Fe or other Pt-free magnetic metals. This unique combination of properties makes *ftc*-FePt nanoparticles potentially useful for applications in ultrahigh density magnetic storage as well as a precursor to advanced magnetic materials.

The first synthesis of monodispersed FePt nanoparticles was demonstrated by Sun and coworkers via the simultaneous reduction of $\text{Pt}(\text{acac})_2$ and thermal decomposition of $\text{Fe}(\text{CO})_5$ in a mixture of oleic acid and oleylamine.[97] The composition of the FePt alloyed nanoparticles could be controlled by adjusting the molar ratio of the two precursors. As prepared, these FePt nanocrystals had the chemically disordered *fcc* crystal structure and took a truncated cubic shape (Figure 29b); however, they could be transformed to the chemically ordered *ftc*-structure by annealing at 500 °C. The annealed nanocrystals appeared rounded. Since this work, both $\text{Fe}(\text{acac})_2$ and FeCl_3 have been shown to be suitable Fe

sources for the synthesis of FePt alloy nanoparticles.[193e,193j] In these cases, the FePt alloys were formed via the co-reduction of the Fe and Pt precursor salts.

The formation of *fcc*-FePt nanoparticles does not always require the two-step process: synthesis of *fcc*-FePt and then annealing. A direct synthesis of *fcc*-FePt nanocrystals was realized with a solution-phase method, in which $\text{Fe}(\text{acac})_2$ and $\text{Pt}(\text{acac})_2$ were used as precursors in the presence of tetraethylene glycol.[195a] X-ray diffraction (XRD) analysis showed that the products are partially in the *fcc*-phase. Most recently, a synthesis of partially ordered *fcc*-FePt nanoparticles using a stoichiometric mixture of $\text{Na}_2\text{Fe}(\text{CO})_4$ and $\text{Pt}(\text{acac})_2$ in tetracosane at 389 °C was reported.[195b] In the product, site ordering of the constituent metals reached as high as 73%. As the *fcc*-to-*fcc* phase transition occurs around 400 °C, the improved crystalline order of these samples was attributed to the higher reaction temperature.[193b,193c]

FePt nanoparticles have also been produced by sequentially reducing $\text{Pt}(\text{acac})_2$ then thermally decomposing $\text{Fe}(\text{CO})_5$. [193f] In this case, Pt nanocrystals first were formed in solution, on which a layer of Fe_2O_3 was coated to form $\text{Pt}@\text{Fe}_2\text{O}_3$ core-shell nanocrystals (Figure 29c). These core-shell particles could be transformed into *fcc*-FePt alloy nanocrystals by annealing the sample under an $\text{Ar}(95\%)/\text{H}_2(5\%)$ environment.

6. Stability of the Shape

Extensive studies have shown that the shape of a metal nanocrystal can undergo dynamic (and sometimes reversible) changes in response to variations in temperature and the surrounding environment. Such behavior has been extensively studied by the catalysis community and can be attributed to the interfacial free energy density being strongly dependent on both temperature and the adsorption of molecules on the surface of a nanocrystal.[196] As a result, any variation in these two parameters may induce the formation of new facets and/or changes to the relative areas of existing facets. As discussed in Section 4.1, surface capping can have a profound effect on the final shape assumed by a growing nanocrystal; however, until recently few studies looked at the stability of the novel nanocrystal shapes after formation. As capping agents are likely to remain on the surface of a nanocrystal and stabilize its shape, their removal (or reduction in coverage) could lead to changes in the shape of a nanocrystal. Such changes could alter the properties of a given nanocrystal, while also potentially providing an easy way to access new nanocrystal shapes if controlled appropriately.

In fact, recent work indicates that metal nanocrystals can undergo such shape evolution in solution. For example, when Ag nanocubes with sharp corners are heated in ethylene glycol containing a small amount of PVP, the characteristically sharp corners become truncated, generating nanocrystals with a rounded profile (Figure 30a).[197] In this case, the PVP adsorbed on the surfaces of a Ag nanocube is gradually released into the solution until equilibrium is established. As a result, the {100} facets with higher energies become exposed to the solvent and the more stable {111} planes develop at the expense of the {100} facets so to minimize the total interfacial free energy. Through a similar mechanism, Ag nanobars with sharp corners and edges can be transformed into nanorice with a rounded profile.[64d] In a third demonstration, Ag nanoplates with triangular or hexagonal cross sections evolved into circular disks (Figure 30b) when aged in deionized water at room temperature for one month.[58b] As indicated by high-resolution TEM study, the nanoplates kept their {111} planes as their top and bottom faces while their cross sections became rounded to get rid of the sharp corners.

In addition to Ag, similar shape changes have been observed in the Pd system. For example, Pd nanocubes capped with Br^- were transformed into cuboctahedrons with a rounded profile

when aged in the reaction solution for two weeks at room temperature (Figure 30c).[64d] In this case, the Br^- was desorbed from the nanocube to expose the otherwise protected surface, thus altering the interfacial free energy density. As a result, the sharp corners become truncated to form $\{111\}$ facets with a lower energy. The same occurrence has been observed with anisotropic Pd nanocrystals. For example, Pd nanorods, whose anisotropic growth is thought to be induced by localized oxidative etching of a specific facet on a cuboctahedral seed, experience a gradual increase in diameter and decrease in length, causing the shape to move toward that of cuboctahedron (Figure 30d).[64d] These results demonstrate that anisotropic nanocrystals slowly transform into their thermodynamically favorable shape even if they can be rapidly formed under specific reaction conditions. Such effects have also been observed in Au nanorod systems, with recent work by Stucky and coworkers showing that single-crystal Au nanorods can be shortened with the addition of HCl to such aging processes.[198]

The shape transformation of a metal nanocrystal can be considered as a special example of Ostwald ripening, which is guided by both thermodynamics and kinetics. In terms of driving force, shape transformation occurs because of a need to minimize the total interfacial free energy at a fixed volume. The kinetics is most likely determined by the surface diffusion of atoms, which can be expedited by heating, stirring, and oxidative etching. The observations from these types of studies then can be immediately applied to the synthesis of metal nanocrystals with controlled shapes. For instance, starting with pre-synthesized Wulff polyhedrons of Ag or Pd, the capping effect of various compounds, polymers, and ions can be quickly screened for inducing the formation of a specific set of facets. One only needs to mix the polyhedrons with a specific compound, polymer, or ionic species in ethylene glycol and then reflux the suspension until a new equilibrium shape is reached! Such a study is also technologically important because it will allow for the identification of conditions under which the nanocrystal shape (and thus the catalytic activity and selectivity, for example) can be preserved.

7. Properties and Applications Enabled by Shape-Controlled Synthesis

The synthesis of metal nanocrystals with well-controlled shapes and sizes has been motivated by both the potential enhancements new materials may bring to industrial applications and the prospect for new technology development. It is well-known that changing the shape of a metal nanocrystal can profoundly alter its properties and thus its performance in a given application. In the following sections, we look at the optical, catalytic, electronic, and magnetic properties of metal nanocrystals, with an emphasis on how these properties can be predictably tuned by shape-controlled syntheses to enhance performance or bring about new opportunities in applications as diverse as chemical sensing and data storage. It is our hope that this discussion will motivate further explorations into the shape-dependant properties of metal nanocrystals as well as lead to the identification of new metal nanocrystals worth targeting synthetically.

7.1. Optical Properties and Applications

Under the irradiation of light, the free electrons in a metal are driven by the alternating electric field to collectively oscillate in phase with the incident light. Known as surface plasmon resonance (SPR),[199] this collective oscillation enables effective scattering and absorption of light under a resonant condition and gives metal (especially, Ag and Au) colloids their brilliant colors. Associated with electron oscillation, polarization of surface charges also occurs on the metal surface when excited by light. Unlike bulk metals, the induced charges of a nanoparticle cannot propagate as a wave along the flat surface but are confined to and concentrated on the particle surface, in which case it is called localized surface plasmon resonance (LSPR).[199] LSPR creates intense local electric fields within a

few nanometers of the particle surface. As a direct application of LSPR, this near-field effect enhances the Raman scattering cross sections of molecules adsorbed on a nanoparticle surface, providing a “fingerprint” spectrum rich with chemical information. Since its first demonstration by Fleischman and Van Dyne in the 70's, this technique has been widely known as SERS.[200]

It has been known for nearly 100 years that the shape of a nanocrystal affects its interaction with light. To demonstrate how shape can affect the absorption and scattering of light, a series of simulated spectra were obtained using Mie's theory for a Ag nanosphere or by the discrete dipole approximation (DDA) method for other Ag nanocrystals.[16d] The simplest shape is also the most symmetric: the sphere. Figure 31a shows the extinction, absorption, and scattering spectra for a 40-nm Ag sphere dispersed in water. Two resonance peaks were found in the spectra: a strong dipole resonance at 410 nm and a weak quadrupole resonance as a shoulder at 370 nm. At this size, the resonance is mostly due to light absorption. As a result, the nanosphere primarily absorbs blue light, giving Ag colloids a yellow appearance. In the spectra, the dipole resonance arises from the polarization of electron density across the sphere, giving the sphere itself a dipole moment that reverses sign at the same frequency as the incident light.[16] The weak quadrupole resonance, which is characterized by two parallel dipoles of opposite sign, arises from the non-uniformity of the incident light across the sphere as a result of energy losses.

In principle, the charge separation that results from the polarization of electron density relative to the lattice of positive ions provides the main restoring force for electron oscillation and largely determines the frequency and intensity of the resonance peak for a given metal. Thus, variations in nanocrystal size, shape, and dielectric environment can affect the surface polarization and alter the spectral profile of the resonance. For simple geometrical shapes, both corner sharpness and shape symmetry can alter the surface polarization and thus the LSPR peak. Considering corner sharpness, recent calculations of the near-fields around nanoparticles show that surface charges are accumulated at sharp corners.[201] As a result of this enhanced charge separation, the restoring force for electron oscillation will be reduced, which can manifest as a red-shift in the spectra when all other things are comparable.[202] For example, Figure 31b shows the spectra calculated for a 40-nm cube. Compared to the 40-nm sphere, the most intense peak is red-shifted by ~100 nm. Red-shifts also are observed for the tetrahedron (Figure 31c) and octahedron (Figure 31d), with the tetrahedron having the most red-shifted resonance peak because it has the sharpest corners. Yet, varying the degree of corner sharpness cannot explain all of the spectral features illustrated in these examples.

As it turns out, shape symmetry can alter the plasmon resonance too, with the number of peaks observed correlating with the number of ways in which the electron density can be polarized (i.e., lower symmetry means more peaks).[203] Additionally, shape symmetry affects the intensity of the resonance peak. When the surface charges on a nanoparticle are separated by mirror symmetry (without the mirror plane bisecting through a vertex), the effective dipole moment will be very large, and the greater the effective dipole moment is the greater the intensity of the dipole resonance. For example, when considering a Ag nanocube in which charge accumulation occurs at the corners of the cube, a strong dipole will result as indicated by its O_h symmetry in which the corners are always directly opposite one another. In contrast, even though charge accumulation occurs at the corners of a tetrahedron, a strong dipole will not result as indicated by its T_d symmetry in which the corners are opposite a face.

The LSPR spectra of nanocrystals with 2-D anisotropy (e.g., triangular nanoplates) are also interesting to consider because large charge separation can occur when polarization occurs

along their edges. Considering Ag nanoplates, their LSPR peaks tend to be further into the red than other Ag nanocrystals because of their sharp corners (Figure 31e). Interestingly, if the corners of the nanoplates are snipped, the main dipole peak will blue-shift.[204] In fact, as Figure 31f shows, getting rid of the sharp corners and forming a circular disc results in a blue-shift of ~100 nm. Yet, the circular symmetry of the disc provides this structure with an effective dipole moment greater than that of a triangular plate. As a result, the intensity of its LSPR peak is much greater.

It is worth pointing out that many of these simulated spectra have been validated by synthesizing the corresponding shapes and measuring their absorbance spectra. For example, the plasmon resonance of 1-D nanostructures has been experimentally investigated by a number of research groups.[128,205] In contrast to spheres, 1-D nanostructures display two dipole resonances: one transverse resonance (polarized along the short axis) and one longitudinal resonance. When the diameter is held constant, increasing the length will red-shift the position of the longitudinal resonance while the transverse resonance will remain unaltered. Figure 32 shows LSPR spectra recorded from Ag nanobars with different aspect ratios,[63c] which are consistent with theoretical prediction. Interestingly, when the Ag nanobars are transformed into nanorice through corner and edge truncation (see Section 6), both the transverse and longitudinal resonances blue-shift relative to those of the nanobars. This observation reiterates the role corner sharpness plays in determining the peak position. From these examples, the design rules for identifying metal nanocrystals with specific LSPR properties can be summarized as: *i*) the number of resonant peaks is determined by the number of ways in which the electron density of a nanoparticle can be polarized, *ii*) the position of LSPR peaks can be tuned by altering corner sharpness and/or shape anisotropy, and *iii*) the intensity of LSPR peaks is affected by shape symmetry.

The ability to tailor the plasmonic features of Ag and Au nanocrystals is enabling the research community to enhance the sensitivity of SERS, a useful technique for molecular sensing. Although each organic molecule has a distinct Raman spectrum, signal enhancement is needed for detection of low-concentration analytes. The intense local electric fields generated by LSPR can enhance the Raman signal of molecules adsorbed onto the metal nanocrystal by many orders in magnitude. As the intensity and position of LSPR peaks can be fine-tuned via shape control, significant Raman signal enhancement can be achieved by simply selecting nanocrystals with an appropriate shape. To illustrate this point, Ag nanocubes with sharp and rounded corners were used as SERS substrates with 1,4-benzenedithiol (1,4-BDT) as the probe molecule and a 785 nm laser for SERS measurement.[206] Compared to nanocubes with sharp corners, the LSPR peak for the nanocubes with rounded corners was slightly blue-shifted. The Raman signals from 1,4-BDT was enhanced by ~49,000 times when Ag nanocubes with sharp corners were used as the substrate and by ~27,000 times when Ag nanocubes with rounded corners were used. While a greater SERS enhancement from those particles with LSPR closer to the excitation wavelength would be expected, such a significant difference in the enhancement factors is more likely explained by the difference in shape. Mainly, the sharp corners on the nanocubes likely provide greater localized electric field enhancement than the rounded ones.

When a nanoparticle is deposited from a solution onto a solid support, it will lose its rotational freedom in three-dimensional space. If the nanoparticle is not a perfect sphere, the direction of laser polarization will become a critical factor in determining the efficiency of charge separation and thus the enhancement factor. We recently discovered this angular dependence while measuring the SERS spectra of supported Ag nanocubes.[207] Figure 33 (left panel, a-c) shows an SEM image of a Ag nanocube with sharp corners and the corresponding SERS spectra from 1,4-BDT adsorbed on the cube at different azimuthal angles relative to the polarization of the excitation laser. When the cube was orientated with

a diagonal axis (corner to corner) parallel to the laser polarization (a and c), the Raman peak from 1,4-BDT at 1565 cm^{-1} was much stronger than when the cube was oriented with one of the faces parallel to the polarization of the laser (b). We also conducted the same experiment on a highly truncated cube (Figure 33, right panel, d-f). It is clear that the SERS spectra for the truncated cube (d-f) was essentially unaffected by the direction of laser polarization while the sharp cube (a-c) showed dramatic variations as their orientations were changed. Because the nanocubes adopt random orientations when deposited on a substrate and the polarization of the laser is fixed, significant variations in the SERS intensity can be observed. These results clearly demonstrate that extra cautions must be taken in order to achieve reproducible and meaningful SERS measurements when nanoparticles are immobilized on substrates. In general, optical studies have to be correlated with high-resolution imaging in order to draw any conclusion about the enhancement factor.

The optimization of LSPR features through shape control is leading to good SERS substrate design for coinage metals (Ag, Au, and Cu) and may also result in a diversification of SERS substrate materials. For instance, the ubiquitous application of Pd in heterogeneous catalysis makes the extension of SERS to Pd attractive; however, the SERS enhancement factors of Pd substrates have been low due to the absorption/scattering of light by Pd only in the UV region. Recently, we successfully prepared Pd nanocrystals with their LSPR bands in the visible region by controlling their shapes; this achievement now enables their use as SERS substrates.[208] As these examples illustrate, it is critical to control the morphology of metal nanocrystals if Raman enhancement is to be maximized for sensing applications.

7.2. Catalytic Properties and Applications

Catalysis has long relied on noble metals to facilitate a wide variety of chemical transformations.[7] On the most basic level, nanocrystals of noble metals are attractive for use as catalysts because of their high surface-to-volume ratios which can minimize the costs associated with their usage. Such nanocrystals have been employed to catalyze oxidation, cross-coupling, electron-transfer, and hydrogenation reactions, among others, with industrial-scale catalytic applications for specific metals stated in Section 5. Yet, as the demands for noble metals are increasing with the advent of emerging technologies like fuel cells, the need for catalysts that are both more active and selective is increasing.[209] Nanocatalysts with well-controlled shapes could help meet this growing demand.

Both the reactivity and selectivity of a catalyst can be tailored by controlling the shape of a nanocrystal. As a first approximation, shape determines which crystal facets comprise the surface of a nanocrystal. For example, consider a tetrahedron and a cube made of an *fcc* metal: all the exposed facets of a tetrahedron are {111} and all the exposed facets of a cube are {100}. Assuming no surface reconstructions, the {111} faces are represented by a hexagonal array of metal atoms while the {100} faces are represented by a square array of metal atoms. Such a difference can give rise to different catalytic activity and selectivity. For example, from studies with single crystals, the Pt(111) surface was found to be 3 to 7 times more active than the Pt(100) surface for aromatization reactions.[210] Also, shape determines the number of atoms located at the edges or corners, which can have a profound effect on catalytic performance.[211]

Recently, El-Sayed and coworkers studied the effect shape had on the catalytic performance of Pt nanocrystals.[18a] In one study, they considered samples of Pt tetrahedrons, cubes, and nearly spherical cuboctahedrons for the electron-transfer reaction between $[\text{Fe}(\text{CN})_6]^{3-}$ and $\text{S}_2\text{O}_3^{2-}$ ions to form $[\text{Fe}(\text{CN})_6]^{4-}$ and $\text{S}_4\text{O}_6^{2-}$. From electron microscopy analysis, they estimated that for tetrahedrons, cuboctahedrons, and cubes of 5 nm in size ~35%, ~13%, and 6% of the surface atoms, respectively, were located at either corners or edges. When used as catalysts, they found that the average rate constant increased exponentially as the

percentage of surface atoms at corners and edges increased. In a second study, they looked at the Suzuki cross-coupling reaction between phenylboronic acid and iodobenzene to form biphenyl.[18a] While similar shape effects were expected, they found little difference in performance. Analysis of the catalysts after use revealed that the well-defined nanocrystal shapes were lost during catalysis, reiterating the need to understand effects on shape-stability as discussed in Section 6.

Using a similar approach, Somorjai and coworkers recently looked at the shape effects of cubic and cuboctahedral Pt nanocrystals by considering the hydrogenation of benzene.[143e] Regardless of shape, a 3-fold increase in turnover rate was measured as compared to bulk single crystals; however, differences in selectivity were observed. Specifically, when cuboctahedrons bound by both {111} and {100} facets were used as catalysts, both cyclohexane and cyclohexene were produced. Yet, when cubic nanocrystals, bound by only {100} facets, were used as catalysts, only cyclohexane was produced. These results are consistent with the product selectivity obtained from bulk Pt(111) and Pt(100) single crystals and illustrate how nanocrystals with well-defined shapes can be used to improve the selectivity of a catalyst. Additionally, Somorjai and coworkers found that for cubic nanocrystals the apparent activation energy for cyclohexane production was 10.9 ± 0.4 kcal/mol while for cuboctahedral nanoparticles the apparent activation energies for cyclohexane and cyclohexene production were 8.3 ± 0.2 and 12.2 ± 0.4 kcal/mol, respectively. These activation energies are significantly lower than those obtained with Pt single crystals, and these differences were attributed to either the increase of corner and edge sites available for reaction or a change in the electronic structure of the Pt nanocrystals as compared to larger single crystals.

In related work, Sun and coworkers recently considered Pt nanocubes, truncated cubes, and polyhedrons as catalysts for the oxygen reduction reaction in a H_2SO_4 -containing medium.[212] They found that the measured current density was 4 times greater when Pt nanocubes were used as compared to the systems where either polyhedral or truncated cubic Pt nanocrystals were used. This difference in activity was attributed to the different adsorption rates of sulfates on Pt(100) and Pt(111) facets[213] and illustrates the enhancement nanocrystals of different shapes may bring to fuel cell applications.

Given the importance of edge and corner sites to catalysis, there has been a growing interest in preparing metal nanocrystals with high-index planes that have a greater percentage of unsaturated atomic steps, edges, and kinks which can serve as intrinsically more active sites for catalysis. Fundamental studies on the single-crystal surfaces of bulk Pt have shown that high-index planes exhibit much higher catalytic activity than that of common and stable, low-index planes such as {111} and {100}.[209] As discussed in Section 5.4, Pt THHs with high-index {730}, {210}, and/or {520} surfaces have recently been prepared, providing a unique opportunity to study their catalytic performance.[145] In an initial study, it was found that the Pt THHs were ~200 times more efficient per unit surface area for the electro-oxidation of ethanol and ~400 times more efficient for formic acid electro-oxidation as compared to a commercial 3.2 nm Pt/C catalyst.

From the results discussed in this section, it becomes clear that maximization of surface, edge, and corner sites should be the criteria for designing superior nanocatalysts. In the selection of nanocatalysts, the stability of nanoparticles and the capping agents on their surfaces are also worth noting. In many cases, the surface atoms of nanocatalysts are so active that their size and shape change during the catalytic reaction.[18b] Such changes can dramatically alter their performance and lifetime. Additionally, capping agents might deactivate catalytic sites, with recent work demonstrating that Pt nanoparticles prepared with TTAB exhibit much higher activity than PVP-capped Pt nanocrystals.[143e] These issues

regarding catalyst stability and poisoning will need to be addressed for shape-controlled nanocrystals to be fully implemented as industrial catalysts.

7.3. Electronic Properties and Applications

As integrated circuits become smaller, the incentive to incorporate metal nanocrystals as interconnects and transport materials increases. In Section 5, a number of metal nanocrystals were discussed that could be attractive for use in electronic applications. For example, Ag has the highest electrical and thermal conductivity of any metal, making 1-D Ag nanocrystals such as Ag nanowires or nanobeams (see Section 5.2) promising nanoscale conduits for electricity or heat. In a recent study, we looked at the electrical properties of Ag nanobeams.[69] In particular, the resistivity and current-carrying ability were measured for a collection of nanobeams with different lengths and widths. It was found that for a nanobeam with a diameter of 20 nm the resistivity was only twice that of bulk silver (with the resistivity decreasing with increasing diameter, as expected). This result illustrates that Ag nanobeams, despite their diminished sizes, largely preserve the unparalleled electrical conductivity of bulk Ag. Additionally, it was found that the maximum current that the nanobeams could support increased with increasing beam cross section, with a maximum current density of $\sim 1.8 \times 10^8 \text{ A cm}^{-2}$ being obtained. This value is comparable to the highest current densities reported for multi-wall carbon nanotubes ($\sim 10^9 \text{ A cm}^{-2}$).[214] While these results exemplify the potential for nanoscale building blocks of Ag in electronic applications, they do not reveal any shape-dependant properties. As resistivity depends on the nature of electron scatter from the metal surface, it is possible that shape could influence the conduction properties of a metal nanocrystal. Unfortunately, studies of this nature have not been conducted. At least, shape-controlled synthesis allows for the generation of 1-D nanocrystals, to which electrodes can be easily applied for transport measurements.

7.4. Magnetic Properties and Applications

With their diminished sizes and single domain magnetism, ferromagnetic nanoparticles (e.g., Co, Ni, Fe) have garnered a significant amount of attention recently for their potential use as high-density storage media for magnetic memory devices.[10] Yet, attempts to use such materials are complicated by the so-called “superparamagnetic limit” in which the miniaturization of magnetic particles is coupled with a reduction in the magnetic energy barrier for flipping spin orientation.[215] It thus becomes desirable to overcome this limit as well as to understand the factors that govern magnetic phenomena on the nanoscale so that such nanomaterials may be integrated appropriately. For magnetic recording media, it is advantageous to have high magnetizations and coercive fields while maintaining small particle size.

As with the other properties of metals, changing the size and shape of a ferromagnetic metal nanocrystal can have a profound impact on its fundamental magnetic properties, with superparamagnetism representing one of the fascinating new properties discovered by preparing these metals as nanocrystals of suitably small size.[216] In a superparamagnetic crystal, the thermal energy (kT) is sufficient to switch the magnetic spin direction (i.e., from a spin-up to a spin-down state), resulting in a net magnetization of zero. The transition temperature from ferromagnetism to superparamagnetism (i.e., the blocking temperature, T_b) is dependant on the size of the nanocrystal according to:[217]

$$T_b = K_u V / 25k \quad (4)$$

where K_u is the magnetic anisotropic constant and V is the volume of the nanocrystal. Thus, it is expected that as the size of a nanocrystal decreases, the ferromagnetic to

superparamagnetic transition will occur at increasingly lower temperatures. Using a superconducting quantum interference device (SQUID), Cheon and coworkers validated this relationship by analyzing the size-dependent magnetic properties of monodisperse Co nanocrystals similar to those discussed in Section 5.7.[218] As expected, the T_b was found to gradually increase with increasing nanocrystal size, with $T_b > RT$ for particles with diameters >10.3 nm only. Additionally, magnetic coercivity (H_c) is affected by nanocrystal size. Outside of the superparamagnetic regime where H_c is zero, sufficiently small nanocrystals still possess a single magnetic domain in which all magnetic spins can align unidirectionally. Within this regime, the magnetic coercivity increases with increasing nanocrystal size according to the relationship:[217]

$$H_c = 2K_u/m_s [1 - 5(kt/K_u V)^{1/2}] \quad (5)$$

where m_s is the saturation magnetization value. It is important to note that above a critical nanocrystal size this trend breaks down due to the formation of multiple magnetic domains. Cheon and coworkers also validated this relationship using monodisperse Co nanoparticles, and as expected, H_c was found to increase with increasing size within the single magnetic domain regime.[219]

These trends illustrate the potential limitations of ferromagnetic nanoparticles for magnetic storage media; however, it has been found that within the single magnetic domain regime, both T_b and H_c are dependent on the shape of a magnetic nanocrystal, providing a potentially powerful way to tune the properties of a magnetic nanoparticle. Specifically, K_u is no longer constant and varies with anisotropies in shape. This relationship can be expressed as:[217]

$$K_u = [H_a + (N_1 - N_2)M_s] M_s / 2 \quad (6)$$

where H_a is the anisotropy field, N_1 and N_2 are the shape-dependent demagnetization factors parallel and perpendicular to the easy axis of the magnetic nanocrystal, and M_s is the saturation magnetization of bulk materials. Shape effects have been studied most extensively in Co nanorods and nanowires prepared either by electrodeposition or template methods. [220] For example, Co nanorods of three lengths (14, 3.8, and 0.75 μm) were prepared while keeping the diameter constant.[220a] Hysteresis curve measurements at 300 K with the sample held perpendicular to the applied field (the easy axis of magnetization is along the axis of these nanorods) showed that the saturation magnetization increased, with greatly enhanced coercivities, as the nanorod length increased. This trend was attributed to an increase in K_u . Interestingly, recent studies have shown that the easy axis of magnetization for Co nanorods can be reoriented perpendicular to the long axis of the rod and that this reorientation can lead to dramatic changes in the overall magnetic anisotropy.[220c]

Presumably, analogous materials prepared by wet-chemical methods would display similar effects, pending any anomalous surface capping effects from surfactants;[174a] however, such extensive work has not been done. As one promising example, Cheon and coworkers evaluated the magnetic properties of Co nanorods (4×20 nm) and compared them to Co nanospheres (diameter 4 nm).[219] They found that the T_b of the Co nanorods exceeded 360 K (compared to 20 K for the nanospheres). For the low temperature (5 K) hysteresis curve measurements, the nanorods showed a larger H_c than the nanospheres: 460 versus 370 Oe (Oersted; unit of magnetic field strength). At room temperature, the nanorods maintained an H_c of ~ 35 Oe. In related work, it was recently shown that triangular and hexagonal Ni plates

such as those discussed in Section 5.7 display significantly higher coercivity as compared to other Ni nanostructures, and this enhancement was attributed to the increase in anisotropic energy due to their unique 2-D structure.[221] It is anticipated that suitable magnetic nanocrystals with narrow size distribution (<5%) will be self-assembled into ordered arrays with controlled magnetic alignment so to achieve high-density information storage.

7.5. Nanocrystals as Building Blocks for Self-Assembly

Self-assembly provides an effective route to well-defined structures that are close to or at a thermodynamic equilibrium state.[222] The essence of self-assembly is that pre-designed building blocks spontaneously organize themselves into a relatively stable structure through non-covalent interactions. The final structure is determined by the characteristics of the building blocks, as the information that defines a self-assembly process (and thus the final structure) is often encoded into the building blocks in the form of shape and/or surface functionality. Nanocrystals are ideal building blocks for self-assembly, which can be potentially employed to fabricate functional devices and complex systems. Significantly, the shape of nanocrystals can provide a useful knob for controlling the self-assembled structures.[178d,222-225] For instance, nanorods tend to form liquid crystalline phases, while nanospheres and nanocubes tend to form long-range ordered lattices. As limited by space, here we only illustrate two examples from our group.

As discussed in Section 5.8, metals (e.g., Bi and Pb) with low melting points can be easily processed as monodispersed colloidal spheres with diameters in the range of 100-600 nm and size variations well below 5%. These metal nanospheres could be further coated with uniform, conformal shells made of a dielectric material such as silica. Because of their spherical shape and uniform size, the as-synthesized spheres self-assembled into 3-D metallodielectric photonic crystals.[178d] As shown by computational studies, crystalline lattices consisting of metal spheres or dielectric-coated metal spheres may exhibit complete photonic band gaps extending over the entire optical regime. Figure 34 shows the reflectance spectra taken from two typical crystals obtained from Pb and Pb@SiO₂ colloidal spheres, and their corresponding top-view SEM images are shown as the insets. Both crystals have an *fcc* structure with their (111) planes oriented parallel to the surfaces of the supporting substrates. A strong reflection band at 775 nm was observed for the crystals based on Pb colloidal spheres, while the Pb@SiO₂ crystals displayed additional peaks at 415 and 530 nm in the visible region. These results suggest that large photonic band gaps could be obtained from this system to cover optical wavelengths from the visible up to the near infrared region.

In a recent study, we demonstrated the self-assembly of Ag nanocubes into specific structures by modifying their side faces with hydrophobic and hydrophilic self-assembled monolayers (SAMs).[226] In terms of monodispersity and availability, Ag nanocubes are unrivaled as a new class of building blocks for self-assembly. The nanocube itself has a non-spherical shape, and significantly, one can control the structures of resultant assemblies by functionalizing the six faces of a nanocube with hydrophobic and hydrophilic SAMs in different schemes. When one side of each cube is functionalized with a hydrophobic, octadecanethiol (ODT) SAM and all others are functionalized with a hydrophilic, mercaptohexadecanoic acid (MHA) SAM, the nanocubes tended to form dimers, as shown in Figure 35a. When two opposing faces of each cube were functionalized with the ODT and the remaining four faces with the MHA, linear chains of three or more cubes could be readily found during SEM characterization (Figure 35b). When the Ag nanocubes were functionalized in an inverse manner, such that four of their sides were modified with ODT and the other two were modified with an MHA, they tended to form 2-D sheets as shown in Figure 35c. These sheets were typically square or rectangular with lengths of 500 nm and had a structure similar to computer simulations of nanocubes with strong face-to-face

interactions. When the entire surface of each Ag nanocube was covered by ODT, the building blocks were hydrophobic and aggregated shortly after being dispersed into water. The formed structures are shown in Figure 35d: a 3-D lattice of the Ag nanocubes. Over time the size of these structures appeared to grow but ultimately plateaued at 1.2 μm in length (ten to twelve nanocubes along the edge). The cubic nature of the final structures suggests that the assembly occurred equally in all three dimensions

8. Summary and Outlook

The last decade has witnessed significant progress in the shape-controlled synthesis of metal nanocrystals. Thanks to the efforts of many research groups, a rich variety of nanocrystal shapes have been achieved for a large number of different metals (Table 1). Controlling the shape of a nanocrystal may initially seem like a scientific curiosity, but its goal goes far beyond aesthetic appeal. As showcased in Section 7, the shape of a metal nanocrystal determines not only its intrinsic physical and chemical properties but also its relevance for optical, catalytic, electronic, and magnetic applications. In discussing the various systems, we strived to elaborate on the plausible nucleation and growth mechanisms involved; however, a quantitative description of crystal nucleation and growth is still challenging. For example, there is little knowledge of the actual nature of the nuclei involved in the formation of nanocrystals. Such information would be invaluable in correlating experimental results with synthetic conditions. Additionally, there is no conclusive account of the roles played by solvent molecules, capping agents, and the trace impurities present in all commercial chemical reagents. Yet, as illustrated in Section 5, all of these species influence the outcome of a synthesis. Because of these unanswered questions, *what is presented in this review article should be considered as a collection of protocols, working hypotheses, and guiding principles for generating metal nanocrystals of different shapes*. We hope that these protocols and rules can serve as a valuable resource, allowing for the production of metal nanocrystals with specific properties sought for applications in the areas of electronics, photonics, catalysis, information storage, sensing, imaging, and biomedical research. It cannot be over emphasized though that most of the conclusions drawn about metal nanocrystal syntheses are to be challenged and refined as our understanding of the nucleation and growth mechanisms is advanced.

Why is it so difficult to decipher the secrets that lead to the formation of nanocrystals with a specific shape? There is no simple answer to this question. Based on our experience, however, we believe it can be addressed from the following aspects:

- i. We should never overlook the seemingly simple reaction involved in a chemical synthesis. For example, it has been assumed that in a typical polyol synthesis, acetaldehyde, derived from the dehydration of ethylene glycol, was the reductant. Our most recent results, however, indicate that at least for Ag and in the temperature range of 140 to 160 $^{\circ}\text{C}$, the primary reductant is glycolaldehyde, being produced via thermal oxidation of ethylene glycol by the oxygen in air.[227] With this new reaction pathway identified, it now becomes possible to explain many experimental observations that were poorly understood previously. Notable examples include the influence of reaction temperature, ionic impurities, and reaction environment. In another example, Brus and coworkers recently found that citrate, a stabilizer commonly used in the synthesis of Ag nanoplates, was directly consumed as the reaction proceeded.[228] They proposed a new mechanism that involves the coupling between oxidative etching of the seed and subsequent photoreduction of aqueous Ag^+ ions. The reduced Ag deposits onto a Ag nanoplate of specific size that has a cathodic photovoltage resulting from plasmon “hot hole” citrate photo-oxidation. In the future, one should consider all possible reaction

pathways for the reduction or decomposition of a precursor. Then, through the identification of reaction intermediates or byproducts, it should be possible to identify with certainty which reagents or experimental parameters play pivotal roles in controlling the reduction kinetics, and thus the nucleation and growth pathway.

- ii. We should never underestimate the roles of trace amounts of impurities that might be present in commercial chemical reagents. For production and storage reasons, essentially all chemical reagents are contaminated with certain amounts of known or unknown impurities. As we have shown for the polyol synthesis of Ag nanocrystals, even the presence of a ppm level of Fe^{2+} , Fe^{3+} or Cl^- impurity can drastically alter the morphology of the final product. This high level of sensitivity might help explain many of the mysteries as well as the irreproducible results associated with shape-controlled syntheses of metal nanocrystals. In many cases, the unexpected effects of an impurity can be greatly amplified due to the autocatalytic nature of nanocrystal growth. Also, it should be noted that the effects of an impurity in one system could differ greatly when transferred to another system (e.g., iron salts in the Ag and Pt systems).
- iii. We need to pay closer attention to the chemical composition of a reaction system. This need is particularly important for metals like Ag and Au because most of their salt precursors (e.g., AgNO_3 and AuCl) are sensitive to light. As we have shown for AgNO_3 , a freshly prepared aqueous solution of this salt can contain a significant amount of trimeric clusters. Due to the autocatalytic nature of metal nanocrystal growth, the presence of such clusters can drastically change the reduction kinetics and reaction pathway, and thus the shape of the final product.
- iv. We need to pay closer attention to the gaseous species from air (including O_2 , N_2 , CO , and water vapor) and as reaction by-products. These species may influence both the reduction kinetics of a precursor and the growth rates of different crystallographic planes. For example, both O_2 and CO (a common product of Pt-catalyzed decomposition of an organic species) have been shown to play important roles in influencing the morphology of Pt nanocrystals due to chemisorption. Unfortunately, their presence and potential roles have been largely ignored in previous studies.
- v. We need to pay closer attention to H^+ and OH^- , two species commonly associated with a redox reaction whenever water is involved. These two species might have strong affinity towards specific crystal facets – for example, H^+ for the $\{100\}$ facets of Ag, Au, Pd, and Pt – which could contribute to shape control.

It should be pointed out that most of the available strategies for shape-controlled synthesis are built upon manipulation of the growth processes rather than nucleation. This observation is likely because very little is known about the nucleation process. To address this long-standing, fundamental problem in chemistry and physics, tools capable of capturing, identifying, and quantifying the nuclei are badly needed. Parallel to this advancement, computational methods need to proceed so that an atomistic-level understanding of the elementary steps involved in a nucleation process can be achieved. Molecular dynamic (MD) simulations are well-suited for this purpose. With little or no *a priori* knowledge about the specific agglomeration reactions, *ab initio* MD simulations provide a useful tool for reaction sampling or identification of the key reaction conditions that control nucleus formation, a starting point for calculating the energy barriers and reaction rates of different pathways. An integration of experimental studies and theoretical modeling will greatly advance our understanding of nucleation and should offer new methods for controlling the assembly of atoms into clusters and then nanocrystals with specific shapes. From such work, the design rules for producing metal nanocrystals (as well as for other types of solid

materials) with exact shapes will be developed. Only at that point, we will have a scientific basis for manufacturing nanocrystals with specific electronic, photonic, magnetic, and catalytic properties sought for a broad range of applications.

Acknowledgments

This work was supported in part by research grants from NSF (DMR-0804088 and DMR-0451788), ACS (PRF-44353-AC10), and ONR (N-00014-01-1-0976); a CAREER Award from NSF (DMR-9983893); a DARPA-DURINT subcontract from Harvard University; an AFOSR-DURINT subcontract from SUNY Buffalo; a MRSEC subcontract from the NSF-funded GEMSEC program at the UW; and a 2006 Director's Pioneer Award from NIH (1DPOD000798). Y.X. was a Camille Dreyfus Teacher Scholar, an Alfred P. Sloan Research Fellow, and a David and Lucile Packard Fellow in Science and Engineering. B.L. was also partially supported by the Postdoctoral Fellowship Program of the Korea Research Foundation (KRF).

References

1. Fahlman, BD. *Materials Chemistry*. Vol. 1. Springer; Mount Pleasant, MI: 2007. p. 282-283.
2. See, for example, a) Halperin WP. *Rev Mod Phys*. 1986; 58:533. b) Kreibitz, U.; Vollmer, M. *Optical Properties of Metal Clusters*. Springer; New York: 1995. c) <http://esi-topics.com/nanocrystals/>
3. Reviews: a) Bawendi MG, Steigerwald ML, Brus LE. *Annu Rev Phys Chem*. 1990; 41:477. b) Weller H. *Adv Mater*. 1993; 5:88. c) Alivisatos AP. *Science*. 1996; 271:933. d) Murray CB, Kagan CR, Bawendi MG. *Annu Rev Mater Sci*. 2000; 30:545.
4. See, for example, a) Likharev KK. *IBM J Res Develop*. 1988; 32:144. b) Maheshwari V, Kane J, Saraf R. *Adv Mater*. 2008; 20:284.
5. See, for example, a) Mott NF. *Rev Mod Phys*. 1968; 40:677. b) Markovich G, Collier CP, Henrichs SE, Remacle F, Levine RD, Heath JR. *Acc Chem Res*. 1999; 32:415.
6. Reviews: a) Hyeon T. *Chem Commun*. 2003; 8:927. b) Sun S. *Adv Mater*. 2006; 18:393. c) Jeong U, Teng X, Wang Y, Yang H, Xia Y. *Adv Mater*. 2007; 19:33.
7. a) Lewis LN. *Chem Rev*. 1993; 93:2693. b) Somorjai GA. *Chem Rev*. 1996; 96:1223. [PubMed: 11848787] c) Ertl, G. *Handbook of Heterogeneous Catalysis*. Wiley-VCH; Weinheim: 2008.
8. See, for example, a) Davey NM, Seymour RJ. *Platinum Met Rev*. 1985; 29:2. b) Jeong S, Woo K, Kim D, Lim S, Kim JS, Shin H, Xia Y, Moon J. *Adv Func Mater*. 2008; 18:679.
9. See, for example, a) Hamilton JF. *Adv Phys*. 1988; 37:359. b) Tani T. *Phys Today*. 1989 September.:36.
10. Reviews: a) A special issue on magnetic recording materials. *MRS Bull*. 1990; 15:12. b) Murray CB, Sun S, Doyle H, Betley T. *MRS Bull*. 2001; 26:985.
11. See, for example, a) Templeton AC, Wuelfing WP, Murray RW. *Acc Chem Res*. 2000; 33:27. [PubMed: 10639073] b) Nicewarner-Peña SR, Freeman RG, Reiss BD, He L, Peña DJ, Walton ID, Cromer R, Keating CD, Natan MJ. *Science*. 2001; 294:137. [PubMed: 11588257]
12. See, for example, a) Maier SA, Brongersma ML, Kik PG, Meltzer S, Requicha AAG, Atwater HA. *Adv Mater*. 2001; 13:1501. b) Sanders AW, Routenberg DA, Wiley BJ, Xia Y, Dufresne ER, Reed MA. *Nano Lett*. 2006; 6:1822. [PubMed: 16895380]
13. a) Taton TA, Mirkin CA, Letsinger RL. *Science*. 2000; 289:1757. [PubMed: 10976070] b) Tkachenko AG, Xie H, Coleman D, Glomm W, Ryan J, Anderson MF, Franzen S, Feldheim DL. *J Am Chem Soc*. 2003; 125:4700. [PubMed: 12696875] c) Zhang X, Young MA, Lyandres O, Van Duyne RP. *J Am Chem Soc*. 2005; 127:4484. [PubMed: 15783231] d) Cheng MMC, Cuda G, Bunimovich YL, Gaspari M, Heath JR, Hill HD, Mirkin CA, Nijdam AJ, Terracciano R, Thundat T, Ferrari M. *Curr Opin Chem Bio*. 2006; 10:11. [PubMed: 16418011] e) Wang H, Brandl DW, Nordlander P, Halas NJ. *Acc Chem Res*. 2007; 40:53. [PubMed: 17226945]
14. See, for example, a) Chen J, Saeki F, Wiley BJ, Cang H, Cobb MJ, Li ZY, Au L, Zhang H, Kimmey MB, Li X, Xia Y. *Nano Lett*. 2005; 5:473. [PubMed: 15755097] b) Cang H, Sun T, Li ZY, Chen J, Wiley BJ, Xia Y, Li X. *Opt Lett*. 2005; 30:3048. [PubMed: 16315717] c) Yang X, Skrabalak SE, Li ZY, Xia Y, Wang LV. *Nano Lett*. 2007; 7:3798. [PubMed: 18020475]
15. Reviews: a) West JL, Halas NJ. *Annu Rev Biom Eng*. 2003; 5:285. b) Jain PK, El-Sayed IH, El-Sayed MA. *Nano Today*. 2007; 2:18. c) Skrabalak SE, Chen J, Au L, Lu X, Li X, Xia Y. *Adv*

- Mater. 2007; 19:3177. [PubMed: 18648528] d) Skrabalak SE, Au L, Lu X, Li X, Xia Y. Nanomedicine. 2007; 2:657. [PubMed: 17976028] e) Fortina P, Kricka LJ, Graves DJ, Park J, Hyslop T, Tam F, Halas N, Surrey S, Waldman SA. Trends in Biotech. 2007; 24:145. f) Jain PK, Huang X, El-Sayed IH, El-Sayed MA. Acc Chem Res. 2008 in press. 10.1021/ar7002804 g) Au L, Zheng D, Zhou F, Li ZY, Li X, Xia Y. ACS Nano. 2008 in press. 10.1021/nn800370j
16. a) Jensen TR, Kelly L, Lazarides A, Schatz GC. J Cluster Sci. 1999; 10:295. b) Kottmann JP, Martin OJF, Smith DR, Schultz S. Phys Rev B. 2001; 64:235–402. c) El-Sayed MA. Acc Chem Res. 2001; 34:257. [PubMed: 11308299] d) Sosa IO, Noguez C, Barrera RG. J Phys Chem B. 2003; 107:6269. e) Wiley BJ, Im SH, Li ZY, McLellan JM, Siekkinen A, Xia Y. J Phys Chem B. 2006; 110:15666. [PubMed: 16898709]
17. See, for example, a) Haruta M. Catal Today. 1997; 36:153. b) Valden M, Lai X, Goodman DW. Science. 1998; 281:1647. [PubMed: 9733505] c) Campbell CT, Parker SC, Starr DE. Science. 2002; 298:811. [PubMed: 12399586]
18. a) Narayanan R, El-Sayed MA. J Phys Chem B. 2005; 109:12663. [PubMed: 16852568] b) Zecchina A, Groppo E, Bordiga S. Chem Eur J. 2007; 13:2440.
19. a) Falicov LM, Somorjai GA. Proc Natl Acad Sci. 1985; 82:2207. [PubMed: 16593551] b) Shi AC, Masel RI. J Catal. 1989; 120:421.
20. a) Wulff G. Zeits F Kristallog. 1901; 34:449. b) Marks LD. Rep Prog Phys. 1994; 57:603. c) Pimpinelli, A.; Villain, J. Physics of Crystal Growth. Cambridge University Press; Cambridge, UK: 1998.
21. Venables, JA. Introduction to Surface and Thin Film Processes. Cambridge University Press; Cambridge: 2000. p. 9-11.
22. a) Faraday M. Philos Trans R Soc London. 1857; 147:145. b) Edwards PP, Thomas JM. Angew Chem. 2007; 119:5576. Angew Chem Int Ed. 2007; 46:5480.
23. a) Henglein A. Chem Rev. 1989; 89:1861. b) Fendler JH. Adv Mater. 1995; 7:607. c) Schmid G, Chi LF. Adv Mater. 1998; 10:515. d) Link S, El-Sayed MA. J Phys Chem B. 1999; 103:8410.
24. a) Wiley B, Sun Y, Mayers B, Xia Y. Chem Eur J. 2005; 11:454. b) Wiley B, Sun Y, Chen J, Cang H, Li ZY, Li X, Xia Y. MRS Bull. 2005; 30:356. c) Wiley B, Sun Y, Xia Y. Acc Chem Res. 2007; 40:1067. [PubMed: 17616165] d) Tao AR, Habas S, Yang P. Small. 2008; 4:310.
25. a) Murphy CJ, Jana NR. Adv Mater. 2002; 14:80. b) Murphy CJ, Sau TK, Gole AM, Orendorff CJ, Gao J, Gao L, Hunyadi SE, Li T. J Phys Chem B. 2005; 109:13857. [PubMed: 16852739] c) Murphy CJ, Gole AM, Hunyadi SE, Orendorff CJ. Inorg Chem. 2006; 45:7544. [PubMed: 16961339]
26. Xiong Y, Xia Y. Adv Mater. 2007; 19:3385.
27. Oxtoby DW. Nature. 2000; 406:464. [PubMed: 10952291]
28. Auer S, Frenkel D. Nature. 2001; 409:1020. [PubMed: 11234006]
29. Gasser U, Weeks ER, Schfield A, Pusey PN, Weitz DA. Science. 2001; 292:258. [PubMed: 11303095]
30. a) Hiller AC, Ward MD. Science. 1994; 263:1261. [PubMed: 17817430] b) Zhang Z, Lagally MG. Science. 1997; 276:377. [PubMed: 9103189] c) Bruce H, Giovannini M, Bromann K, Kern K. Nature. 1998; 394:451. d) Yau ST, Vekilov PG. Nature. 2000; 406:494. [PubMed: 10952306]
31. a) Lee SM, Wong WT. J Cluster Sci. 1998; 9:417. b) Richmond MG. Coord Chem Rev. 2003; 241:273.
32. a) Roesky HW, Singh S, Yusuff KKM, Maguire JA, Hosmane NS. Chem Rev. 2006; 106:3813. [PubMed: 16967922] b) Melnik M, Ondrejovicova I, Miklos D, Segla P, Holloway CE. Rev Inorg Chem. 2007; 27:67. c) Sevryugina Y, Rogachev AY, Petrukhnina MA. Inorg Chem. 2007; 46:7870. [PubMed: 17696424] d) Hartig J, Stöber A, Hauser P, Schnöckel H. Angew Chem. 2007; 119:1687. Angew Chem Int Ed. 2007; 46:1658. e) Anson CE, Eichhöfer A, Issac I, Fenske D, Fuhr O, Sevilano P, Persau C, Stalke D, Zhang J. Angew Chem. 2008; 120:1346. Angew Chem Int Ed. 2008; 47:1326.
33. LaMer VK, Dinegar RH. J Am Chem Soc. 1950; 72:4847.
34. Watzky MA, Finke RG. J Am Chem Soc. 1997; 119:10382.
35. a) Ciacchi LC, Mertig M, Pompe W, Meriani S, De Vita A. Platinum Met Rev. 2003; 47:98. b) Colombi Ciacchi L, Pompe W, De Vita A. J Am Chem Soc. 2001; 123:7371. [PubMed: 11472168]

- c) Mertig M, Colombi Ciacchi L, Seidel R, Pompe W, De Vita A. *Nano Lett.* 2002; 2:841. d) Colombi Ciacchi L, Pompe W, De Vita A. *J Phys Chem B.* 2003; 107:1755.
36. a) Huang ZY, Mills G, Hajek B. *J Phys Chem.* 1993; 17:11542. b) Ciacchi LC, Mertig M, Seidel R, Pompe W, De Vita A. *Nanotechnology.* 2003; 14:840. c) Finney EE, Finke RG. *J Coll Interf Sci.* 2008; 317:351.
37. Xiong Y, Washio I, Chen J, Sadilek M, Xia Y. *Angew Chem.* 2007; 119:5005. *Angew Chem Int Ed.* 2007; 46:4917.
38. a) Mitchell JW. *Imaging Sci J.* 1997; 45:2. b) Lam DMK, Rossiter BW. *Sci Am.* 1991; 265:80.
39. a) Flad J, Igelmann G, Preuss H, Stoll H. *Chem Phys.* 1984; 90:257. b) Cheng PY, Duncan MA. *Chem Phys Lett.* 1988; 152:341. c) Balasubramanian K, Feng PY. *Chem Phys Lett.* 1989; 159:452. d) Partridge H, Bauschlicher CW Jr, Langhoff SR. *Chem Phys Lett.* 1990; 175:531.
40. a) Boo DW, Ozaki Y, Andersen LH, Lineberger WC. *J Phys Chem A.* 1997; 101:6688. b) Leisner T, Vajda S, Wolf S, Wöste L. *J Chem Phys.* 1999; 111:1017. c) Hartmann M, Heidenreich A, Pittner J, Bonačić-Koutecký V, Jortner J. *J Phys Chem A.* 1998; 102:4069.
41. Fayet P, Granzer F, Hegenbart G, Meisar E, Pischel B, Wöste L. *Phys Rev Lett.* 1985; 55:3002. [PubMed: 10032297]
42. a) Kéki S, Nagy L, Deák G, Zsuga M, Somogyi L, Lévai A. *Am Soc Mass Spec.* 2004; 15:879. b) McLean JA, Stumpo KA, Russell DH. *J Am Chem Soc.* 2005; 127:5304. [PubMed: 15826152]
43. Li X, Kuznetsov AE, Zhang HF, Boldyrev AI, Wang LS. *Science.* 2001; 291:859. [PubMed: 11157162]
44. a) Li J, Li X, Zhai HJ, Wang LS. *Science.* 2003; 299:864. [PubMed: 12574622] b) Zhang HF, Stender M, Zhang R, Wang CM, Li J, Wang LS. *J Phys Chem B.* 2003; 108:12259.
45. a) Peyser LA, Vinson AE, Bartko AP, Dickson RM. *Science.* 2001; 291:103. [PubMed: 11141556] b) Zheng J, Dickson RM. *J Am Chem Soc.* 2002; 124:13982. [PubMed: 12440882] c) Petty JT, Zheng J, Hud NV, Dickson RM. *J Am Chem Soc.* 2004; 126:5207. [PubMed: 15099104]
46. a) Henglein A. *Chem Phys Lett.* 1989; 154:473. b) Linnert T, Mulvaney P, Henglein A, Weller H. *J Am Chem Soc.* 1990; 112:4657. c) Ershov BG, Janata E, Henglein A. *J Phys Chem.* 1993; 97:339.
47. a) König L, Rabin I, Schultze W, Ertl G. *Science.* 1996; 274:1353. [PubMed: 8910270] b) Félix C, Sieber C, Harbich W, Buttet J, Rabin I, Schultze W, Ertl G. *Phys Rev Lett.* 2001; 86:2992. [PubMed: 11290090] c) Watanabe Y, Namikawa G, Onuki T, Nishio K, Tsuchiya T. *Appl Phys Lett.* 2001; 78:2125. d) Belharouak I, Weill F, Parent C, Le Flem G, Moine B. *J Non-Cryst Solids.* 2001; 293-295:649. e) Podlipensky AV, Grebenev V, Seifert G, Graener H. *J Luminescence.* 2004; 109:135. f) Treguer M, Rocco F, Lelong G, Nestour AL, Cardinal T, Maali A, Lounis B. *Solid State Sci.* 2005; 7:812.
48. Qu L, Yu WW, Peng X. *Nano Lett.* 2004; 4:465.
49. a) Schmid G. *Chem Rev.* 1992; 92:1709. b) van Leeuwen DA, van Ruitenbeek JM, Schmid G, de Jongh LJ. *Phys Lett A.* 1992; 170:325. c) Aiken JD III, Finke RG. *J Mol Catal A.* 1999; 145:1. d) Zhang H, Schmid G, Hartmann U. *Nano Lett.* 2003; 3:305.
50. a) Wang ZL. *J Phys Chem B.* 2000; 104:1153. b) Zhang JM, Ma F, Xu KW. *Appl Surf Sci.* 2004; 229:34.
51. a) Smith DJ, Petford-Long AK, Wallenberg LR, Bovin JO. *Science.* 1986; 233:872. [PubMed: 17752214] b) Iijima S, Ichihashi T. *Phys Rev Lett.* 1986; 56:616. [PubMed: 10033240] c) Doraiswamy N, Marks LD. *Surf Sci.* 1996; 348:67. d) Yacaman MJ, Ascencio JA, Liu HB, Gardea-Torresdey J. *J Vac Sci Technol B.* 2001; 19:1091. e) Liu HB, Ascencio JA, Perez-Alvarez M, Yacaman MJ. *Surf Sci.* 2001; 491:88.
52. a) Gai PL, Harmer MA. *Nano Lett.* 2002; 2:771. b) Lofton C, Sigmund W. *Adv Func Mater.* 2005; 15:1197. c) Elechiguerra JL, Reyes-Gasga J, Yacaman MJ. *J Mater Chem.* 2006; 16:3906.
53. a) Hofmeister H, Nepijko SA, Levlev DN, Schulze W, Ertl G. *J Cryst Growth.* 2002; 234:773. b) Nepijko SA, Levlev DN, Schulze W, Urban J, Ertl G. *ChemPhysChem.* 2000; 1:140.
54. a) Baletto F, Ferrando R. *Phys Rev B.* 2001; 63:155408. b) Baletto F, Ferrando R, Fortunelli A, Montalenti F, Mottet C. *J Chem Phys.* 2002; 116:3856. c) Baletto F, Ferrando R. *Rev Mod Phys.* 2005; 77:371.
55. Ajayan PM, Marks LD. *Phys Rev Lett.* 1998; 60:585. [PubMed: 10038590]

56. Cleveland C, Landman U. *J Chem Phys.* 1991; 94:7376.
57. a) Kirkland AI, Jefferson DA, Duff DG, Edwards PP, Gameson I, Johnson BFG, Smith DJ. *Proc R Soc Lond A.* 1993; 440:589. b) Germain V, Li J, Ingert D, Wang ZL, Pileni MP. *J Phys Chem B.* 2003; 107:8717.
58. a) Ho PF, Chi KM. *Nanotechnology.* 2004; 15:1059. b) Xiong Y, Siekkinen AR, Wang J, Yin Y, Kim MJ, Xia Y. *J Mater Chem.* 2007; 17:2600.
59. a) Washio I, Xiong Y, Yin Y, Xia Y. *Adv Mater.* 2006; 18:1745. b) Xiong Y, Washio I, Chen J, Cai H, Li ZY, Xia Y. *Langmuir.* 2006; 22:8563. [PubMed: 16981776] c) Lim B, Camargo PHC, Xia Y. *Langmuir.* 2008 in press.
60. Xiong Y, McLellan JM, Chen J, Yin Y, Li ZY, Xia Y. *J Am Chem Soc.* 2005; 127:17118. [PubMed: 16316260]
61. a) Sun Y, Xia Y. *Adv Mater.* 2003; 15:695. b) Sun Y, Mayers B, Xia Y. *Nano Lett.* 2003; 3:675.
62. Wiley B, Herricks T, Sun Y, Xia Y. *Nano Lett.* 2004; 4:1733.
63. a) Wiley BJ, Xiong Y, Li ZY, Yin Y, Xia Y. *Nano Lett.* 2006; 6:765. [PubMed: 16608280] b) Wiley BJ, Chen Y, McLellan J, Xiong Y, Li ZY, Ginger D, Xia Y. *Nano Lett.* 2007; 7:1032. [PubMed: 17343425]
64. a) Xiong Y, Chen J, Wiley B, Xia Y, Aloni S, Yin Y. *J Am Chem Soc.* 2005; 127:7332. [PubMed: 15898780] b) Xiong Y, Wiley B, Chen J, Li ZY, Yin Y, Xia Y. *Angew Chem.* 2005; 117:8127. *Angew Chem Int Ed.* 2005; 44:7913. c) Zetsu N, McLellan JM, Wiley B, Yin Y, Li ZY, Xia Y. *Angew Chem.* 2006; 118:1310. *Angew Chem Int Ed.* 2006; 45:1288. d) Xiong Y, Cai H, Wiley BJ, Wang J, Kim MJ, Xia Y. *J Am Chem Soc.* 2007; 129:3665. [PubMed: 17335211]
65. Wiley B, Sun Y, Xia Y. *Langmuir.* 2005; 21:8077. [PubMed: 16114903]
66. Xiong Y, McLellan JM, Yin Y, Xia Y. *Angew Chem.* 2007; 119:804. *Angew Chem Int Ed.* 2007; 46:790.
67. a) Tao A, Sinsersuksakul P, Yang P. *Angew Chem.* 2006; 118:4713. *Angew Chem Int Ed.* 2006; 45:4597. b) Korte KE, Skrabalak SE, Xia Y. *J Mater Chem.* 2008; 18:437.
68. Xiong Y, Cai H, Yin Y, Xia Y. *Chem Phys Lett.* 2007; 440:273.
69. Wiley BJ, Wang Z, Wei J, Yin Y, Cobden DH, Xia Y. *Nano Lett.* 2006; 6:2273. [PubMed: 17034096]
70. Sun Y, Mayers B, Herricks T, Xia Y. *Nano Lett.* 2003; 3:955.
71. a) Campbell CT. *Surf Sci.* 1997; 27:1. b) Ozin GA. *Catal Rev - Sci Eng.* 1977; 16:191. c) Roberts MW. *Surf Sci.* 1994; 299:769. d) Chen Q, Richardson NV. *Prog Surf Sci.* 2003; 73:59.
72. Harris PJF. *Nature.* 1986; 323:792.
73. a) Spendelow JS, Wieckowski A. *Phys Chem Chem Phys.* 2004; 6:5094. b) Bernhardt TM. *Int J Mass Spectr.* 2005; 243:1. c) Baranova EA, Bock C, Ilin D, Wang D, MacDougall B. *Surf Sci.* 2006; 600:3502. d) Joshi AM, Tucker MH, Delgass WN, Thomson KT. *J Chem Phys.* 2006; 125:194707. [PubMed: 17129150]
74. a) Potapenko SY. *J Cryst Growth.* 1993; 133:147. b) van Enckevort WJP, van den Berg ACJF. *J Cryst Growth.* 1998; 183:441. c) Land TA, Martin TL, Potapenko S, Palmore GT, De Yoreo JJ. *Nature.* 1999; 399:442.
75. Narayanan R, El-Sayed MA. *Nano Lett.* 2004; 4:1343.
76. a) Habermehl-Cwirzen K, Lahtinen J. *Surf Sci.* 2004; 573:183. b) Meyer R, Lemire C, Shaikhutdinov SK, Freund H. *Gold Bull.* 2004; 37:72. c) McAllister B, Hu P. *J Chem Phys.* 2005; 122:084709.
77. a) Campbell CT. *Surf Sci.* 1983; 157:43. b) Sexton BA, Madix RJ. *Chem Phys Lett.* 1980; 76:294. c) Guo X, Hoffman A, Yates JT Jr. *J Chem Phys.* 1989; 90:5787. d) Buatier de Mongeot F, Cupilillo A, Valbusa V, Rocca M. *Chem Phys Lett.* 1997; 270:345. e) Gijzeman OJL, Voogt EH, Mens AJM, Geus JW. *Surf Sci.* 1997; 373:210.
78. a) Sun Y, Xia Y. *Science.* 2002; 298:2176. [PubMed: 12481134] b) Xiong Y, Chen J, Wiley B, Xia Y, Yin Y, Li ZY. *Nano Lett.* 2005; 5:1237. [PubMed: 16178217]
79. a) Jana NR, Gearheart L, Murphy CJ. *J Phys Chem B.* 2001; 105:4065. b) Jana NR, Geraheart L, Obare SO, Murphy CJ. *Langmuir.* 2002; 18:922. c) Johnson CJ, Dujardin E, Davis SA, Murphy CJ, Mann S. *J Mater Chem.* 2002; 12:1765. d) Gole A, Murphy CJ. *Chem Mater.* 2004; 16:3633.

- e) Wei Z, Mieszawska AJ, Zamborini FP. *Langmuir*. 2004; 20:4322. [PubMed: 15969133] f) Wei Z, Zamborini FP. *Langmuir*. 2004; 20:11301. [PubMed: 15595748] g) Ha TH, Koo HJ, Chung BH. *J Phys Chem C*. 2007; 111:1123.
80. Lim B, Xiong Y, Xia Y. *Angew Chem*. 2007; 119:9439. *Angew Chem Int Ed*. 2007; 46:9279.
81. a) Schimpf JA, Abreu JB, Soriaga MP. *J Electroanal Chem*. 1994; 364:247. b) Carrasquillo A Jr, Jeng JJ, Barriga RJ, Temesghen WF, Soriaga MP. *Inorg Chim Acta*. 1997; 255:249. c) Lucas CA, Marković NM, Ross PN. *Phys Rev B*. 1997; 55:7964. d) Zou S, Gao X, Weaver MJ. *Surf Sci*. 2000; 452:44.
82. a) Huang HH, Ni XP, Loy GL, Chew CH, Tan KL, Loh FC, Deng JF, Xu GQ. *Langmuir*. 1996; 12:909. b) Zhang Z, Zhao B, Hu L. *J Solid State Chem*. 1996; 121:105. c) Bonet F, Tekaiia-Elhsissen K, Sarathy KV. *Bull Mater Sci*. 2000; 23:165. d) Gao Y, Jiang P, Liu DF, Yuan HJ, Yan XQ, Zhou ZP, Wang JX, Song L, Liu LF, Zhou WY, Wang G, Wang CY, Xie SS, Zhang JM, Shen DY. *J Phys Chem B*. 2004; 108:12877.
83. Rupprechter G. *Adv Catal*. 2007; 51:133.
84. Kilin DS, Prezhdo OV, Xia Y. *Chem Phys Lett*. 2008; 458:113.
85. a) Mammen M, Choi SK, Whitesides GM. *Angew Chem*. 1998; 110:2908. *Angew Chem Intl Ed*. 1998; 37:2754. b) Kane RS. *AIChE J*. 2006; 52:3638. c) Borodko Y, Humphrey SM, Tilley TD, Frei H, Somorjai GA. *J Phys Chem C*. 2007; 111:6288.
86. Gao J, Bender CM, Murphy CJ. *Langmuir*. 2003; 19:9065.
87. Bögels G, Meekes H, Bennema P, Bollen D. *J Phys Chem B*. 1999; 103:7577.
88. a) Dahmen U, Hetherington C, Radmilovic V, Johnson E, Xiao S, Luo C. *Microsc Microanal*. 2002; 8:247. [PubMed: 12533222] b) Frøseth AG, Derlet PM, Van Swygenhoven H. *Adv Eng Mater*. 2005; 7:16.
89. a) Ming, Nb; Sunagawa, I. *J Cryst Growth*. 1988; 87:13. b) Bogels G, Meekes H, Bennema P, Bollen D. *Imaging Sci J*. 2001; 49:33. c) Lee JW, Chung UJ, Hwang NM, Kim DY. *Acta Crystallogr Sect A*. 2005; 61:405. [PubMed: 15972993]
90. a) Holden, A.; Singer, P. *Crystals and Crystal Growing*. Doubleday & Company; Garden City, NY: 1960. b) Mullin, JW. *Crystallization*. Butterworths; London: 1961. c) Hulliger J. *Angew Chem*. 1994; 106:151. *Angew Chem Intl Ed*. 1994; 33:143.
91. Kim F, Connor S, Song H, Kuykendall T, Yang P. *Angew Chem*. 2004; 116:3759. *Angew Chem Int Ed*. 2004; 43:3673.
92. Jana NR, Gearheart L, Murphy CJ. *Adv Mater*. 2001; 13:1389.
93. a) Chambers SA. *Adv Phys*. 1991; 40:357. b) Ledentsov NN, Ustinov VM, Shchulan VA, Kop'ev PS, Alferov ZhI, Bimbers D. *Semiconductors*. 1998; 32:343.
94. a) Habas SE, Lee H, Radmilovic V, Somorjai GA, Yang P. *Nat Mater*. 2007; 6:692. [PubMed: 17618289] b) Fan FR, Liu DY, Wu YF, Duan S, Xie ZX, Jiang ZY, Tian ZQ. *J Am Chem Soc*. 2008; 130:6949. [PubMed: 18465860] c) Lim B, Wang J, Camargo PHC, Jiang M, Kim MJ, Xia Y. *Nano Lett*. 2008 in press. 10.1021/nl8016434
95. Ahmadi TS, Wang ZL, Green TC, Henglein A, El-Sayed MA. *Science*. 1996; 272:1924. [PubMed: 8662492]
96. Yu YY, Chang SS, Lee CL, Wang CRC. *J Phys Chem B*. 1997; 101:6661.
97. Sun S, Murray CB, Weller D, Folks L, Moser A. *Science*. 2000; 287:1989. [PubMed: 10720318]
98. Jin R, Cao Y, Mirkin CA, Kelly KL, Schatz GC, Zheng JG. *Science*. 2001; 294:1901. [PubMed: 11729310]
99. See, for example, a) Reetz MT, Westermann E. *Angew Chem*. 2000; 112:170. *Angew Chem Int Ed*. 2000; 39:165. b) Franzén R. *Can J Chem*. 2000; 78:957. c) Li Y, Hong XM, Collard DM, El-Sayed MA. *Org Lett*. 2000; 2:2385. [PubMed: 10930290] d) Kim SW, Kim M, Lee WY, Hyeon T. *J Am Chem Soc*. 2002; 124:7642. [PubMed: 12083902] e) Son SU, Jang Y, Park J, Na HB, Park HM, Yun HJ, Lee J, Hyeon T. *J Am Chem Soc*. 2004; 126:5026. [PubMed: 15099059] f) Yin L, Liebscher J. *Chem Rev*. 2007; 107:133. [PubMed: 17212474]
100. Rupprechter G, Weilach C. *Nano Today*. 2007; 2:27.
101. Sun Y, Mayers B, Xia Y. *Adv Mater*. 2003; 15:641.
102. Veisz B, Király Z. *Langmuir*. 2003; 19:4817.

103. a) Sun Y, Zhang L, Zhou H, Zhu Y, Sutter E, Ji Y, Rafailovich MH, Sokolov JC. *Chem Mater.* 2007; 19:2065. b) Zhang Y, Grass ME, Kuhn JN, Tao F, Habas SE, Huang W, Yang P, Somorjai GA. *J Am Chem Soc.* 2008; 130:5868. [PubMed: 18399628]
104. a) Turkevich J, Kim G. *Science.* 1970; 169:874. b) Bradley JS, Tesche B, Busser W, Maase M, Reetz MT. *J Am Chem Soc.* 2000; 122:4631. c) Choo HP, Liew KY, Mahmood WAK, Liu H. *J Mater Chem.* 2001; 11:2906. d) Schlotterbeck U, Aymonier C, Thomann R, Hofmeister H, Tromp M, Richtering W, Mecking S. *Adv Funct Mater.* 2004; 14:999.
105. a) Gugliotti LA, Feldheim DL, Eaton BE. *Science.* 2004; 304:850. [PubMed: 15087507] b) Gugliotti LA, Feldheim DL, Eaton BE. *J Am Chem Soc.* 2005; 127:17814. [PubMed: 16351112] c) Liu D, Gugliotti LA, Wu T, Dolska M, Tkachenko AG, Shipton MK, Eaton BE, Feldheim DL. *Langmuir.* 2006; 22:5862. [PubMed: 16768520]
106. Nagy A, Mestl G. *Appl Catal A Gen.* 1999; 188:337.
107. a) Im SH, Lee YT, Wiley B, Xia Y. *Angew Chem.* 2005; 117:2192. *Angew Chem Int Ed.* 2005; 44:2154. b) Lee YT, Im SH, Wiley B, Xia Y. *Chem Phys Lett.* 2005; 411:479.
108. a) Siekkinen AR, McLellan JM, Chen J, Xia Y. *Chem Phys Lett.* 2006; 432:491. [PubMed: 18496589] b) Skrabalak SE, Au L, Li X, Xia Y. *Nature Protocols.* 2007; 2:2182.
109. a) Kryukov AI, Zin'chuk NN, Korzhak AV, Kuchmii SY. *Theor Exp Chem.* 2001; 37:355. b) Kryukov AI, Stroyuk AL, Zin'chuk NN, Korzhak AV, Kuchmii SY. *J Mol Catal A: Chem.* 2004; 221:209.
110. a) Yu D, Yam VWW. *J Am Chem Soc.* 2004; 126:13200. [PubMed: 15479055] b) Yu D, Yam VWW. *J Phys Chem B.* 2005; 109:5497. [PubMed: 16851589]
111. a) Jana NR, Gearheart L, Murphy CJ. *Chem Commun.* 2001:617. b) Sun Y, Gates B, Mayers B, Xia Y. *Nano Lett.* 2002; 2:165. c) Sun Y, Xia Y. *Adv Mater.* 2002; 14:833. d) Sun Y, Yin Y, Mayers BT, Herricks T, Xia Y. *Chem Mater.* 2002; 14:4736.
112. a) Lee GJ, Shin SI, Kim YC, Oh SG. *Mater Chem Phys.* 2004; 84:197. b) Aslan K, Leonenko Z, Lakowicz JR, Geddes CD. *J Phys Chem B.* 2005; 109:3157. [PubMed: 16851335] c) Ni C, Hassan PA, Kaler EW. *Langmuir.* 2005; 21:3334. [PubMed: 15807571] d) Gao Y, Jiang P, Song L, Liu L, Yan X, Zhou Z, Liu D, Wang J, Yuan H, Zhang Z, Zhao X, Dou X, Zhou W, Wang G, Xie S. *J Phys D: Appl Phys.* 2005; 38:1061. e) Yang Y, Xiong L, Shi J, Nogami M. *Nanotechnology.* 2006; 17:2670. f) Lee KH, Huang KM, Tseng WL, Chiu TC, Lin YW, Chang HT. *Langmuir.* 2007; 23:1435. [PubMed: 17241070] g) Tsuji M, Matsumoto K, Miyamae N, Tsuji T, Zhang X. *Cryst Growth Des.* 2007; 7:311. h) Tsuji M, Nishizawa Y, Matsumoto K, Miyamae N, Tsuji T, Zhang X. *Coll Surf A.* 2007; 293:185.
113. a) Xiong Y, Xie Y, Du G, Liu X, Tian X. *Chem Lett.* 2002:98. b) Gao Y, Jiang P, Liu DF, Yuan HJ, Yan XQ, Zhou ZP, Wang JX, Song L, Liu LF, Zhou WY, Wang G, Wang CY, Xie SS. *Chem Phys Lett.* 2003; 380:146. c) Xiong Y, Xie Y, Wu C, Yang J, Li Z, Xu F. *Adv Mater.* 2003; 15:405. d) Gao Y, Song L, Jiang P, Liu LF, Yan XQ, Zhou ZP, Liu DF, Wang JX, Yuan HJ, Zhang ZX, Zhao XW, Dou XY, Zhou WY, Wang G, Xie SS, Chen HY, Li JQ. *J Cryst Growth.* 2005; 276:606.
114. a) Liu FK, Chang YC, Huang PW, Ko FH, Chu TC. *Chem Lett.* 2004; 33:1050. b) Hu JQ, Chen Q, Xie ZX, Han GB, Wang RH, Ren B, Zhang Y, Yang ZL, Tian ZQ. *Adv Funct Mater.* 2004; 14:183.
115. a) Jin R, Cao Y, Hao E, Métraux GS, Schatz GC, Mirkin CA. *Nature.* 2003; 425:487. [PubMed: 14523440] b) Deivaraj TC, Lala NL, Lee JY. *J Coll Interf Sci.* 2005; 289:402. c) Yang J, Zhang Q, Lee JY, Too HP. *J Coll Interf Sci.* 2007; 308:157. d) Rocha TCR, Zanchet D. *J Phys Chem C.* 2007; 111:6989. e) Rocha TCR, Winnischofer H, Westphal E, Zanchet D. *J Phys Chem C.* 2007; 111:2885. f) Maillard M, Huang P, Brus L. *Nano Lett.* 2003; 3:1611. g) Xue C, Millstone JE, Li S, Mirkin CA. *Angew Chem.* 2007; 119:8588. *Angew Chem Int Ed.* 2007; 46:8436. h) An J, Tang B, Ning X, Zhou J, Xu S, Zhao B, Xu W, Corredor C, Lombardi JR. *J Phys Chem C.* 2007; 111:18055.
116. a) Chen S, Carroll DL. *Nano Lett.* 2002; 2:1003. b) Chen S, Fan Z, Carroll DL. *J Phys Chem B.* 2002; 106:10777. c) Pastoriza-Santos I, Liz-Marzán LM. *Nano Lett.* 2002; 2:903. d) Maillard M, Giorgio S, Pileni MP. *Adv Mater.* 2002; 14:1084.
117. a) Métraux GS, Mirkin CA. *Adv Mater.* 2005; 17:412. f) Lu L, Kobayashi A, Tawa K, Ozaki Y. *Chem Mater.* 2006; 18:4894. b) Yang J, Lu L, Wang H, Shi W, Zhang H. *Cryst Growth Des.*

- 2006; 6:2155. c) Xie J, Lee JY, Wang DIC, Ting YP. *ACS Nano*. 2007; 1:429. [PubMed: 19206664]
118. a) Hvolbæk B, Janssens TVW, Clausen BS, Falsig H, Christensen CH, Nørskov JK. *Nano Today*. 2007; 2:14. b) Hashmi ASK. *Chem Rev*. 2007; 107:3180. [PubMed: 17580975]
119. Jin R, Egusa S, Scherer NF. *J Am Chem Soc*. 2004; 126:9900. [PubMed: 15303846]
120. a) Zhang J, Gao Y, Alvarez-Puebla RA, Buriak JM, Fenniri H. *Adv Mater*. 2006; 18:3233. b) Li C, Shuford KL, Park QH, Cai W, Li Y, Lee EJ, Cho SO. *Angew Chem*. 2007; 119:3328. *Angew Chem Int Ed*. 2007; 46:3264. c) Zhang J, Liu H, Wang Z, Ming N. *Appl Phys Lett*. 2007; 90:163122. d) Xu J, Li S, Weng J, Wang X, Zhou Z, Yang K, Liu M, Chen X, Cui Q, Cao M, Zhang Q. *Adv Funct Mater*. 2008; 18:277. e) Seo D, Yoo CI, Chung IS, Park SM, Ryu S, Song H. *J Phys Chem C*. 2008; 112:2469.
121. a) Sau TK, Murphy CJ. *J Am Chem Soc*. 2005; 127:8648. b) Seo D, Park JC, Song H. *J Am Chem Soc*. 2006; 128:14863. [PubMed: 17105296] c) Kundu S, Panigrahi S, Praharaj S, Basu S, Ghosh SK, Pal A, Pal T. *Nanotechnology*. 2007; 18:075712.
122. a) Shankar SS, Rai A, Ankamwar B, Singh A, Ahmad A, Sastry M. *Nat Mater*. 2004; 3:482. [PubMed: 15208703] b) Sun X, Dong S, Wang E. *Angew Chem*. 2004; 116:6520. *Angew Chem Int Ed*. 2004; 43:6360. c) Shao Y, Jin Y, Dong S. *Chem Commun*. 2004; 1104. d) Millstone JE, Park S, Shuford KL, Qin L, Schatz GC, Mirkin CA. *J Am Chem Soc*. 2005; 127:5312. [PubMed: 15826156] e) Huang H, Yang X. *Coll Surf A*. 2005; 255:11. f) Yamamoto M, Kashiwagi Y, Sakata T, Mori H, Nakamoto M. *Chem Mater*. 2005; 17:5391. g) Ah CS, Yun YJ, Park HJ, Kim WJ, Ha DH, Yun WS. *Chem Mater*. 2005; 17:5558. h) Porel S, Singh S, Radhakrishnan TP. *Chem Commun*. 2005:2387. i) Liu B, Xie J, Lee JY, Ting YP, Chen JP. *J Phys Chem B*. 2005; 109:15256. [PubMed: 16852932] j) Kan C, Zhu X, Wang G. *J Phys Chem B*. 2006; 110:4651. [PubMed: 16526697] k) Chu HC, Huo CH, Huang MH. *Inorg Chem*. 2006; 45:808. [PubMed: 16411718] l) Chandran SP, Chaudhary M, Pasricha R, Ahmad A, Sastry M. *Biotechnol Prog*. 2006; 22:577. [PubMed: 16599579] m) Liu Q, Liu H, Zhou Q, Liang Y, Yin G, Xu Z. *J Mater Sci*. 2006; 41:3657. n) Xie J, Lee JY, Wang DIC, Ting YP. *Small*. 2007; 3:672. [PubMed: 17299827] o) Jiang P, Zhou JJ, Li R, Gao Y, Sun TL, Zhao XW, Xiang YJ, Xie SS. *J Nanoparticle Res*. 2006; 8:927. p) Geriche M, Pinches A. *Hydrometallurgy*. 2006; 83:132. q) Li C, Cai W, Li Y, Hu J, Liu P. *J Phys Chem B*. 2006:110–1546. r) Mallikarjuna NN, Varma RS. *Cryst Growth Des*. 2007; 7:686.
123. Besson C, Finney EE, Finke RG. *J Am Chem Soc*. 2005; 127:8179. [PubMed: 15926847]
124. Yang S, Zhang T, Zhang L, Wang Q, Zhang R, Ding B. *Nanotechnology*. 2006; 17:5639.
125. Li C, Cai W, Cao B, Sun F, Li Y, Kan C, Zhang L. *Adv Funct Mater*. 2006; 16:83.
126. Zhao N, Wei Y, Sun N, Chen Q, Bai J, Zhao L, Qin Y, Li M, Qi L. *Langmuir*. 2008; 24:991. [PubMed: 18173292]
127. Zhang J, Du J, Han B, Liu Z, Jiang T, Zhang Z. *Angew Chem*. 2006; 118:1134. *Angew Chem Int Ed*. 2006; 45:1116.
128. a) Nikoobakht B, El-Sayed MA. *Chem Mater*. 2003; 15:1957. b) Sau TK, Murphy CJ. *Langmuir*. 2004; 20:6414. [PubMed: 15248731] c) Pérez-Juste J, Liz-Marzán LM, Carnie S, Chan DYC, Mulvaney P. *Adv Funct Mater*. 2004; 14:6. d) Gou L, Murphy CJ. *Chem Mater*. 2005; 17:3668. e) Chen HM, Peng HC, Liu RS, Asakura K, Lee CL, Lee JF, Hu SF. *J Phys Chem B*. 2005; 109:19533. f) Liu M, Guyot-Sionnest P. *J Phys Chem B*. 2005; 109:22192. [PubMed: 16853888] g) Kou X, Zhang S, Tsung CK, Yeung MH, Shi Q, Stucky GD, Sun L, Wang J, Yan C. *J Phys Chem B*. 2006; 110:16377. [PubMed: 16913766] h) Kou X, Zhang S, Tsung CK, Yang Z, Yeung MH, Stucky GD, Sun L, Wang J, Yan C. *Chem Eur J*. 2007; 13:2929. i) Jiang XC, Pileni MP. *Coll Surf A*. 2007; 295:228. j) Xu ZC, Shen CM, Xiao CW, Yang TZ, Zhang HR, Li JQ, Li HL, Gao HJ. *Nanotechnology*. 2007; 18:115608.
129. a) Wang ZL, Mohamed MB, Link S, El-Sayed MA. *Surf Sci*. 1999; 440:L809. b) Wang ZL, Gao RP, Nikoobakht B, El-Sayed MA. *J Phys Chem B*. 2000; 104:5417.
130. Orendorff CJ, Murphy CJ. *J Phys Chem B*. 2006; 110:3990. [PubMed: 16509687]
131. a) Hao E, Bailey RC, Schatz GC, Hupp JT, Li S. *Nano Lett*. 2004; 4:327. b) Hu J, Zhang Y, Liu B, Liu J, Zhou H, Xu Y, Jiang Y, Yang Z, Tian ZQ. *J Am Chem Soc*. 2004; 126:9470. [PubMed: 15291513] c) Song JH, Kim F, Kim D, Yang P. *Chem Eur J*. 2005; 11:910. d) Xu X, Cortie MB. *Adv Funct Mater*. 2006; 16:2170. e) Kou X, Zhang S, Yang Z, Tsung CK, Stucky GD, Sun L,

- Wang J, Yan C. *J Am Chem Soc.* 2007; 129:6402. [PubMed: 17461586] f) Jena BK, Raj CR. *Langmuir.* 2007; 23:4064. [PubMed: 17315899]
132. Kim F, Song JH, Yang P. *J Am Chem Soc.* 2002; 124:14316. [PubMed: 12452700]
133. a) Sánchez-Iglesias A, Pastoriza-Santos I, Pérez-Juste J, Rodríguez-González B, De Abajo FJG, Liz-Marzán LM. *Adv Mater.* 2006; 18:2529. b) Carbó-Argibay E, Rodríguez-González B, Pacifico J, Pastoriza-Santos I, Pérez-Juste J, Liz-Marzán LM. *Angew Chem.* 2007; 119:9141. *Angew Chem Int Ed.* 2007; 46:8983. c) Seo D, Yoo CI, Park JC, Park SM, Ryu S, Song H. *Angew Chem.* 2008; 120:775. *Angew Chem Int Ed.* 2008; 47:763.
134. a) Lu X, Yavuz MS, Tuan HY, Korgel BA, Xia Y. *J Am Chem Soc.* 2008; 130:8900. [PubMed: 18540574] b) Wang C, Hu Y, Lieber CM, Sun S. *J Am Chem Soc.* 2008; 130:8902. [PubMed: 18540579] c) Huo Z, Tsung Ck, Huang W, Zhang X, Yang P. *Nano Lett.* 2008; 8:2041. [PubMed: 18537294]
135. a) Chen J, Herricks T, Geissler M, Xia Y. *J Am Chem Soc.* 2004; 126:10854. [PubMed: 15339165] b) Chen J, Herricks T, Xia Y. *Angew Chem.* 2005; 117:2645. *Angew Chem Int Ed.* 2005; 44:2.
136. Chen S, Kimura K. *J Phys Chem B.* 2001; 105:5397.
137. a) Ahmadi TS, Wang ZL, Henglein A, El-Sayed MA. *Chem Mater.* 1996; 8:1161. b) Tang Z, Geng D, Lu G. *Mater Lett.* 2005; 59:1567. c) Kinge S, Bönemann H. *Appl Organometal Chem.* 2006; 20:784. d) Yu YT, Xu BQ. *Appl Organometal Chem.* 2006; 20:638. e) Inaba M, Ando M, Hatanaka A, Nomoto A, Matsuzawa K, Tasaka A, Kinumoto T, Iriyama Y, Ogumi Z. *Electrochim Acta.* 2006; 52:1632. f) Ferreira PJ, Shao-Horn Y. *Electrochem Solid-State Lett.* 2007; 10:B60. g) Ren J, Tilley RD. *Small.* 2007; 3:1508. [PubMed: 17647261]
138. a) Song H, Kim F, Connor S, Somorjai GA, Yang P. *J Phys Chem B.* 2005; 109:188. [PubMed: 16851003] b) Rioux RM, Song H, Grass M, Habas S, Niesz K, Hoefelmeyer JD, Yang P, Somorjai GA. *Topics in Catal.* 2006; 39:167.
139. Ren J, Tilley RD. *J Am Chem Soc.* 2007; 129:3287. [PubMed: 17311381]
140. Mahmoud MA, Tabor CE, El-Sayed MA, Ding Y, Wang ZL. *J Am Chem Soc.* 2008; 130:4590. [PubMed: 18345676]
141. a) Lee EP, Chen J, Yin Y, Campbell CT, Xia Y. *Adv Mater.* 2006; 18:3271. b) Lee EP, Peng Z, Cate D, Yang H, Campbell CT, Xia Y. *J Am Chem Soc.* 2007; 129:10634. [PubMed: 17685620] Formo E, Lee EP, Campbell D, Xia Y. *Nano Lett.* 2008; 8:668. [PubMed: 18205427]
142. Krishnaswamy R, Remita H, Impéror-Clerc M, Even C, Davidson P, Pansu B. *ChemPhysChem.* 2006; 7:1510. [PubMed: 16810723]
143. a) Zhao SY, Chen SH, Wang SY, Li DG, Ma HY. *Langmuir.* 2002; 18:3315. b) Song Y, Yang Y, Medforth CJ, Pereira E, Singh AK, Xu H, Jiang Y, Brinker CJ, Swol F, Shelnutt JA. *J Am Chem Soc.* 2004; 126:635. [PubMed: 14719963] c) Niesz K, Grass M, Somorjai GA. *Nano Lett.* 2005; 5:2238. [PubMed: 16277460] d) Lee H, Habas SE, Kweskin S, Butcher D, Somorjai GA, Yang P. *Angew Chem.* 2006; 118:7988. *Angew Chem Int Ed.* 2006; 45:7824.
144. a) Bratlie KM, Lee H, Komvopoulos K, Yang P, Somorjai GA. *Nano Lett.* 2007; 7:3097. [PubMed: 17877408] b) Song Y, Garcia RM, Dorin RM, Wang H, Qiu Y, Coker EN, Steen WA, Miller JE, Shelnutt JA. *Nano Lett.* 2007; 7:3650. [PubMed: 17999549]
145. Tian N, Zou ZY, Sun SG, Ding Y, Wang ZL. *Science.* 2007; 316:732. [PubMed: 17478717]
146. Xiong Y, Wiley BJ, Xia Y. *Angew Chem.* 2007; 119:7291. *Angew Chem Int Ed.* 2007; 46:7157.
147. a) Fu X, Wang Y, Wu N, Gui L, Tang Y. *Langmuir.* 2002; 18:4619. b) Martin JE, Wilcoxon JP, Odinek J, Provencio P. *J Phys Chem B.* 2002; 106:971. c) Herricks T, Chen J, Xia Y. *Nano Lett.* 2004; 4:2367. d) Teng X, Yang H. *Nano Lett.* 2005; 5:885. [PubMed: 15884888] e) Tian N, Zhou ZY, Sun SG, Cui L, Ren B, Tian ZQ. *Chem Commun.* 2006:4090. f) Maksimuk S, Teng X, Yang H. *Phys Chem Chem Phys.* 2006; 8:4660. [PubMed: 17047763]
148. Lou XW, Yuan C, Archer LA. *Chem Mater.* 2006; 18:3921.
149. Maksimuk S, Teng X, Yang H. *J Phys Chem C.* 2007; 111:14312.
150. Curtis AC, Duff DG, Edwards PP, Jefferson DA, Johnson BFG, Kirkland AI, Wallace AS. *J Phys Chem.* 1988; 92:2270.

151. a) Wang Y, Chen P, Liu M. *Nanotechnology*. 2006; 17:6000. b) Kim MH, Lim B, Lee E, Xia Y. *J Mater Chem*. 2008 in press. c) Zhou G, Lu M, Yang Z. *Langmuir*. 2006; 22:5900. [PubMed: 16768527] d) Jana NR, Wang ZL, Sau TK, Pal T. *Curr Sci*. 2000; 79:1367.
152. a) Tanori J, Pileni MP. *Langmuir*. 1997; 13:639. b) Mott D, Galkowski J, Wang L, Luo J, Zhong CJ. *Langmuir*. 2007; 23:5740. [PubMed: 17407333] c) Cha SI, Mo CB, Kim KT, Jeong YJ, Hong SH. *J Mater Res*. 2006; 21:2371.
153. Lisiecki I, Filankembo A, Sack-Kongehl H, Weiss K, Pileni MP, Urban J. *Phys Rev B*. 2000; 61:4968.
154. a) Wang JH, Yang TH, Wu WW, Chen LJ, Chen CH, Chu CJ. *Nanotechnology*. 2006; 17:719. b) Kim C, Gu W, Briceno M, Robertson IM, Choi H, Kim K. *Adv Mater*. 2008; 20:1859. c) Choi H, Park SH. *J Am Chem Soc*. 2004; 126:6248. [PubMed: 15149219]
155. a) Curtis AC, Duff DG, Edwards PP, Jefferson DA, Johnson BFG, Kirkland AI, Wallace AS. *Angew Chem*. 1988; 100:1588. *Angew Chem Int Ed*. 1988; 27:1530. b) Henglein A. *J Phys Chem B*. 2000; 104:1206.
156. a) Liu Z, Yang Y, Liang J, Hu Z, Li S, Peng S, Qian Y. *J Phys Chem B*. 2003; 107:12658. b) Cao X, Yu F, Li L, Yao Z, Xie Y. *J Cryst Growth*. 2003; 254:164. c) Liu CM, Guo L, Xu HB, Wu ZY, Weber J. *Microelect Eng*. 2003; 66:107. d) Li Q, Wang C. *Chem Phys Lett*. 2003; 375:525. e) Yao WT, Yu SH, Zhou Y, Jiang J, Wu QS, Zhang L, Jiang J. *J Phys Chem B*. 2005; 109:14011. [PubMed: 16852759] f) Panigrahi S, Kundu S, Ghosh SK, Nath S, Praharaj S, Basu S, Pal T. *Polyhedron*. 2006; 25:1263.
157. Chang Y, Lye ML, Zeng HC. *Langmuir*. 2005; 21:3746. [PubMed: 15835932]
158. Lu X, Peng Z, Lee E, Yang H, Xia Y. *J Mater Chem*. 2008 submitted.
159. Ressler T, Kniep BL, Kasatkin I, Schögl R. *Angew Chem*. 2005; 117:4782. *Angew Chem Int Ed*. 2005; 44:4704.
160. Vukojević S, Trapp O, Grunwaldt J, Kiener C, Schüth F. *Angew Chem*. 2005; 117:8192. *Angew Chem Int Ed*. 2005; 44:7978.
161. Scherzer, J.; Guia, AJ. *Hydrocracking Science and Technology*. Marcel Dekker; New York: 1996.
162. Robert F, Oehme G, Grassert I, Sinou D. *J Mol Catal A*. 2000; 156:127.
163. a) Wang Y, Ren J, Deng K, Gui L, Tang Y. *Chem Mater*. 2000; 12:1622. b) Papp S, Szél Z, Oszkó A, Dékány I. *Chem Mater*. 2004; 16:1674. c) Ewers TD, Sra AK, Norris BC, Cable RE, Cheng CH, Shantz DF, Schaak RW. *Chem Mater*. 2005; 17:514.
164. a) Hoefelmeyer JD, Niesz K, Somorjai GA, Tilley TD. *Nano Lett*. 2005; 5:435. [PubMed: 15755090] b) Humphrey SM, Grass ME, Habas SE, Niesz K, Somorjai GA, Tilley TD. *Nano Lett*. 2007; 7:785. [PubMed: 17288491] c) Zhang Y, Grass ME, Habas SE, Tao F, Zhang T, Yang P, Somorjai GA. *J Phys Chem C*. 2007; 111:12243. d) Park KH, Jang K, Kim HJ, Son SU. *Angew Chem*. 2007; 119:1170. *Angew Chem Int Ed*. 2007; 46:1152.
165. a) Yee CK, Jordan R, Ulman A, White H, King A, Rafailovich M, Sokolov J. *Langmuir*. 1999; 15:3486. b) Shah PS, Husain S, Johnston KP, Korgel BA. *J Phys Chem B*. 2001; 105:9433. c) Fonseca GS, Umpierre AP, Fichtner PFP, Teixeira SR, Dupont J. *Chem Eur J*. 2003; 9:3263. d) Mévellec V, Roucoux A, Ramirez E, Philippot K, Chaudret B. *Adv Synth Catal*. 2004; 346:72. e) Stowell CA, Korgel BA. *Nano Lett*. 2005; 5:1203.
166. a) Yan X, Liu H, Liew KY. *J Mater Chem*. 2001; 11:3387. b) Viau G, Brayner R, Poul L, Chakroune N, Lacaze E, Fiévet-Vincent F, Fiévet F. *Chem Mater*. 2003; 15:486. c) Tsukatani T, Fujihara H. *Langmuir*. 2005; 21:12093. [PubMed: 16342978] d) Harpeness R, Peng Z, Liu X, Pol VG, Koltypin Y, Gedanken A. *J Coll Interf Sci*. 2005; 287:678.
167. a) O'Handley, RC. *Modern Magnetic Materials: Principles and Applications*. John Wiley & Sons; New York: 1999. b) Spaldin, N. *Magnetic Materials: Fundamentals and Device Applications*. Cambridge University Press; Cambridge: 2003.
168. a) Griffiths CH, Ohoro MP, Smith TW. *J Appl Phys*. 1979; 50:7108. b) Zhao XQ, Zheng F, Liang Y, Hu ZQ, Xu YB. *Mater Lett*. 1994; 21:285. c) Suslick KS, Fang MM, Hyeon T. *J Am Chem Soc*. 1996; 118:11960. d) Park SJ, Kim S, Lee S, Khim ZG, Char K, Hyeon T. *J Am Chem Soc*. 2000; 122:8581. e) Farrell D, Majetich SA, Wilcoxon JP. *J Phys Chem B*. 2003; 107:11022. f) Farrell D, Cheng Y, McCallum RW, Sachan M, Majetich SA. *J Phys Chem B*. 2005; 109:13409. [PubMed: 16852677]

169. a) Dumestre F, Chaudret B, Amiens C, Renaud P, Fejes P. *Science*. 2004; 303:821. [PubMed: 14764874] b) Kim D, Park J, An K, Yang NK, Park JG, Hyeon T. *J Am Chem Soc*. 2007; 129:5812. [PubMed: 17439128]
170. Xiong Y, Xie Y, Li Z, Zhang R, Yang J, Wu C. *New J Chem*. 2003; 27:588.
171. a) Chen JP, Lee KM, Sorensen CM, Klabunde KJ, Hadjipanayis GC. *J Appl Phys*. 1994; 75:5876. b) Sun SH, Murray CB. *J Appl Phys*. 1999; 85:4325. c) Dinega DP, Bawendi MG. *Angew Chem*. 1999; 111:1906. *Angew Chem Int Ed*. 1999; 38:1788. d) Wang ZL, Dai ZR, Sun SH. *Adv Mater*. 2000; 12:1944. e) Puentes VF, Krishnan KM, Alivisatos P. *Appl Phys Lett*. 2001; 78:2187. f) Puentes VF, Krishnan KM, Alivisatos AP. *Science*. 2001; 291:2115. [PubMed: 11251109] g) Murray CB, Sun SH, Gaschler W, Doyle H, Betley TA, Kagan CR. *IBM J Res Dev*. 2001; 45:47. h) Puentes VF, Zanchet D, Erdonmez CK, Alivisatos AP. *J Am Chem Soc*. 2002; 124:12874. [PubMed: 12392435] i) Lisiecki I, Albouy PA, Pileni MP. *Adv Mater*. 2003; 15:712. j) Puentes VF, Gorostiza P, Aruguete DM, Bastus NG, Alivisatos AP. *Nat Mater*. 2004; 3:263. [PubMed: 15048109]
172. Lu Y, Lu X, Mayers BT, Herricks T, Xia Y. *J Solid State Chem*. 2008 in press. 10.1016/j.jssc.2008.02.016
173. a) Dumestre F, Chaudret B, Amiens C, Fromen MC, Casanove MJ, Renaud P, Zurcher P. *Angew Chem*. 2002; 114:4462. *Angew Chem Int Ed*. 2002; 41:4286. b) Dumestre F, Chaudret B, Amiens C, Respaud M, Fejes P, Renaud P, Zurcher P. *Angew Chem*. 2003; 115:5371. *Angew Chem Int Ed*. 2003; 42:5213.
174. a) Cordente N, Respaud M, Senocq F, Casanove MJ, Amiens C, Chaudret B. *Nano Lett*. 2001; 1:565. b) Cheng GJ, Puentes VF, Guo T. *J Colloid Interface Sci*. 2006; 293:430. [PubMed: 16026794] c) Ely TO, Amiens C, Chaudret B. *Chem Mater*. 1999; 11:526.
175. a) Chen DH, Wu SH. *Chem Mater*. 2000; 12:1354. b) Hou Y, Gao S. *J Mater Chem*. 2003; 13:1510. c) Bala T, Bhame SD, Joy PA, Prasad BLV, Sastry M. *J Mater Chem*. 2004; 14:2941.
176. Leng Y, Wang Y, Li X, Liu T, Takahashhi S. *Nanotechnology*. 2006; 17:4834.
177. a) Wang WN, Itoh Y, Lenggara IW, Okuyama K. *Mater Sci Eng B*. 2004; 111:69. b) Liu Z, Li S, Yang Y, Peng S, Hu Z, Qian Y. *Adv Mater*. 2003; 15:11.
178. a) Wang Y, Xia Y. *Nano Lett*. 2004; 4:2047. b) Jeong U, Wang Y, Ibisate M, Xia Y. *Adv Funct Mater*. 2005; 15:1907. c) Wang Y, Cai L, Xia Y. *Adv Mater*. 2005; 17:473. d) Wang Y, Ibisate M, Li ZY, Xia Y. *Adv Mater*. 2006; 18:471.
179. a) Yu H, Gibbons PC, Kelton KF, Buhro WE. *J Am Chem Soc*. 2001; 123:9198. [PubMed: 11552843] b) Goia DV. *J Mater Chem*. 2004; 14:451.
180. a) Rayleigh L. *Proc R Soc London*. 1879; 29:71. b) Tomotika S. *Proc R Soc London*. 1935; A150:322.
181. a) Elemans PHM, Janssen JMH, Meijer HEH. *J Rheol*. 1990; 34:1311. b) Lepers JC, Favis BD, Tabar RJ. *J Polym Sci Part B: Polym Phys*. 1997; 35:2271.
182. a) Foos EE, Stroud RM, Berry AD, Snow AW, Armistead JP. *J Am Chem Soc*. 2000; 122:7114. b) Fang J, Stokes KL, Zhou WL, Wang W, Lin J. *Chem Commun*. 2001:1872.
183. a) Wang J, Cao G, Li Y. *Mater Res Bull*. 2003; 38:1645. b) Gao Y, Niu H, Zeng C, Chen Q. *Chem Phys Lett*. 2003; 367:141. c) Wang J, Wang X, Peng Q, Li Y. *Inorg Chem*. 2004; 43:7552. [PubMed: 15530107] d) Balan L, Schneider R, Billaud D, Fort Y, Ghanbaja J. *Nanotechnology*. 2004; 15:940. e) Wang WZ, Poudel B, Ma Y, Ren ZF. *J Phys Chem B*. 2006; 110:25702. [PubMed: 17181209]
184. Gutiérrez M, Henglein A. *J Phys Chem*. 1996; 100:7656.
185. Zhou B, Ren T, Zhu JJ. *Int J Mod Phys B*. 2005; 19:2829.
186. a) Wang Y, Herricks T, Xia Y. *Nano Lett*. 2003; 3:1163. b) Wang Y, Jiang X, Herricks T, Xia Y. *J Phys Chem B*. 2004; 108:8631. c) Lin XM, Claus H, Welp U, Beloborodow IS, Kwok WK, Crabtree GW, Jaeger HM. *J Phys Chem C*. 2007; 111:3548.
187. a) Trentler TJ, Hickman KM, Geol SC, Viano AM, Gibbons PC, Buhro WE. *Science*. 1995; 270:1791. b) Holmes JD, Johnston KP, Doty RC, Korgel BA. *Science*. 2000; 287:1471. [PubMed: 10688792]
188. a) Soulantica K, Maisonnat A, Senocq F, Fromen MC, Casanove MJ, Chaudret B. *Angew Chem*. 2001; 113:3071. *Angew Chem Int Ed*. 2001; 40:16. b) Zhang Y, Ago H, Liu J, Yumura M,

- Uchida K, Ohshima S, Lijima S, Zhu J, Zhang X. *J Cryst Growth*. 2004; 264:363. c) Hsu YJ, Lu SY, Lin YF. *Small*. 2006; 2:268. [PubMed: 17193034]
189. Chou NH, Ke X, Schiffer P, Schaak RE. *J Am Chem Soc*. 2008; 130:8140. [PubMed: 18540599]
190. Wang YW, Hong BH, Lee JY, Kim JS, Kim GH, Kim KS. *J Phys Chem B*. 2004; 108:16723.
191. a) Stegemann B, Ritter C, Kaiser B, Rademann K. *J Phys Chem B*. 2004; 108:14292. b) Yang B, Wu Y, Hu H, Li C, Yang X, Qian Y. *Mater Chem Phys*. 2005; 92:286.
192. a) Nittmann J, Stanley HE. *Nature*. 1986; 321:663. b) Ben-Jacob E, Garik P. *Nature*. 1990; 343:523.
193. a) Ding Y, Yamamuro S, Farrell D, Majetich SA. *J Appl Phys*. 2003; 93:7411. b) Hai NH, Dempsey NM, Givord D. *J Magn Magn Mater*. 2003; 262:353. c) Liu C, Klemmera T, Shuklaa N, Wu X, Weller D, Tanaseb M, Laughlin D. *J Magn Magn Mater*. 2003; 266:96. d) Anders S, Toney MF, Thomson T, Farrow RFC, Thiele JU, Terris BD, Sun SH, Murray CB. *J Appl Phys*. 2003; 93:6299. e) Sun SH, Anders S, Thomson T, Baglin JEE, Toney MF, Hamann HF, Murray CB, Terris BD. *J Phys Chem B*. 2003; 107:5419. f) Teng XW, Yang H. *J Am Chem Soc*. 2003; 125:14559. [PubMed: 14624605] g) Thomson T, Toney MF, Raoux S, Lee SL, Sun SH, Murray CB, Terris BD. *J Appl Phys*. 2004; 96:1197. h) Zeng H, Sun S, Sandstrom RL, Murray CB. *J Magn Magn Mater*. 2003; 266:227. i) Chen M, Liu JP, Sun S. *J Am Chem Soc*. 2004; 126:8394. [PubMed: 15237993] j) Zeng H, Li J, Wang ZL, Liu JP, Sun S. *Nano Lett*. 2004; 4:187.
194. Gutfleisch O, Lyubina J, Müller KH, Schultz L. *Adv Eng Mater*. 2005; 7:208.
195. a) Jeyadevan B, Urakawa K, Hobo A, Chinnasamy N, Tohij SKK. *Jpn J Appl Phys*. 2003; 42:L350. b) Howard LEM, Nguyen HL, Giblin SR, Tanner BK, Terry I, Hughes AK, Evans JS. *J Am Chem Soc*. 2005; 127:10140. [PubMed: 16028904]
196. a) Rottman C, Wortis M. *Phys Rev B*. 1981; 24:6274. b) Jayaprakash C, Saam WF. *Phys Rev B*. 1984; 30:3916.
197. Chen J, McLellan JM, Siekkinen A, Xiong Y, Li ZY, Xia Y. *J Am Chem Soc*. 2006; 128:14776. [PubMed: 17105266]
198. Tsung CK, Kou X, Shi Q, Zhang J, Yeung MH, Wang J, Stucky GD. *J Am Chem Soc*. 2006; 128:5352. [PubMed: 16620101]
199. Xia Y, Halas NJ. *MRS Bull*. 2005; 30:338.
200. a) Fleischman M, Hendra PJ, McQuillan AD. *Chem Phys Lett*. 1974; 26:163. b) Jeanmaire DL, Van Duyne RP. *J Electroanal Chem*. 1977; 84:1. c) Haynes CL, McFarland AD, Van Duyne RP. *Anal Chem*. 2005:338A.
201. Kottmann JP, Martin OJF, Smith DR, Schultz S. *Phys Rev B*. 2002; 64:235402.
202. Haes AJ, Haynes CL, McFarland AD, Schatz GC, Van Duyne RP, Zou S. *MRS Bull*. 2005; 30:368.
203. Fuchs R. *Phys Rev B*. 1975; 11:1732.
204. Kelly KL, Coronado E, Zhao LL, Schatz GC. *J Phys Chem B*. 2003; 107:668.
205. Hu M, Novo C, Funston A, Wang H, Petrova H, Zou S, Mulvaney P, Xia Y, Hartland GV. *J Mater Chem*. 2008; 18:1949. [PubMed: 18846243]
206. McLellan JM, Siekkinen A, Chen J, Xia Y. *Chem Phys Lett*. 2006; 427:122.
207. McLellan JM, Li ZY, Siekkinen A, Xia Y. *Nano Lett*. 2007; 7:1013. [PubMed: 17375965]
208. McLellan JM, Xiong Y, Hu M, Xia Y. *Chem Phys Lett*. 2006; 417:230.
209. Gates BC, Huber GW, Marshall CL, Ross PN, Siirola J, Wang Y. *MRS Bull*. 2008; 33:429.
210. a) Somorjai GA, Blakely DW. *Nature*. 1975; 258:580. b) Somorjai, GA. *Chemistry in Two Dimensions: Surfaces*. Cornell University Press; Ithaca, NY, USA: 1981.
211. Bond GC. *Platinum Rev*. 1975; 19:126.
212. Wang C, Daimon H, Onodera T, Koda T, Sun S. *Angew Chem*. 2008; 120:3644. *Angew Chem Int Ed*. 2008; 47:3588.
213. Markovic NM, Gasteiger HA, Ross PN. *J Phys Chem*. 1995; 99:3411.
214. a) Bourlon B, Glattli DC, Placais B, Berroir JM, Milko C, Forro L, Bachtold A. *Phys Rev Lett*. 2004; 92:026804. [PubMed: 14753954] b) Wei BQ, Vajtai R, Ajayan PM. *App Phys Lett*. 2001; 79:1172.

215. a) Weller D, Moser A. *IEEE Trans Magn.* 1999; 35:4423. b) Ross CA. *Annu Rev Mater Res.* 2001; 31:203.
216. Jun YW, Seo JW, Cheon J. *Acc Chem Res.* 2008; 41:179. [PubMed: 18281944]
217. Jales, D. *Introduction to Magnetism and Magnetic Materials.* CRC Press; Boca Raton, FL, USA: 1998.
218. Jun Y, Choi J, Cheon J. *Chem Commun.* 2007:1203.
219. Park JI, Kang NJ, Jun Y, Oh SJ, Ri HC, Cheon J. *ChemPhysChem.* 2002; 3:543. [PubMed: 12465496]
220. a) Aslam M, Bhohe R, Alem N, Donthu S, Dravid VP. *J Appl Phys.* 2005; 98:074311. b) Darques M, Piroux L, Encinas A, Bayle-Guillemaud P, Popa A, Ebels U. *Appl Phys Lett.* 2005; 86:072508. c) Darques M, Piroux L, Encinas A. *IEEE Trans Mag.* 2005; 41:3415.
221. Leng Y, Zhang Y, Liu T, Suzuki M, Li Z. *Nanotechnology.* 2006; 17:1797.
222. See, for example, a) Whitesides GM, Grzybowski BA. *Science.* 2002; 295:2418. [PubMed: 11923529] b) Glotzer SC, Solomon MJ. *Nat Mater.* 2007; 6:557. [PubMed: 17667968]
223. See, for example, a) Li LS, Walda J, Manna L, Alivisatos AP. *Nano Lett.* 2002; 2:557. b) Meuer S, Oberle P, Theato P, Tremel W, Zentel R. *Adv Mater.* 2007; 19:2073.
224. a) Kalsin AM, Fialkowski M, Paszewski M, Smoukov SK, Bishop KJM, Grzybowski BA. *Science.* 2006; 312:420. [PubMed: 16497885] b) Chen Z, Moore J, Radtke G, Siringhaus H, O'Brien S. *J Am Chem Soc.* 2007; 129:15702. [PubMed: 18034489]
225. a) Li F, Delo SA, Stein A. *Angew Chem.* 2007; 119:6786. *Angew Chem Int Ed.* 2007; 46:6666. b) Yang S, Gao L. *J Am Chem Soc.* 2006; 128:9330. [PubMed: 16848458]
226. Rycenga M, McLellan JM, Xia Y. *Adv Mater.* 2008; 20:2416.
227. Skrabalak SE, Wiley B, Kim MH, Formo E, Xia Y. *Nano Lett.* 2008; 8:2077. [PubMed: 18507481]
228. Wu X, Redmond PL, Liu H, Chen Y, Steigerwald M, Brus L. *J Am Chem Soc.* 2008 in press. 10.1021/ja8018669

Biographies



Younan Xia was born in Jiangsu, China, in 1965. He received a B.S. degree in chemical physics from the University of Science and Technology of China (USTC) in 1987 and then worked as a graduate student on nonlinear optical crystals for four years at the Fujian Institute of Research on the Structure of Matter, Chinese Academy of Sciences. He came to the United States in 1991, received a M.S. degree in inorganic chemistry from the University of Pennsylvania (with the late Professor Alan G. MacDiarmid) in 1993 and a Ph.D. degree in physical chemistry from Harvard University (with Professor George M. Whitesides) in 1996. After a postdoctoral stint with Professors George M. Whitesides and Mara Prentiss at Harvard University, he started as an Assistant Professor of Chemistry at the University of Washington in Seattle in 1997. He was promoted to Associate Professor and Professor in 2002 and 2004, respectively. In the fall of 2007, he relocated to Washington University in St. Louis to take the position of James M. McKelvey Professor for Advanced Materials in the Department of Biomedical Engineering. He also holds joint appointments in the Departments of Energy, Environmental and Chemical Engineering, Biochemistry and Molecular Biophysics, Radiology, and Chemistry. Currently, his research centers on the

design and synthesis of nanostructured materials with controlled properties for applications in imaging, sensing, drug delivery, cancer treatment, tissue engineering, catalysis, energy conversion, photonics, and electronics.



Yujie Xiong was born in Jiangxi, China, in 1979. He entered the Special Class for the Gifted Young (SCGY) at the University of Science and Technology of China (USTC) in 1996, received a B.S. degree in chemical physics in 2000, and a Ph.D. degree in inorganic chemistry under the tutelage of Prof. Yi Xie in 2004. In the course of his graduate studies, he was the recipient of a number of awards, including the Best Doctoral Dissertation Award from the Chinese Academy of Sciences. From 2004 to 2007, he worked as a postdoctoral fellow with Professor Younan Xia at the University of Washington in Seattle, where his research centered on shape-controlled synthesis of noble-metal nanocrystals and exploration of their novel properties. He is currently working on energy-saving devices with Professor John A. Rogers at the University of Illinois at Urbana-Champaign. His research interests include synthesis and assembly of inorganic nanostructures, nucleation and growth, surface plasmonic properties, micro- and nanofabrication, electronic and photonic devices, surface-enhanced Raman scattering (SERS), and catalysis. He has published more than 60 peer-reviewed papers and book chapters.



Byungkwon Lim was born in Seoul, Korea, in 1975. He received his B.S. (1998), M.S. (2000), and Ph.D. (2004) degrees all from the School of Chemical and Biological Engineering, Seoul National University, Korea. During his graduate study, he worked on the synthesis of polymeric and carbeneous nanostructures using vapor deposition polymerization. He then worked as a senior researcher on the synthesis and structural analysis of polymeric materials for 3 years at LG Chem, Korea. He has been working with Professor Younan Xia as a postdoctoral fellow since March, 2007. His research interests include shape-controlled synthesis of noble-metal nanocrystals, surface plasmonic properties, carbeneous nanostructures, and catalysis.



Sara E. Skrabalak received a B.A. degree in chemistry from Washington University in St. Louis where she was the recipient of the 2002 Sowden Award for her research accomplishments with Professor William E. Buhro. She then received her Ph.D. degree in chemistry from the University of Illinois at Urbana-Champaign under the tutelage of Professor Kenneth S. Suslick. In the course of her graduate studies, she was the recipient of a number of awards including the 2006 T. S. Piper Thesis Research Award. She has been working with Professor Younan Xia as a postdoctoral fellow since 2007 and will begin as an Assistant Professor of Chemistry at Indiana University – Bloomington in fall 2008. Her research interests include shape and architectural controlled synthesis of inorganic solids (metals, metal oxides, and metal sulfides), solar energy conversion, catalysis, environmental remediation, and nanotechnology.

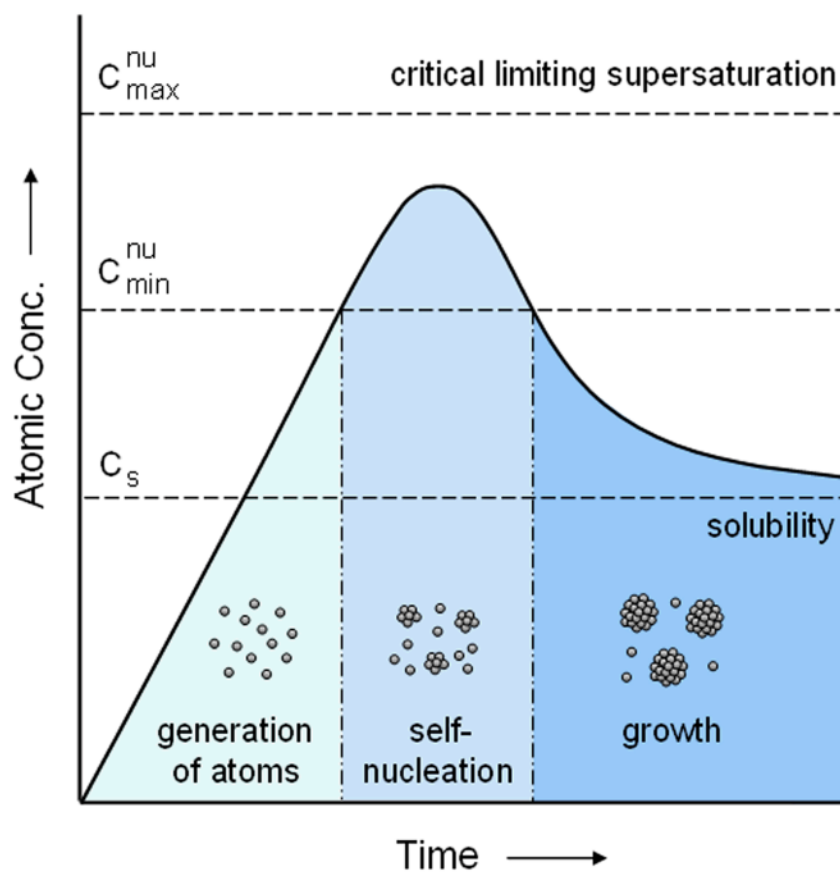


Figure 1. Plot of atomic concentration against time, illustrating the generation of atoms, nucleation, and subsequent growth (modified with permission from [33], copyright 1950 American Chemical Society).

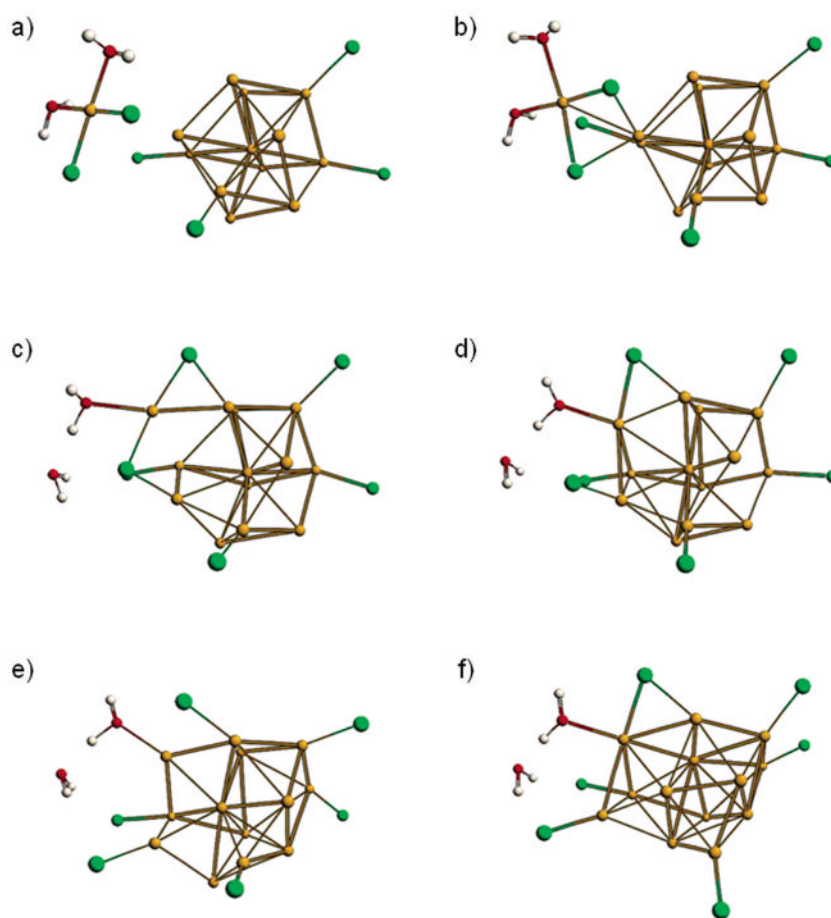


Figure 2. Snapshots from a first-principles molecular dynamics simulation showing the reaction of a PtCl₂(H₂O)₂ complex with a Pt₁₂Cl₄ cluster. Pt: yellow. Cl: green. O: red. H: white. Simulation time: a) 0.0 ps, b) 0.6 ps, c) 1.3 ps, d) 2.0 ps, e) 3.2 ps, and f) 5.0 ps (modified with permission from [35d], copyright 2003 American Chemical Society).

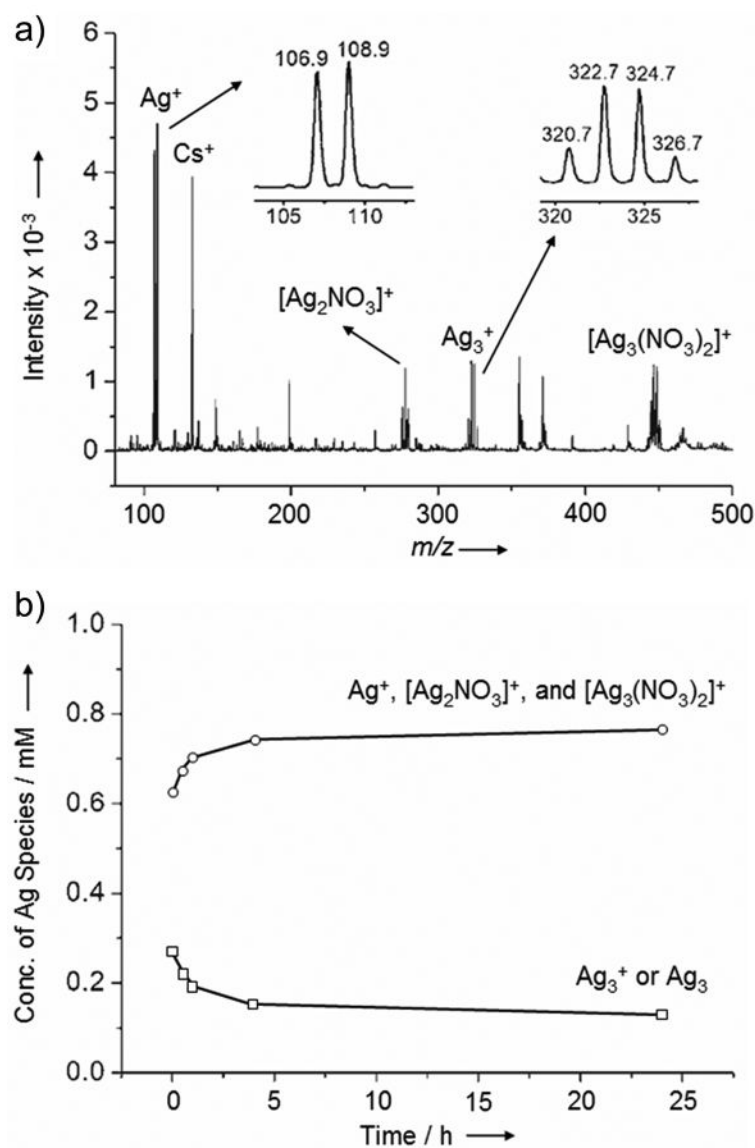


Figure 3.
 a) Positive-mode mass spectrum of a freshly prepared 1 mM aqueous AgNO_3 solution. Note that Cs^+ was added in the form of CsNO_3 as a reference for concentration calibration. b) Plots of the concentrations of different silver species versus time, when a 1 mM aqueous AgNO_3 solution was aged in air (modified with permission from [37], copyright 2007 Wiley-VCH).






Full-shell "magic number" clusters					
Number of shells	1	2	3	4	5
Number of atoms in cluster	13	55	147	309	561
Percentage of surface atoms	92	76	63	52	45

Figure 4. Idealized representation of full-shell metal clusters with "magic numbers" of atoms, which are built upon the densest sphere packing (modified with permission from [49c], copyright 1999 Elsevier).

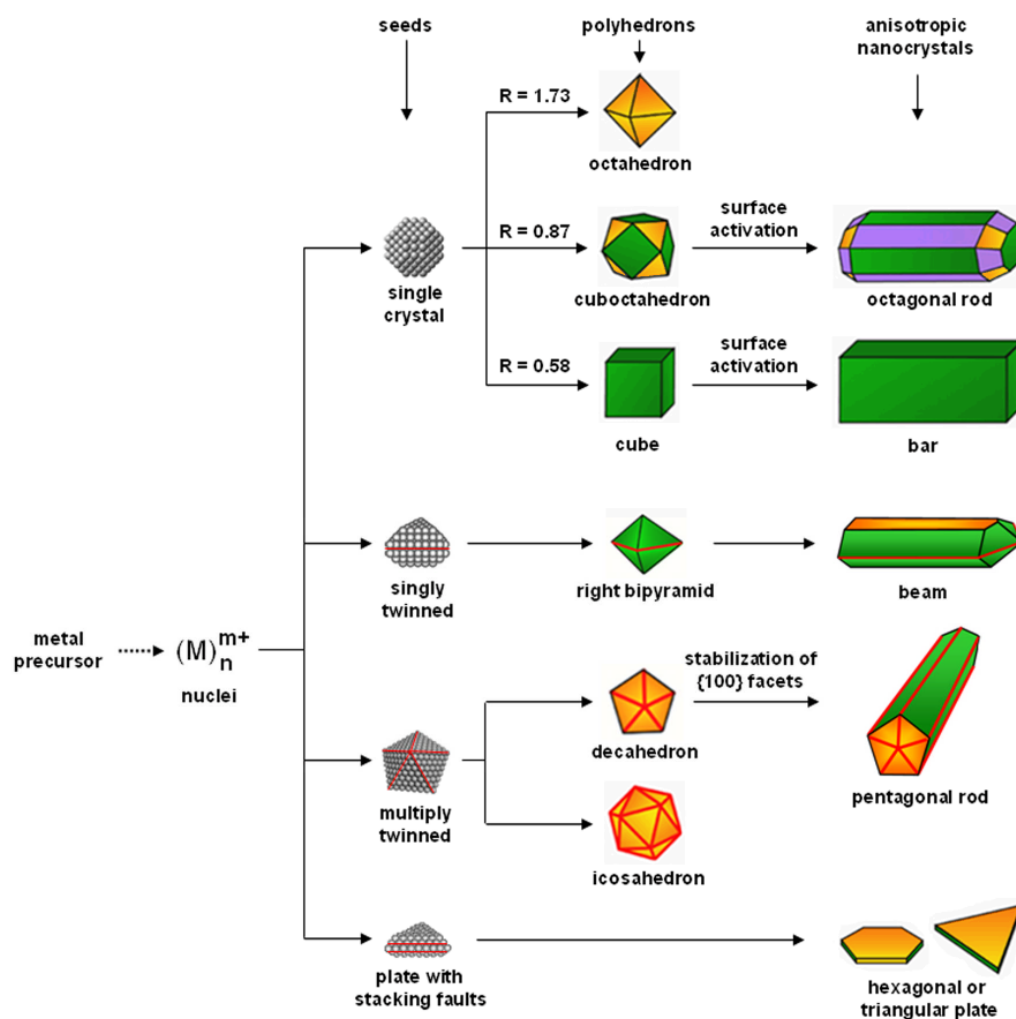


Figure 5.

A schematic illustration of the reaction pathways that lead to *fcc* metal nanocrystals having different shapes. First, a precursor is reduced or decomposed to form the nuclei (small clusters). Once the nuclei have grown past a certain size, they become seeds with a single-crystal, singly twinned, or multiply twinned structure. If stacking faults are introduced, the plate-like seeds will be formed. The green, orange, and purple colors represent the $\{100\}$, $\{111\}$, and $\{110\}$ facets, respectively. Twin planes are delineated in the drawing with red lines. The parameter R is defined as the ratio between the growth rates along the $\langle 100 \rangle$ and $\langle 111 \rangle$ directions (modified with permission from [26], copyright 2007 Wiley-VCH).

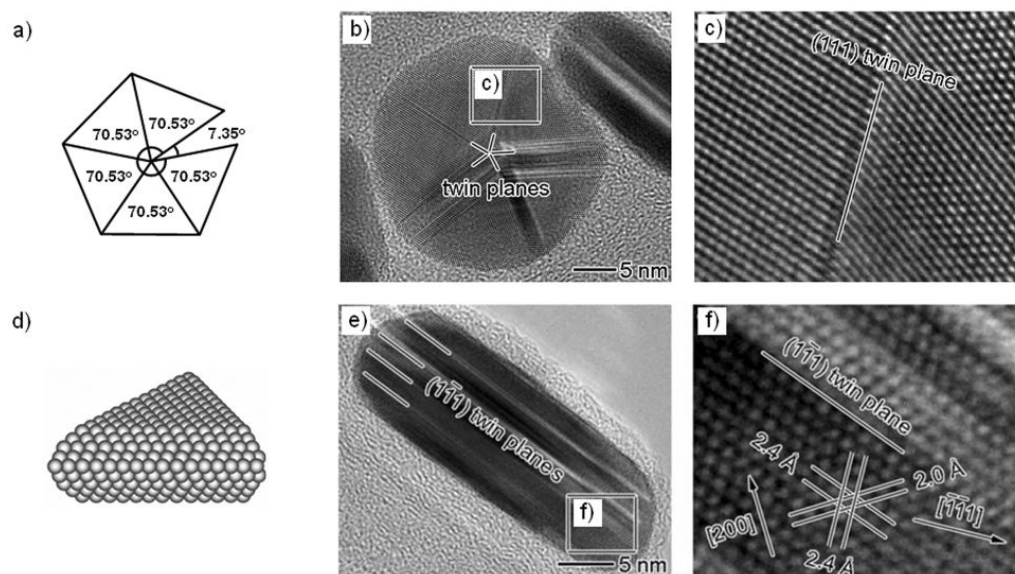


Figure 6.

a) Schematic of a decahedron, which can be considered as the assembly of five single-crystal, tetrahedral units sharing a common edge. Since the theoretical angle between two $\{111\}$ planes of a tetrahedron is 70.53° , five tetrahedrons joined with $\{111\}$ twin planes will leave a gap of 7.35° . b, c) High-resolution TEM images of a decahedral Ag nanocrystal (modified with permission from [58b], copyright 2007 Royal Society of Chemistry). d) Schematic of a plate-like seed with a random hexagonal close-packed (rhcp) structure. Note that stacking faults and/or lamellar twins are introduced into the crystal lattice. e, f) High-resolution TEM images taken from the side face of a Ag nanoplate (modified with permission from [58b], copyright 2007 Royal Society of Chemistry).

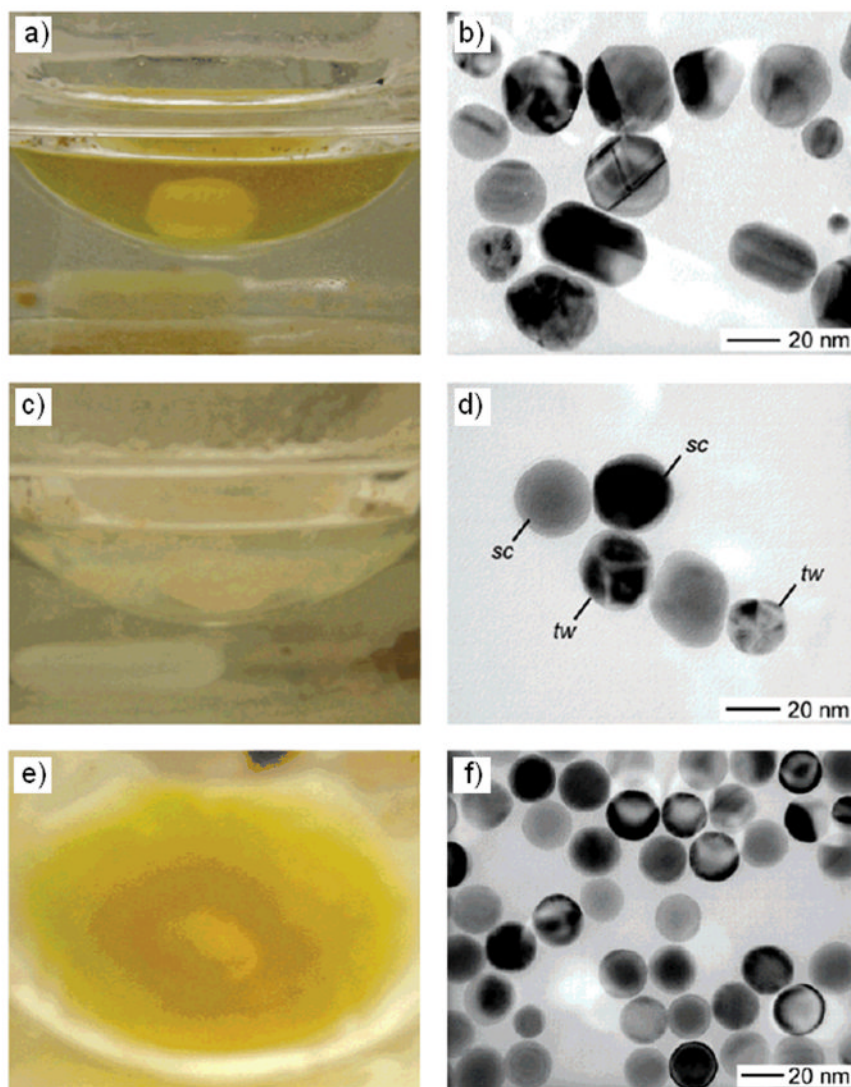


Figure 7. Details of a polyol synthesis of Ag nanocrystals in which AgNO_3 and PVP serve as the Ag precursor and capping agent, respectively. The reaction was performed in air and 0.06 mM NaCl was added. Reaction times: a, b) 10 min, c, d) 2 h, and e, f) 44 h. a, c, e) Photographs of the reaction solution, in which the yellow color indicates the presence of Ag nanocrystals. b, d, f) TEM images of the Ag nanocrystals produced at each time. Single-crystal and twinned nanocrystals are labeled as *sc* and *tw*, respectively. As the reaction proceeded, the twinned nanocrystals were removed due to oxidative etching, but the single-crystal species remained and accumulated in the solution because of their higher resistance to oxidative etching (modified with permission from [62], copyright 2004 American Chemical Society).

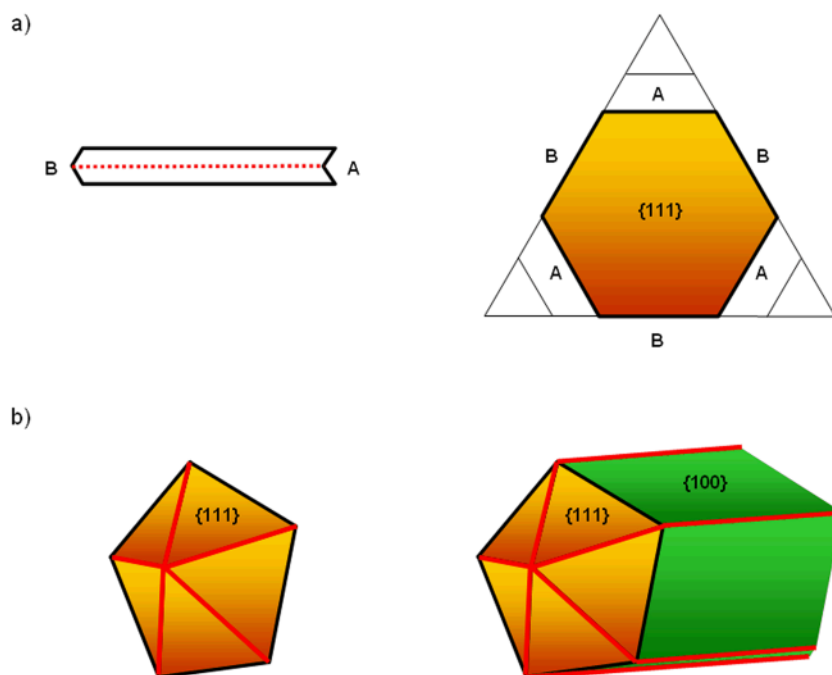


Figure 8.

a) A schematic model of a hexagonal plate with a single twin plane, which contains concave-type (A) and convex-type (B) faces. The concave-type surface serves as the primary site for atomic addition, facilitating the transformation of hexagonal plates into triangular plates. b) Schematic models of a decahedron seed and a five-fold twinned rod. The five variants in the decahedron are separated by $\{111\}$ -type twin planes. In the five-fold twinned rod, the side faces are $\{100\}$ and the end faces are $\{111\}$ faces. The green and orange colors represent the $\{100\}$ and $\{111\}$ facets, respectively. Twin planes are delineated in the figure with red lines (modified with permission from [52b], copyright 2005 Wiley-VCH).

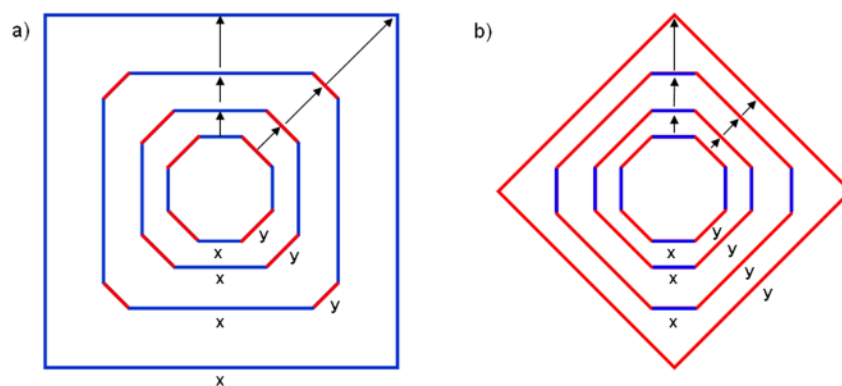


Figure 9. Shape evolution during the successive stages of growth for an imaginary 2-D crystal. a) Rapid addition to the y-edges (relative to the x-edges) results in the elongation of the x-edges and the eventual disappearance of the y-edges, and b) vice versa. The length of arrow is directly proportional to the growth rate. When the crystal is enclosed by a single set of planes, the shape will become stable over growth time unless the surface is modified again due to etching, Ostwald ripening, and/or capping.

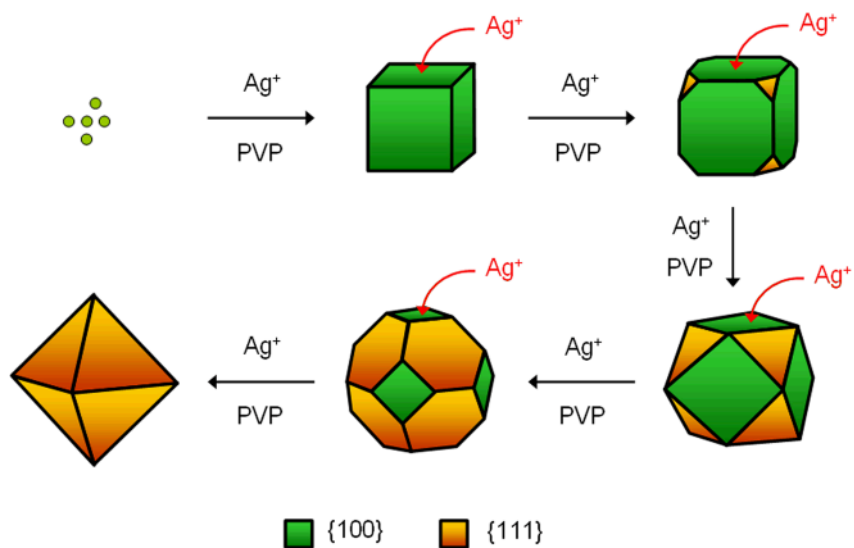


Figure 10.

A schematic illustration of the overgrowth process of Ag nanocrystals, in which Ag atoms are continuously deposited onto the {100} facets of a Ag nanocube to eventually result in an octahedron enclosed by {111} facets (modified with permission from [67a], copyright 2006 Wiley-VCH).

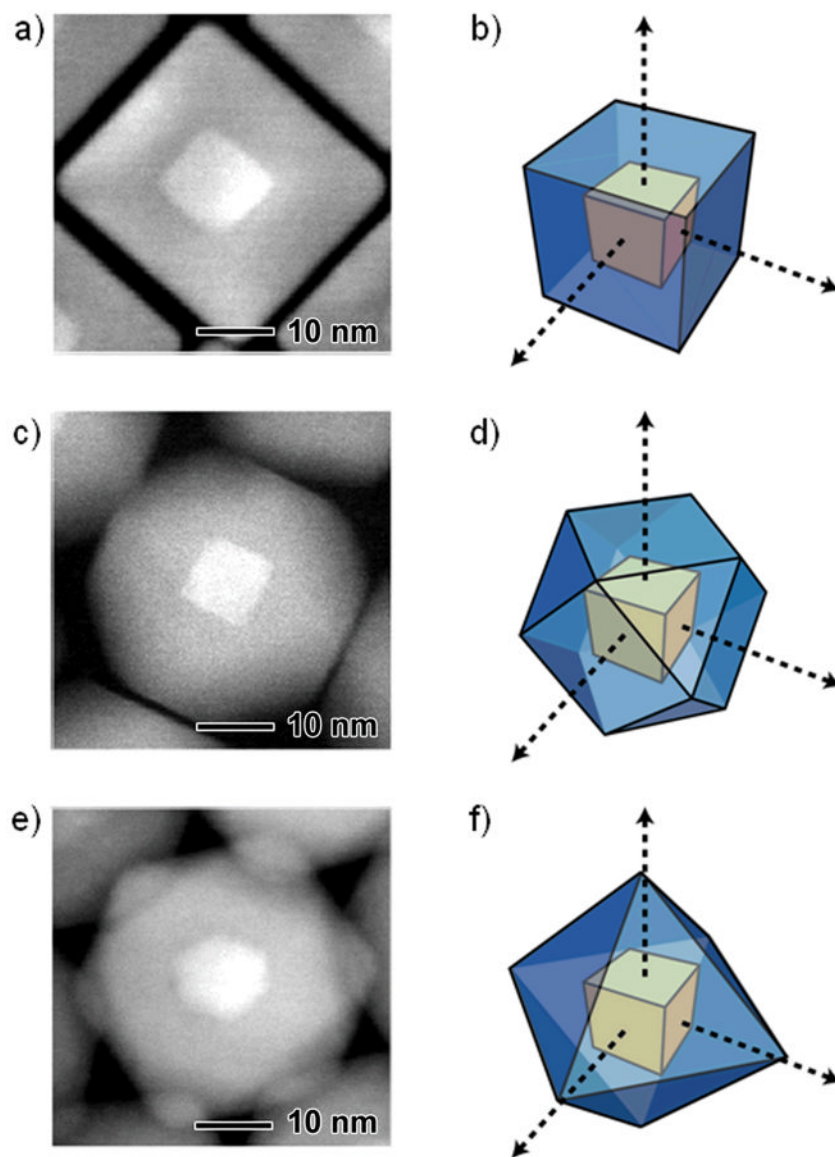


Figure 11. Electron microscopy characterization of the binary Pt/Pd core-shell nanocrystals obtained through the heteroepitaxial deposition of Pd on cubic Pt seeds: a, b) cube; c, d) cuboctahedron; and e, f) octahedron (modified with permission from [94a], copyright 2007 Nature Publishing Group).

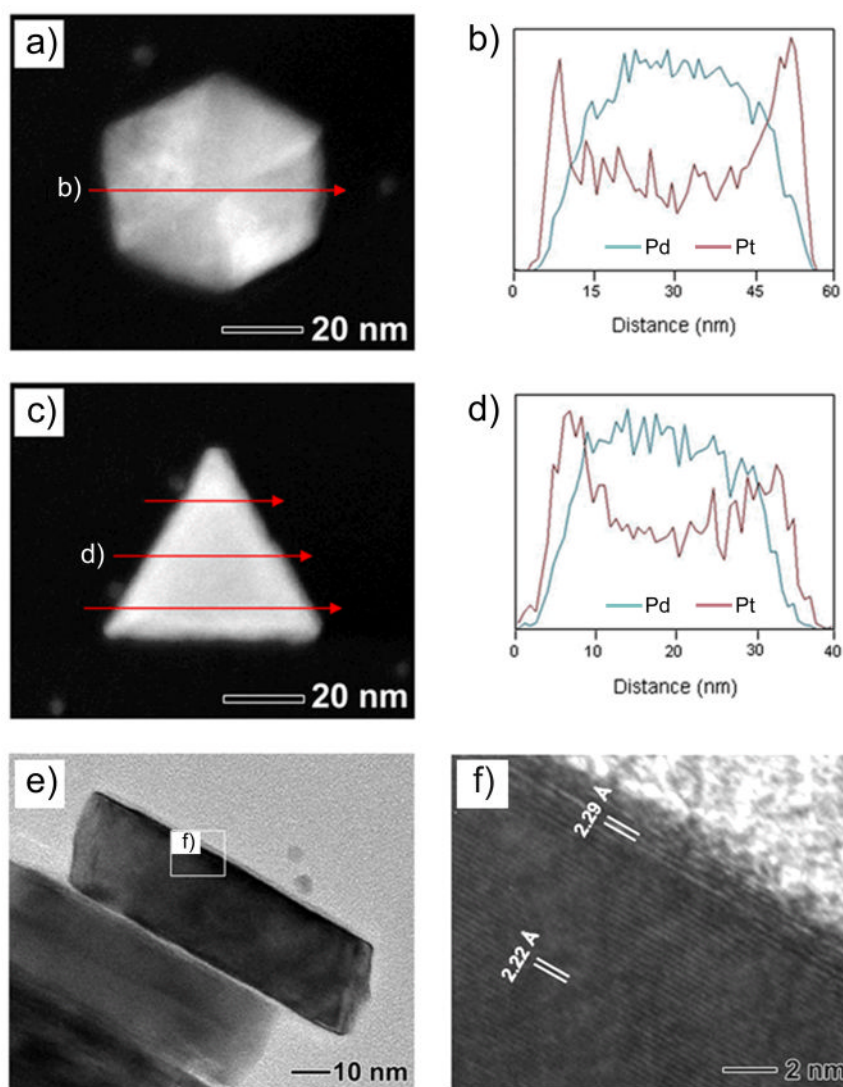


Figure 12. Electron microscopy characterization of the binary Pd/Pt core-shell nanoplates obtained through the heteroepitaxial growth of Pt shells on Pd nanoplate seeds. a-d) STEM images and the corresponding cross-sectional compositional line profiles of Pd/Pt core-shell nanoplates for a, b) hexagonal and c, d) triangular plates. e, f) HRTEM images taken from the side faces of the Pd/Pt core-shell nanoplates, which show the continuous lattice fringes from the Pd core (lattice spacing: 2.22 Å) to the Pt shell (lattice spacing: 2.29 Å) (modified with permission from [94c], copyright 2008 American Chemical Society).

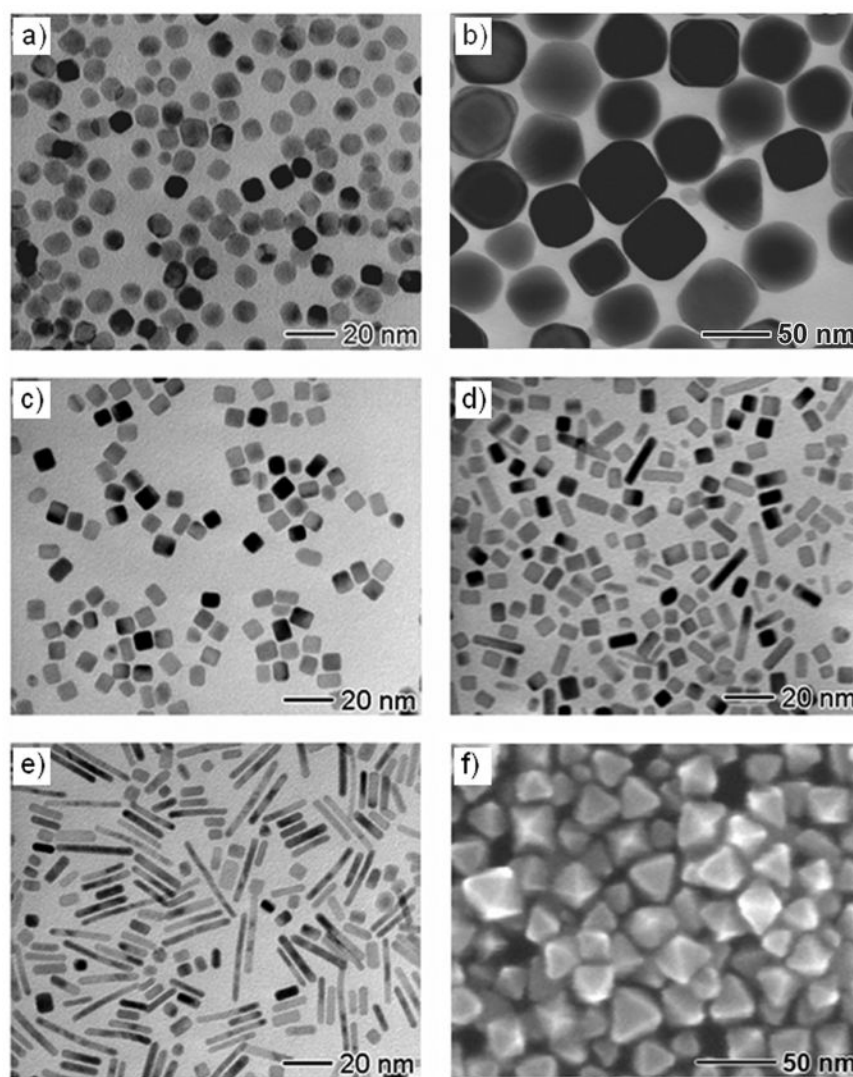


Figure 13.

Electron microscopy images of single-crystal Pd nanocrystals: a) Wulff polyhedrons prepared in ethylene glycol with PVP as a capping agent (modified with permission from [64a], copyright 2005 American Chemical Society); b) slightly truncated nanocubes prepared in ethylene glycol with PVP as a capping agent and Fe^{III} species as an etchant (modified with permission from [78b], copyright 2005 American Chemical Society); c) nanocubes prepared with PVP as a reductant in water and in the presence of KBr; d) nanobars prepared in a mixture of 90.9% water and 9.1% ethylene glycol, in the presence of KBr; e) nanorods prepared in a mixture of 72.7% ethylene glycol and 27.3% water, in the presence of KBr (modified with permission from [64d], copyright 2007 American Chemical Society); and f) octahedrons prepared with citric acid as a reducing agent and capping agent at a high concentration of Pd precursor (modified with permission from [80], copyright 2007 Wiley-VCH).

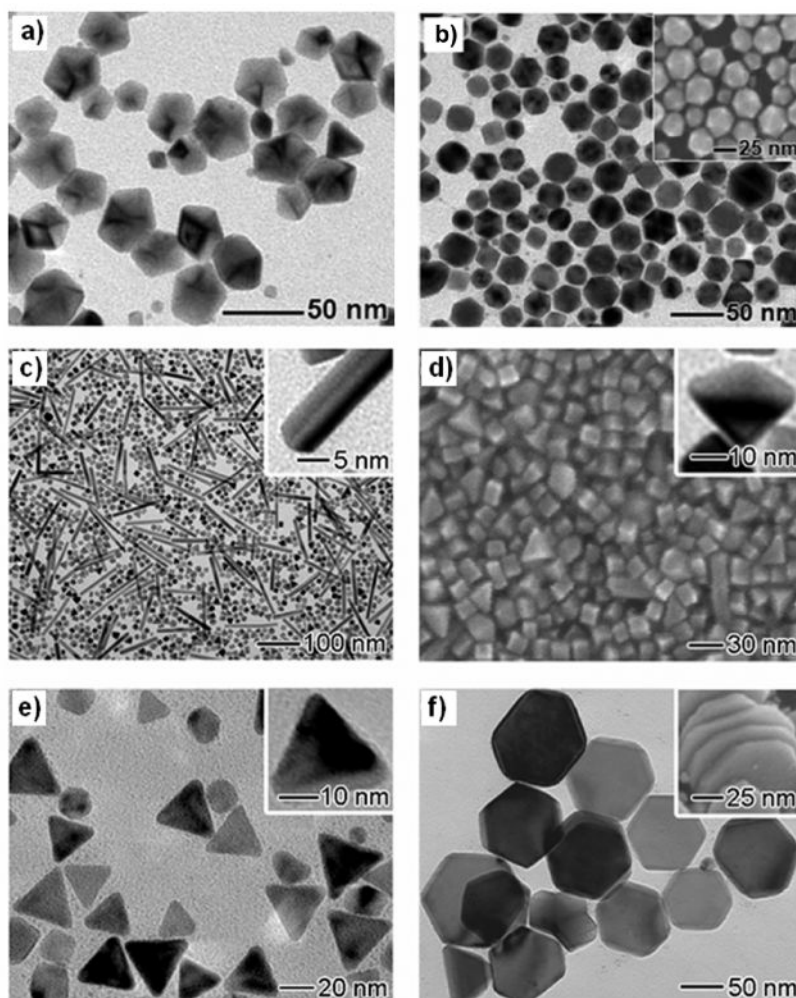


Figure 14.

Electron microscopy images of Pd nanocrystals with twin defects: a) decahedrons prepared with citric acid as a reducing agent and capping agent at high concentrations for both Pd precursor and citric acid (modified with permission from [80], copyright 2007 Wiley-VCH); b) icosahedrons prepared with citric acid as a reducing agent and capping agent at a low concentration of Pd precursor (modified with permission from [80], copyright 2007 Wiley-VCH); c) five-fold twinned nanorods (as a mixture with cubes) prepared with ascorbic acid as a reductant in water and in the presence of bromide; d) single-twinned right bipyramids (as a mixture with cubes) prepared with ascorbic acid as a reductant in water and in the presence of bromide (modified with permission from [68], copyright 2007 Elsevier); e) triangular nanoplates prepared in ethylene glycol and in the presence of FeCl_3 and HCl (modified with permission from [60], copyright 2005 American Chemical Society); and f) hexagonal nanoplates prepared with PVP as a reductant in water (modified with permission from [59b], copyright 2006 American Chemical Society).

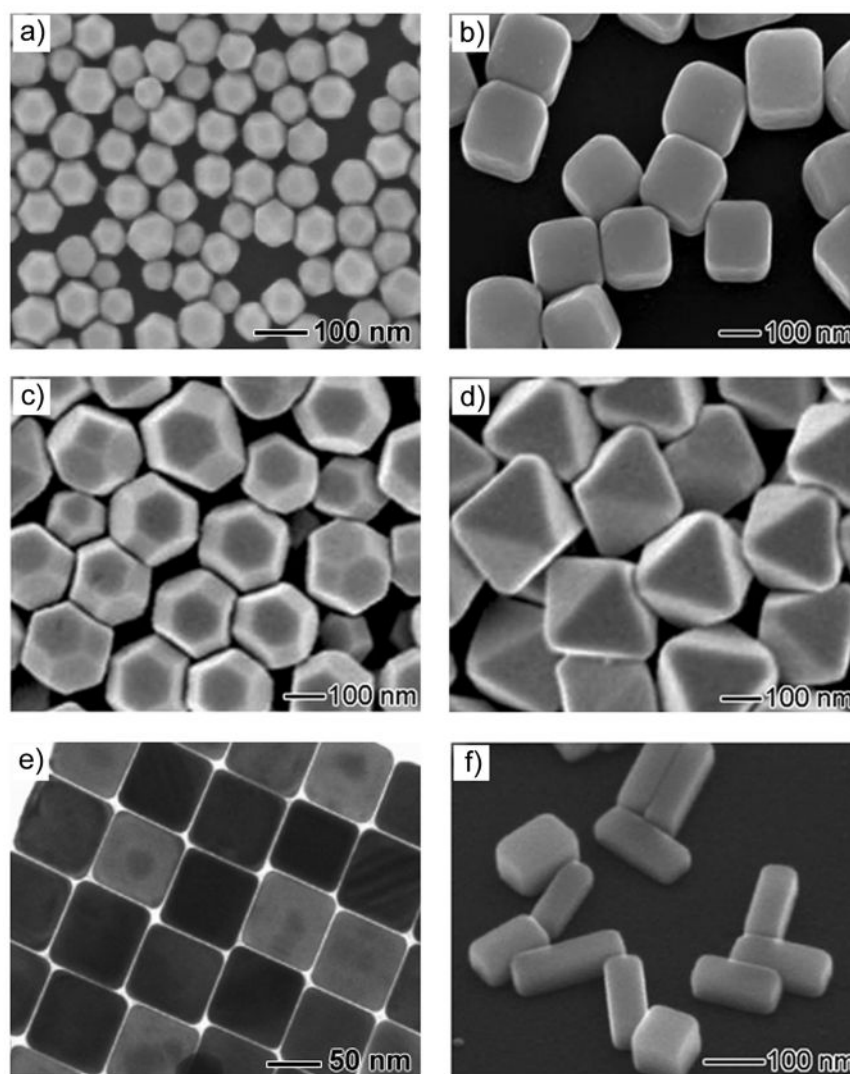


Figure 15. Electron microscopy images of single-crystal Ag nanocrystals: a) cuboctahedrons prepared in ethylene glycol with PVP as a capping agent (modified with permission from [62], copyright 2004 American Chemical Society); b) nanocubes prepared in ethylene glycol with PVP as a capping agent (modified with permission from [78a], copyright 2002 American Association for the Advancement of Science); c) truncated octahedrons prepared in 1,5-pentanediol in the presence of PVP and Cu^{2+} ions; d) octahedrons prepared in 1,5-pentanediol in the presence of PVP and Cu^{2+} ions (modified with permission from [67a], copyright 2006 Wiley-VCH); e) nanocubes prepared by a modified silver mirror reaction in the presence of Br^- with glucose as a reducing agent (modified with permission from [110b], copyright 2005 American Chemical Society); and f) nanobars prepared in ethylene glycol in the presence of PVP and Br^- (modified with permission from [63b], copyright 2007 American Chemical Society).

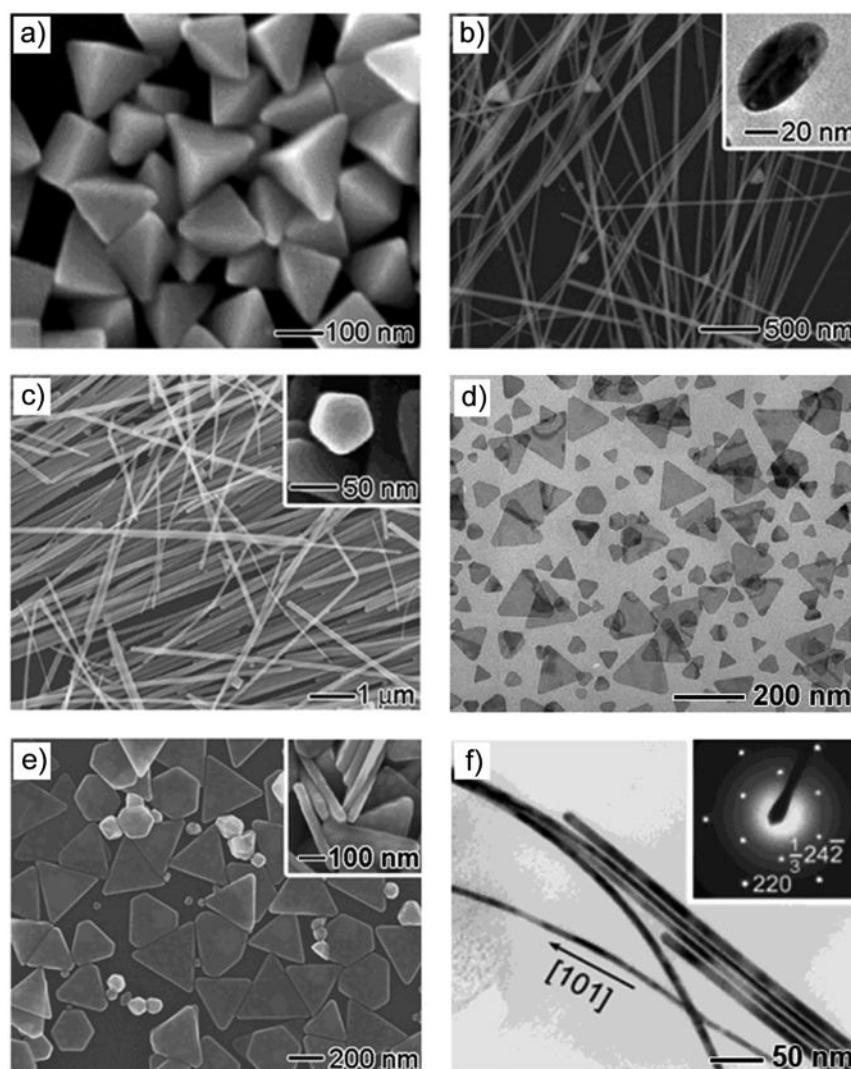


Figure 16.

Electron microscopy images of Ag nanocrystals with twin defects: a) singly twinned right bipyramids prepared in ethylene glycol in the presence of PVP and Br^- (modified with permission from [63a], copyright 2006 American Chemical Society); b) singly twinned nanobeams prepared in ethylene glycol in the presence of PVP and Br^- (modified with permission from [69], copyright 2006 American Chemical Society); c) five-fold twinned nanorods prepared in ethylene glycol with PVP as a capping agent (modified with permission from [65], copyright 2005 American Chemical Society); d) nanoplates prepared via the light-induced conversion of Ag nanospheres (modified with permission from [115a], copyright 2003 Nature Publishing Group); e) nanoplates prepared in water with PVP as a reductant (modified with permission from [59a], copyright 2006 Wiley-VCH); and f) nanobelts formed by refluxing an aqueous dispersion of Ag colloids (modified with permission from [61b], copyright 2003 American Chemical Society).

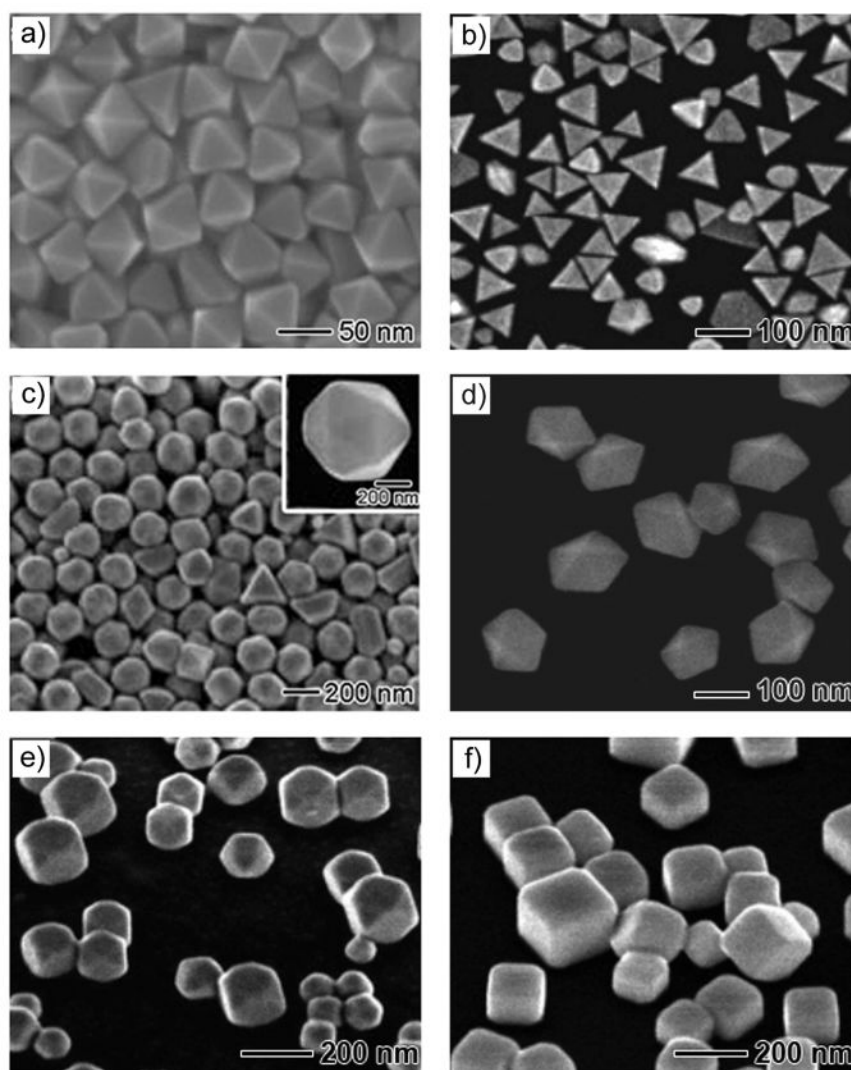


Figure 17.

Electron microscopy images of Au nanocrystals: a) octahedrons prepared with PVP as a capping agent in polyethylene glycol 600 (PEG 600) (modified with permission from [120b], copyright 2007 Wiley-VCH); b) truncated tetrahedrons prepared with PVP as a capping agent in tetraethylene glycol (modified with permission from [120e], copyright 2008 American Chemical Society); c) icosahedrons prepared in ethylene glycol with a low concentration of Au precursor (modified with permission from [91], copyright 2004 Wiley-VCH); d) decahedrons prepared in diethylene glycol with a high concentration of PVP (modified with permission from [120e], copyright 2008 American Chemical Society); e) truncated nanocubes prepared in 1,5-pentanediol in the presence of Ag^+ ions with PVP as a capping agent; and f) nanocubes prepared in 1,5-pentanediol in the presence of Ag^+ ions with PVP as a capping agent (modified with permission from [121b], copyright 2006 American Chemical Society).

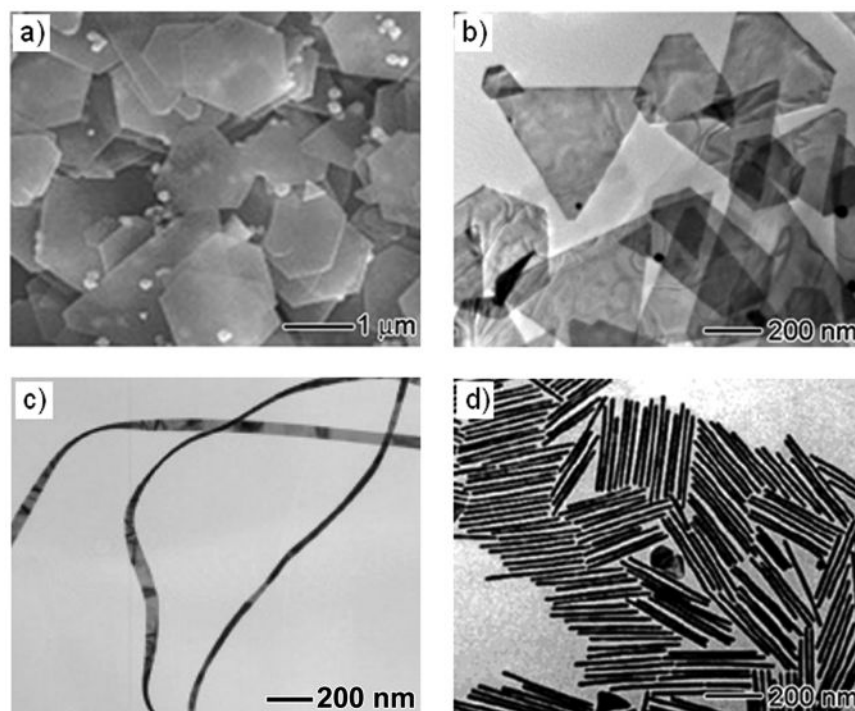


Figure 18. Electron microscopy images of anisotropic Au nanocrystals: a) hexagonal nanoplates prepared with *ortho*-phenylenediamine as a reductant (modified with permission from [122b], copyright 2004 Wiley-VCH); b) triangular nanoplates prepared with *Sargassum sp.* as a reductant (modified with permission from [122i], copyright 2005 American Chemical Society); c) nanobelts prepared with ascorbic acid as a reducing agent and SDSn and CTAB as surfactants (modified with permission from [126], copyright 2008 American Chemical Society); and d) five-fold twinned nanorods prepared via a seeding process with CTAB as a capping agent (modified with permission from [79a], copyright 2001 American Chemical Society).

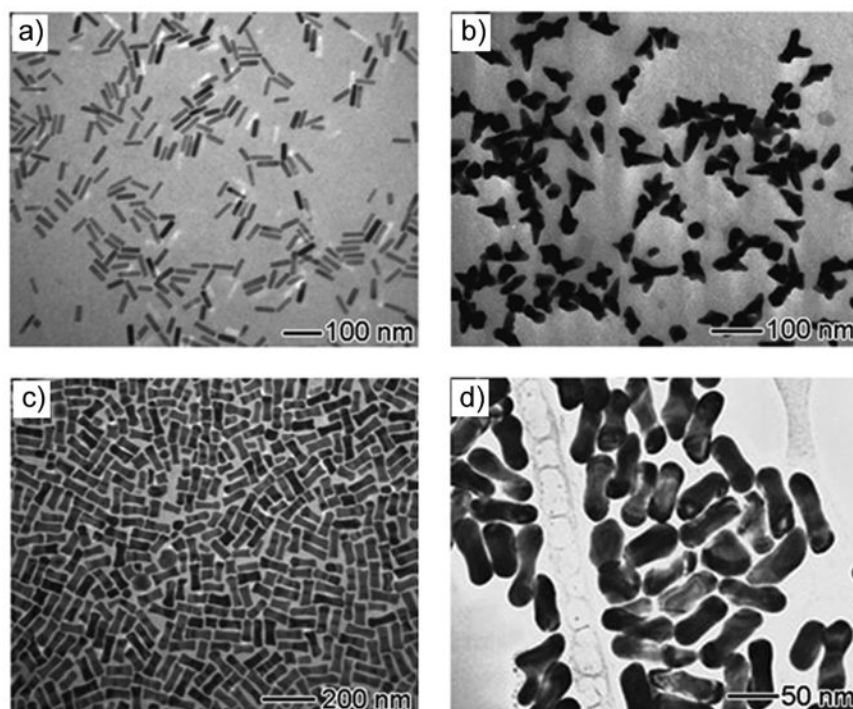


Figure 19. Electron microscopy images of various Au nanocrystals prepared via a seeding process: a) nanorods prepared in the presence of Au seeds and Ag^+ ions and with CTAB as a capping agent (modified with permission from [128d], copyright 2005 American Chemical Society); b) multipods formed through an overgrowth mechanism (modified with permission from [131a], copyright 2004 American Chemical Society); c) dog bone-shaped nanocrystals formed through an overgrowth mechanism (modified with permission from [128d], copyright 2005 American Chemical Society); and d) dumbbell-shaped nanocrystals formed through an overgrowth mechanism (modified with permission from [131c], copyright 2005 Wiley-VCH).

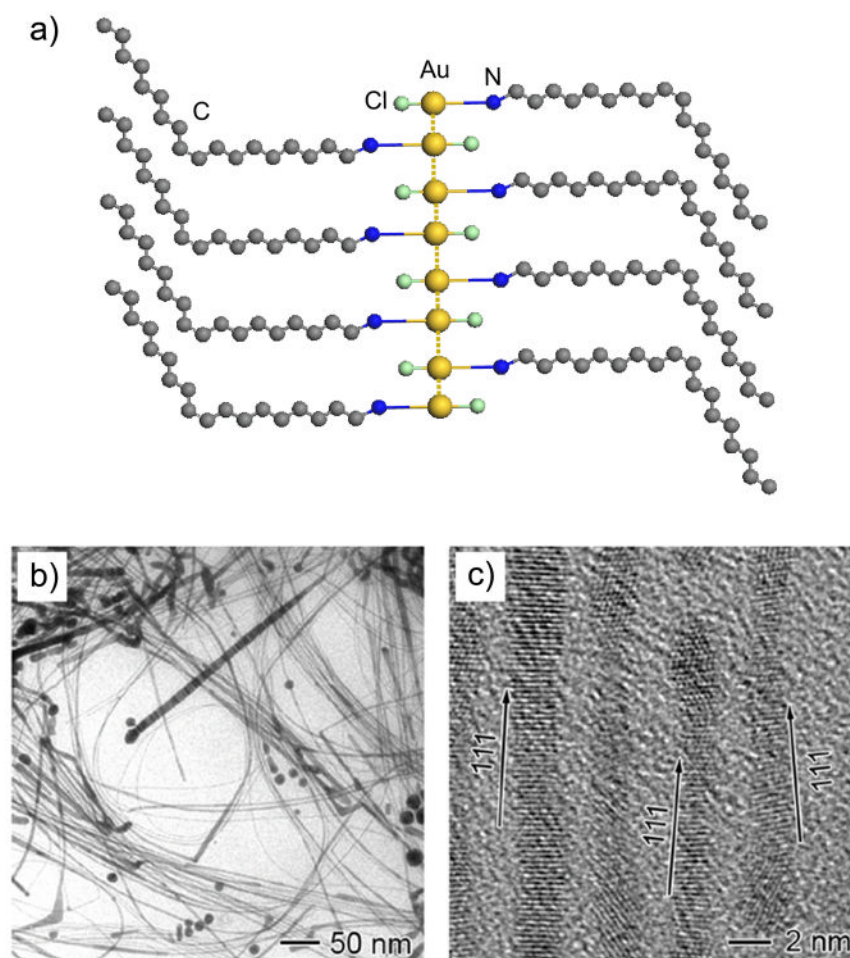


Figure 20.

a) A schematic illustrating the formation of a polymeric strand of oleylamine-AuCl complex; b) TEM image of ultrathin Au nanowires with an average diameter of 1.8 nm obtained by reducing the oleylamine-AuCl complex with 10-nm Ag nanoparticles in hexane; and c) HRTEM image showing $\langle 111 \rangle$ growth direction for most of the nanowires (modified with permission from [134a], copyright 2008 American Chemical Society).

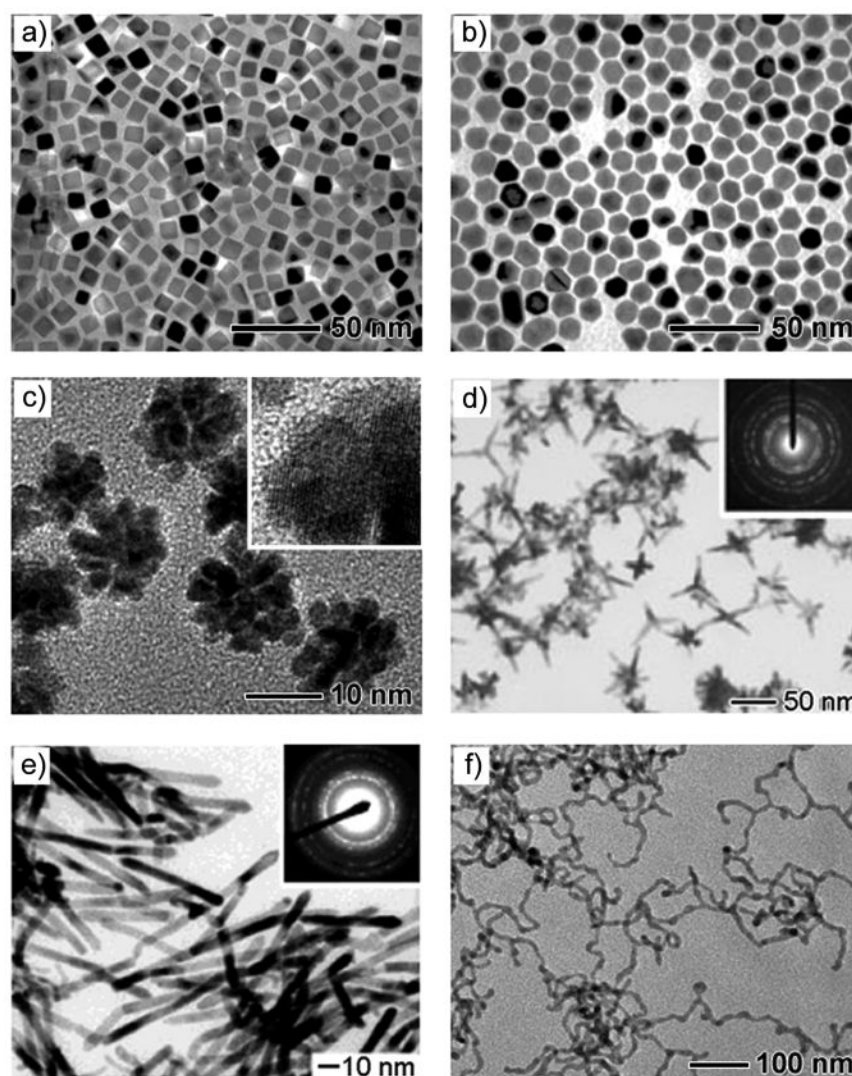


Figure 21. Electron microscopy images of Pt nanocrystals with different shapes: a) nanocubes prepared in the presence of TTAB with a high concentration of NaBH_4 ; b) cuboctahedrons prepared in the presence of TTAB with a low concentration of NaBH_4 (modified with permission from [144a], copyright 2007 American Chemical Society); c) nanodendrites prepared with ascorbic acid as a reducing agent (modified with permission from [143b], copyright 2004 American Chemical Society); d) tetrapods prepared via a polyol process using Fe^{III} species to reduce the number of seeds at the nucleation stage (modified with permission from [135b], copyright 2005 Wiley-VCH); e) nanowires prepared via a polyol process using Fe^{III} species to slow down the reduction (modified with permission from [135a], copyright 2004 American Chemical Society); and f) nanowire network prepared in a two-phase water-chloroform system in the presence of CTAB with NaBH_4 as a reducing agent (modified with permission from [144b], copyright 2007 American Chemical Society).

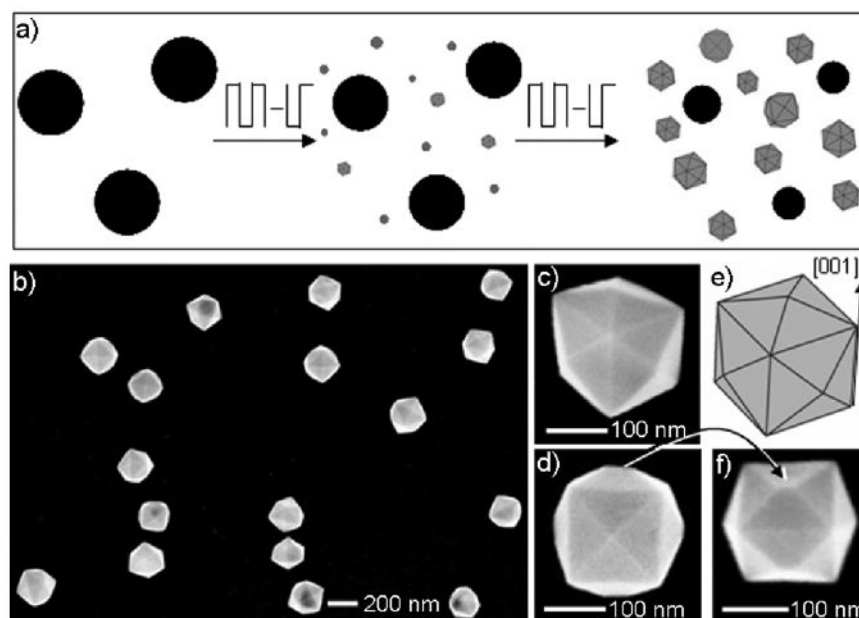


Figure 22.

a) A schematic illustrating the electrochemical preparation of Pt tetrahexahedrons (THHs) from nanospheres: under the influence of the square-wave potential, Pt THHs can nucleate and grow at the expense of spherical particles; b) low-magnification SEM image of the Pt THHs; c, d) high-magnification SEM images of a Pt THH along different orientations, clearly showing the shape of the THH; e) geometrical model of an ideal THH; and f) high-magnification SEM image of a Pt THH, showing the imperfect vertices as a result of unequally sized neighboring facets (modified with permission from [145], copyright 2007 American Association for the Advancement of Science).

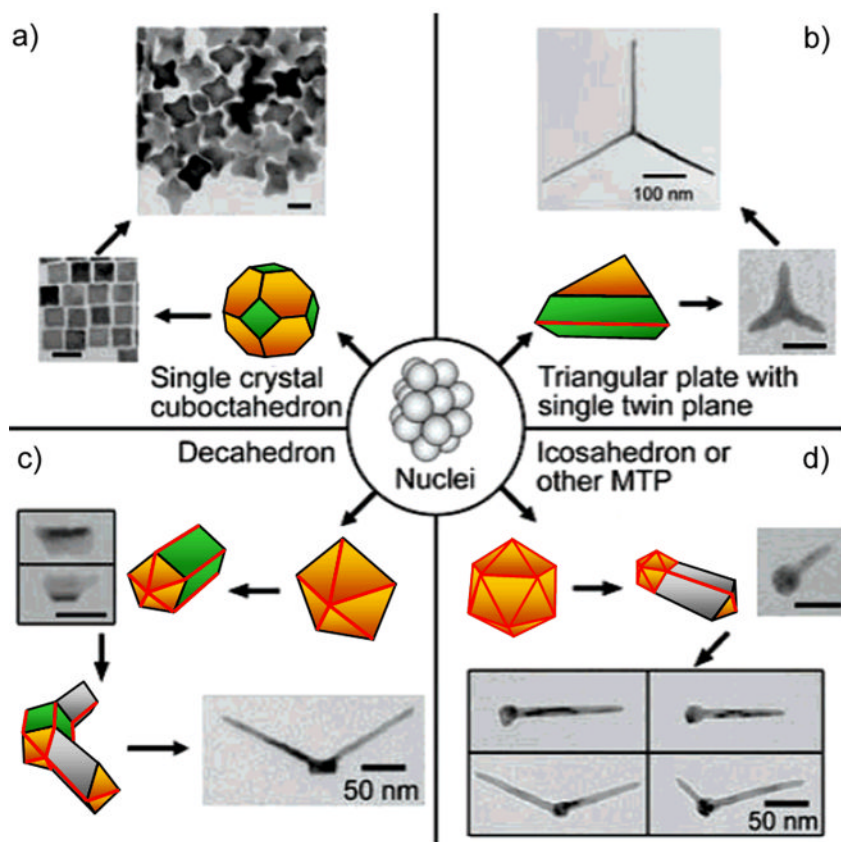


Figure 23. Schematic of Pt nanocrystals formed from seeds with different numbers of twin planes: a) zero, b) single, c) five, and d) multiple. Twin planes are delineated in the figure with red lines. Scale bars are 20 nm if not labeled in the images (modified with permission from [149], copyright 2007 American Chemical Society).

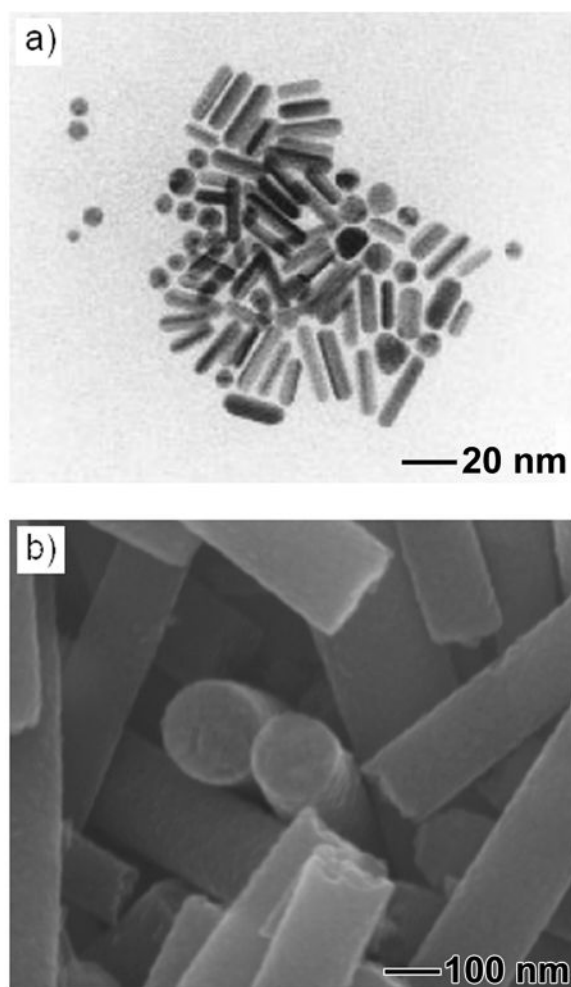


Figure 24.

a) TEM image of five-fold twinned Cu nanorods prepared by reducing copper(II) bis(2-ethylhexyl)sulfosuccinate ($\text{Cu}(\text{AOT})_2$) with hydrazine in a mixture of isooctane and water (modified with permission from [152a], copyright 1997 American Chemical Society). b) SEM image of Cu nanowires with a circular cross-section prepared by reducing $\text{Cu}(\text{NO}_3)_2$ with hydrazine in the presence of sodium hydroxide and ethylenediamine [158].

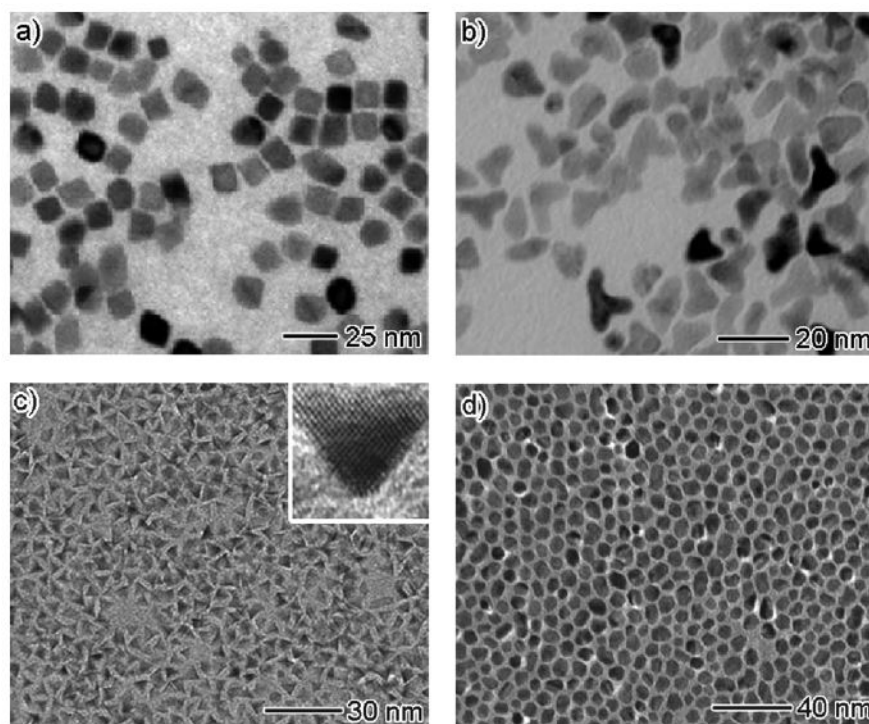


Figure 25.

TEM images of Rh nanocrystals with different shapes: a) nanocubes prepared via a polyol process at 190 °C (modified with permission from [164a], copyright 2005 American Chemical Society); b) multipods prepared via a polyol process at 140 °C (modified with permission from [64c], copyright 2006 Wiley-VCH); c) tetrahedrons prepared through the decomposition of $\text{Rh}_2(\text{CO})_4\text{Cl}_2$; and d) nanorods prepared through the decomposition of $\text{Rh}(\text{C}_5\text{H}_8\text{O}_2)_3$ (modified with permission from [164d], copyright 2007 Wiley-VCH).

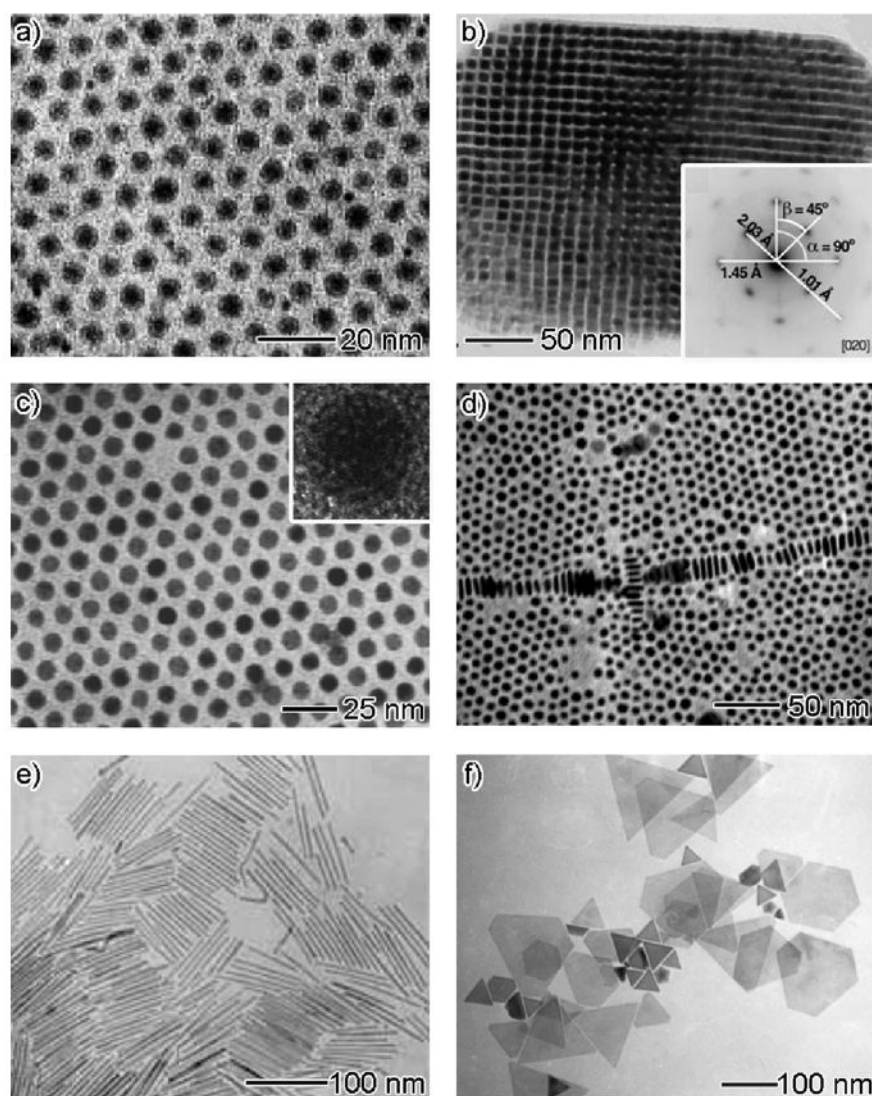


Figure 26. Electron microscopy images of Fe, Co and Ni nanocrystals with different shapes: a) α -Fe nanoparticles prepared by thermal decomposition of $\text{Fe}(\text{CO})_5$ (modified with permission from [168f], copyright 2005 American Chemical Society); b) Fe nanocubes prepared by thermal decomposition of $\text{Fe}[\text{N}(\text{SiMe}_3)_2]_2$ (modified with permission from [169a], copyright 2004 American Association for the Advancement of Science); c) ϵ -Co nanoparticles prepared by reducing CoCl_2 with LiBEt_3H (modified with permission from [171b], copyright 1999 American Institute of Physics); d) *hcp*-Co nanodisks prepared by rapid decomposition of $\text{Co}_2(\text{CO})_8$ (modified with permission from [171h], copyright 2002 American Chemical Society); e) *hcp*-Co nanorods prepared by decomposition of $[\text{Co}(\eta^3\text{-C}_8\text{H}_{13})(\eta^4\text{-C}_8\text{H}_{12})]$ (modified with permission from [173b], copyright 2003 Wiley-VCH); and f) *fcc*-Ni nanoplates prepared by decomposition of $\text{Ni}(\text{COD})_2$ in the presence of $\text{Fe}(\text{CO})_5$ (modified with permission from [176], copyright 2006 Institute of Physics Publishing).

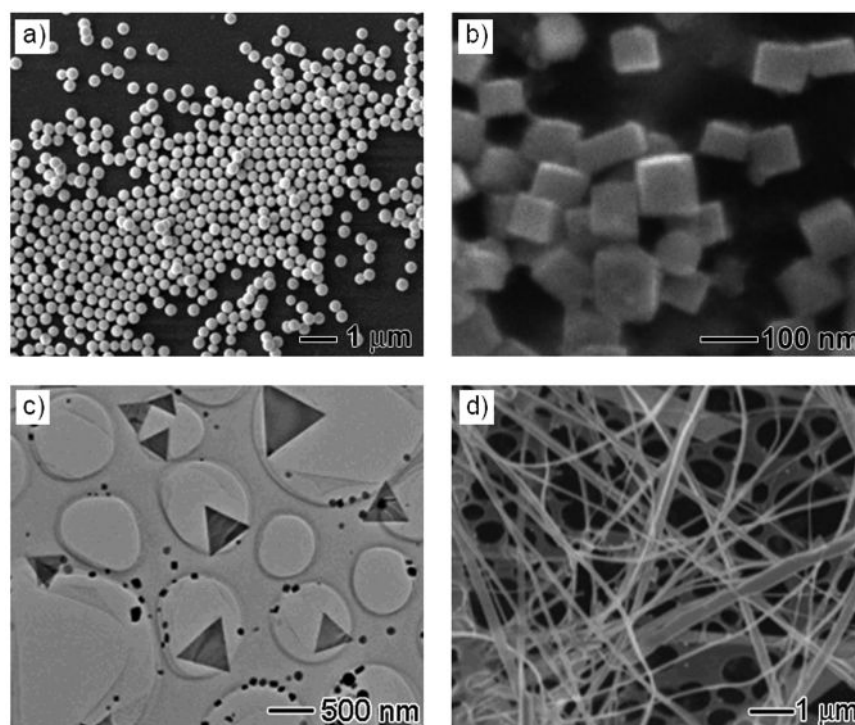


Figure 27. Electron microscopy images of Bi nanocrystals with different shapes: a) nanospheres prepared using a microemulsion-based approach (modified with permission from [178a], copyright 2006 Wiley-VCH); b) nanocubes, c) triangular nanoplates, and d) nanobelts prepared via hydrothermal routes (modified with permission from [183e], copyright 2006 American Chemical Society).

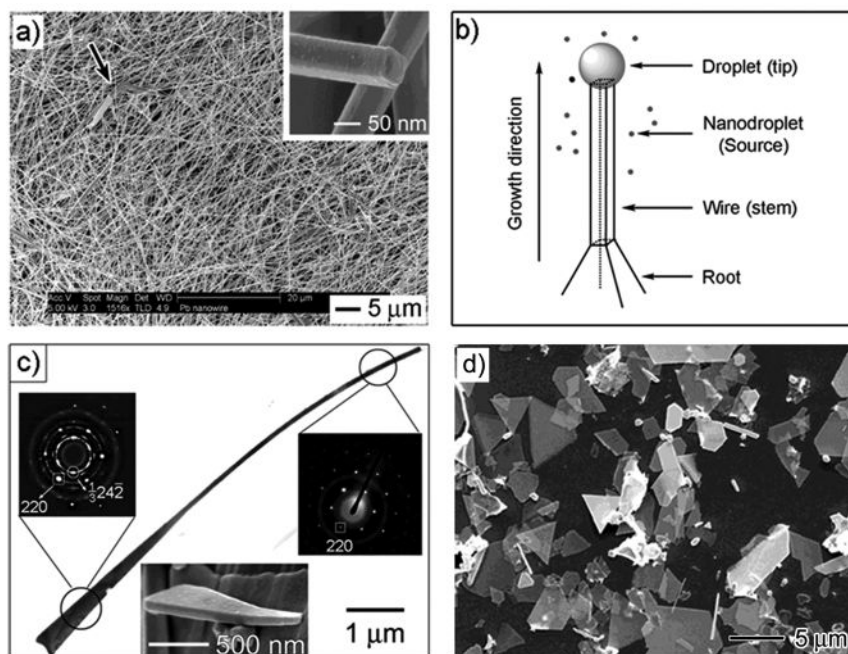


Figure 28.

a) SEM image of Pb nanowires prepared by a polyol process in the presence of PVP; the inset shows the cross-section of a broken nanowire; b) schematic illustrating the growth of a Pb nanowire with three components: root, stem, and tip. The Pb nanodroplets in the solution phase serve as the source of atoms for growth; c) TEM image of an individual Pb nanowire and the SAED patterns (insets) taken from its root and stem, respectively; and d) SEM image of Pb nanoplates prepared by increasing the concentration of PVP (modified with permission from [186b], copyright 2004 American Chemical Society).

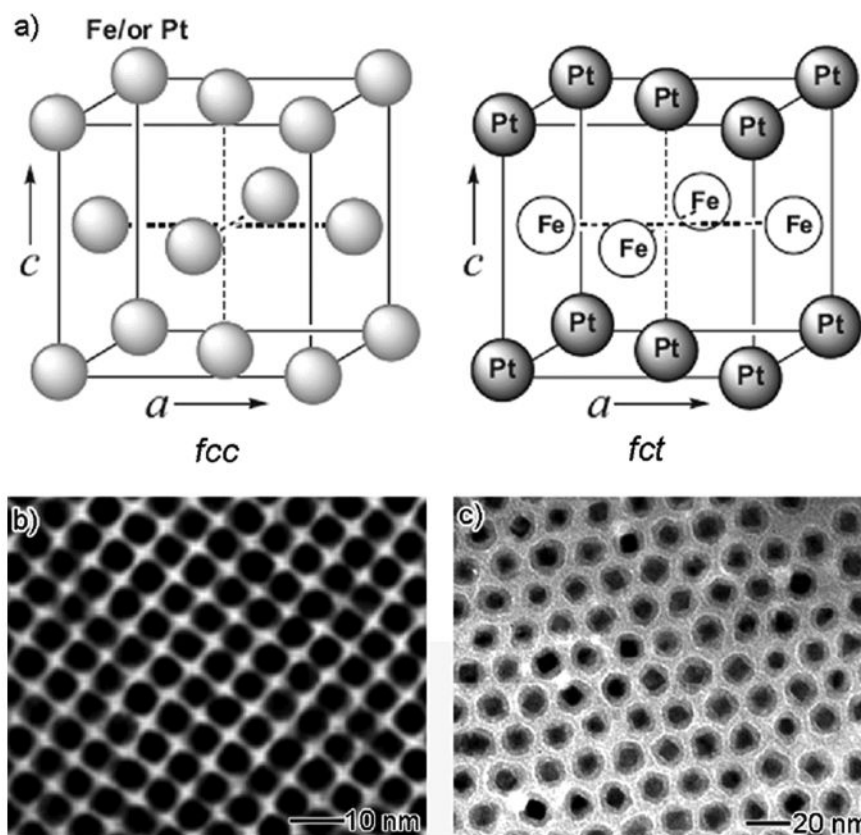


Figure 29.

a) Schematic illustrating the unit cell of chemically disordered *fcc*- and chemically ordered *fct*-FePt (modified with permission from [6b], copyright 2006 Wiley-VCH); b) TEM image of truncated *fcc*-FePt nanocubes prepared by simultaneous reduction of Pt(acac)₂ and thermal decomposition of Fe(CO)₅ (modified with permission from [97], copyright 2000 American Association for the Advancement of Science); and c) TEM image of Pt@Fe₂O₃ core-shell nanostructures prepared via a two-step process (modified with permission from [193f], copyright 2003 American Chemical Society).

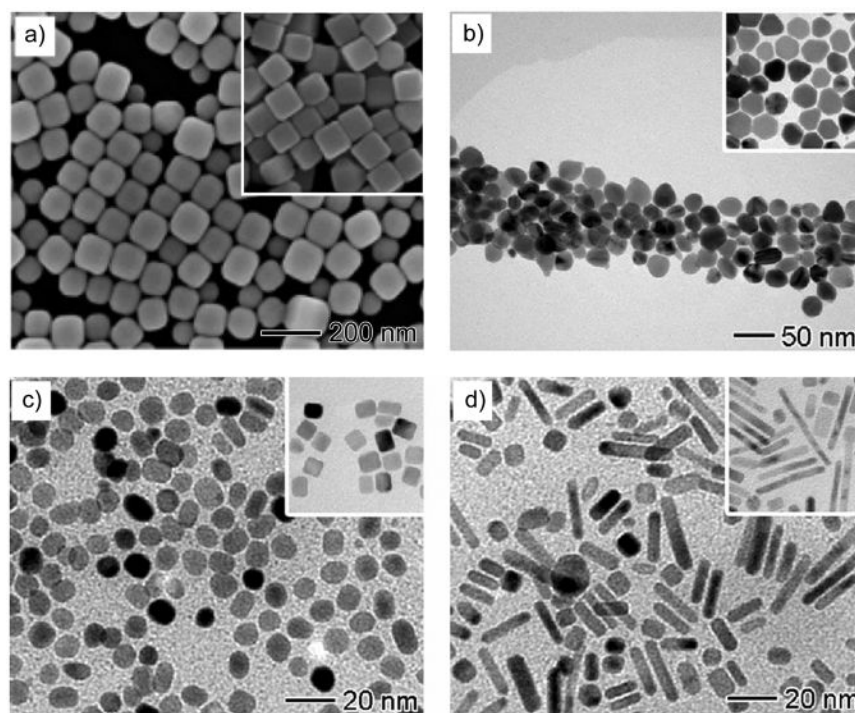


Figure 30.

Electron microscopy images of metal nanocrystals after aging: a) Ag nanocubes aged at 160 °C for 5 min in an ethylene glycol solution containing 1 mM HCl in the presence of 0.1 mM PVP (modified with permission from [197], copyright 2007 American Chemical Society); b) Ag nanoplates aged in water for 1 month at room temperature (modified with permission from [58b], copyright 2007 Royal Society of Chemistry); c) Pd nanocubes and d) Pd single-crystal nanorods aged in the reaction solution for 4 weeks at room temperature (modified with permission from [64d], copyright 2007 American Chemical Society). The insets in panel (a-d) show TEM images of the corresponding nanocrystals before the aging process, at the same magnification as in (a-d).

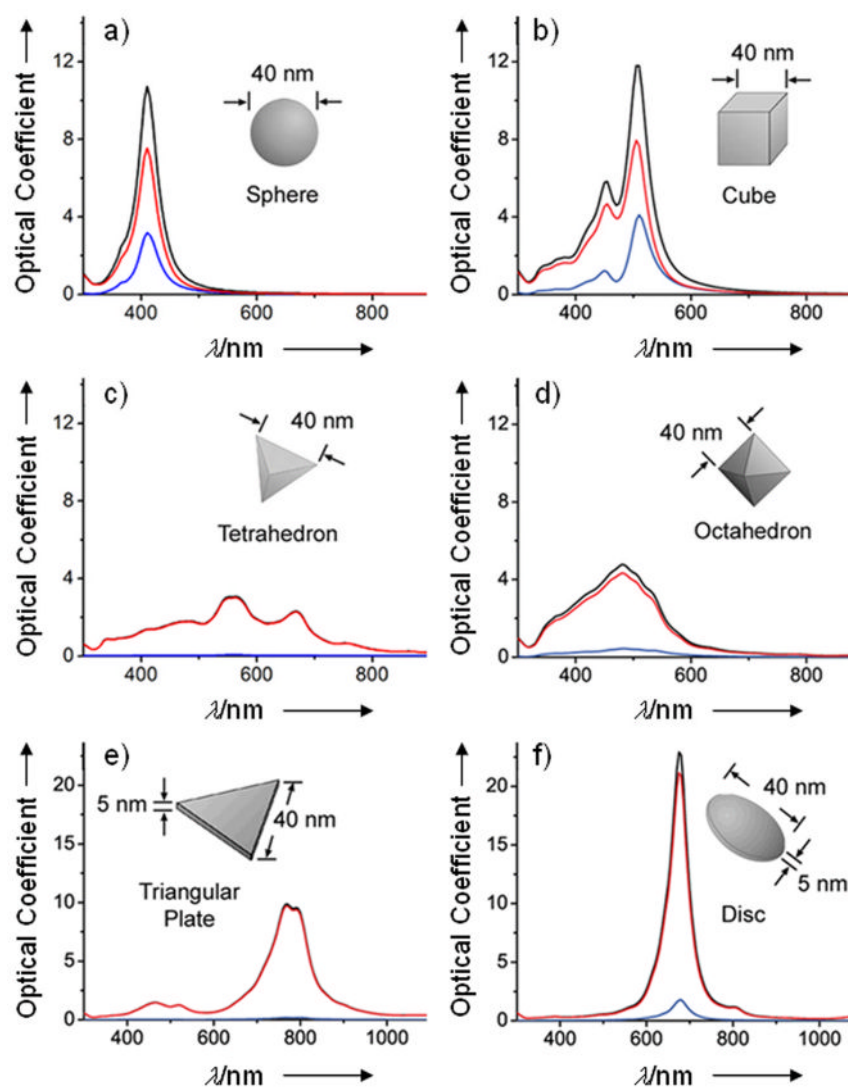


Figure 31. Calculated UV-visible extinction (black), absorption (red), and scattering (blue) spectra of Ag nanocrystals, illustrating the effect of shape on spectral characteristics: a) sphere, b) cube, c) tetrahedron, d) octahedron, e) triangular plate, and f) circular plate (modified with permission from [16e], copyright 2006 American Chemical Society).

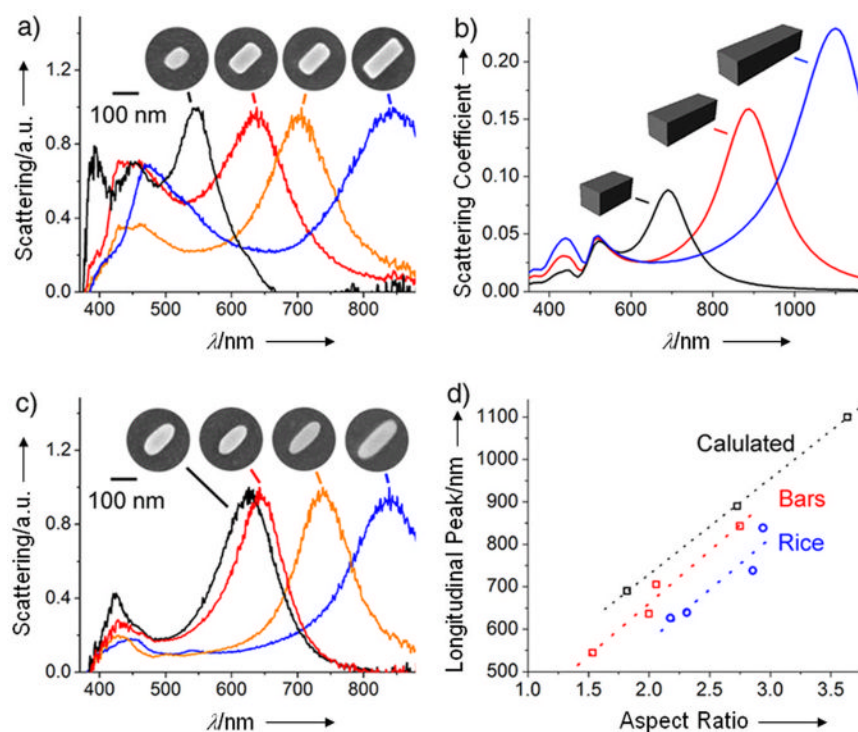


Figure 32.

a) SEM images of individual Ag nanobars and the corresponding normalized LSPR spectra. The longitudinal plasmon peak red-shifts with increasing aspect ratio for the nanobars. b) LSPR (scattering) spectra calculated using the DDA method for Ag nanobars 100, 150, and 200 nm in length, keeping width = 55 nm and height = 50 nm. c) SEM images of individual nanorice with the corresponding normalized LSPR spectra. d) Plot of longitudinal plasmon peak location versus aspect ratio. The peaks of both nanobars and nanorice red-shift with increasing length, but on average the peaks of nanobars are 80 nm red-shifted from nanorice (modified with permission from [63b], copyright 2007 American Chemical Society).

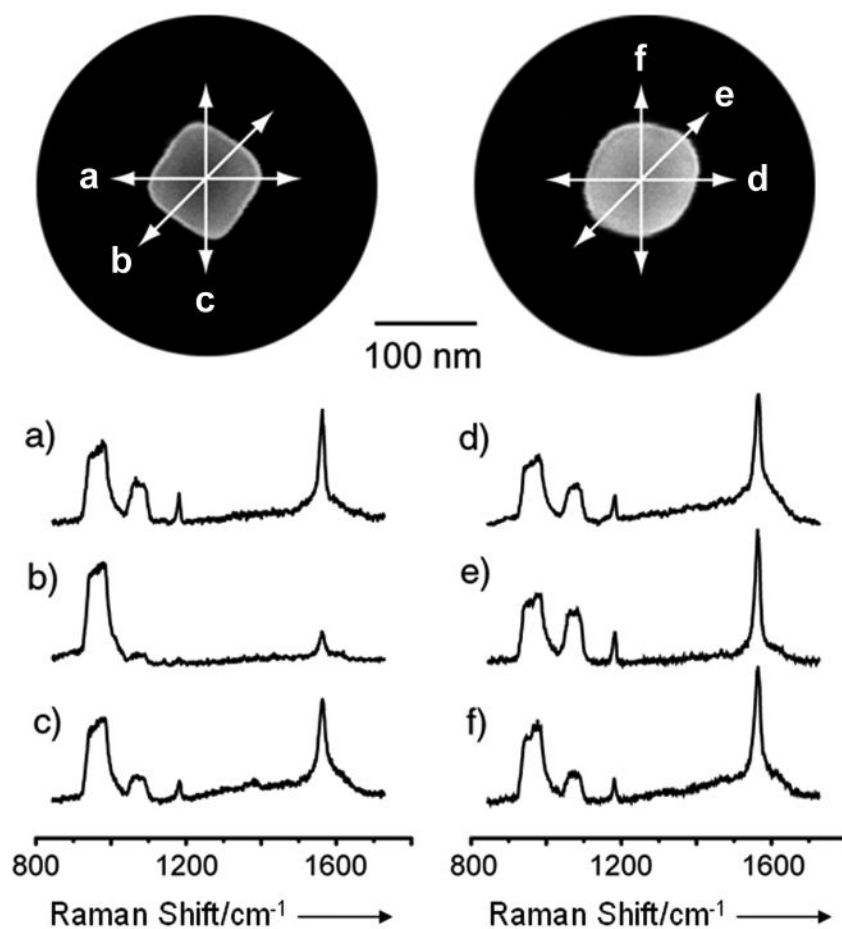


Figure 33. The normalized SERS spectra of 1,4-BDT adsorbed on a Ag nanocube with sharp corners (left panel, a-c) and a highly truncated Ag nanocube (right panel, d-f), at various angles relative to the polarization of the excitation laser. Each SEM image shows the nanocube used and the arrows indicate the polarization directions of incident laser. The scale bar applies to both images. The broad peak at 900-1000 cm^{-1} from the underlying silicon substrate was used as the reference for normalization (modified with permission from [207], copyright 2007 American Chemical Society).

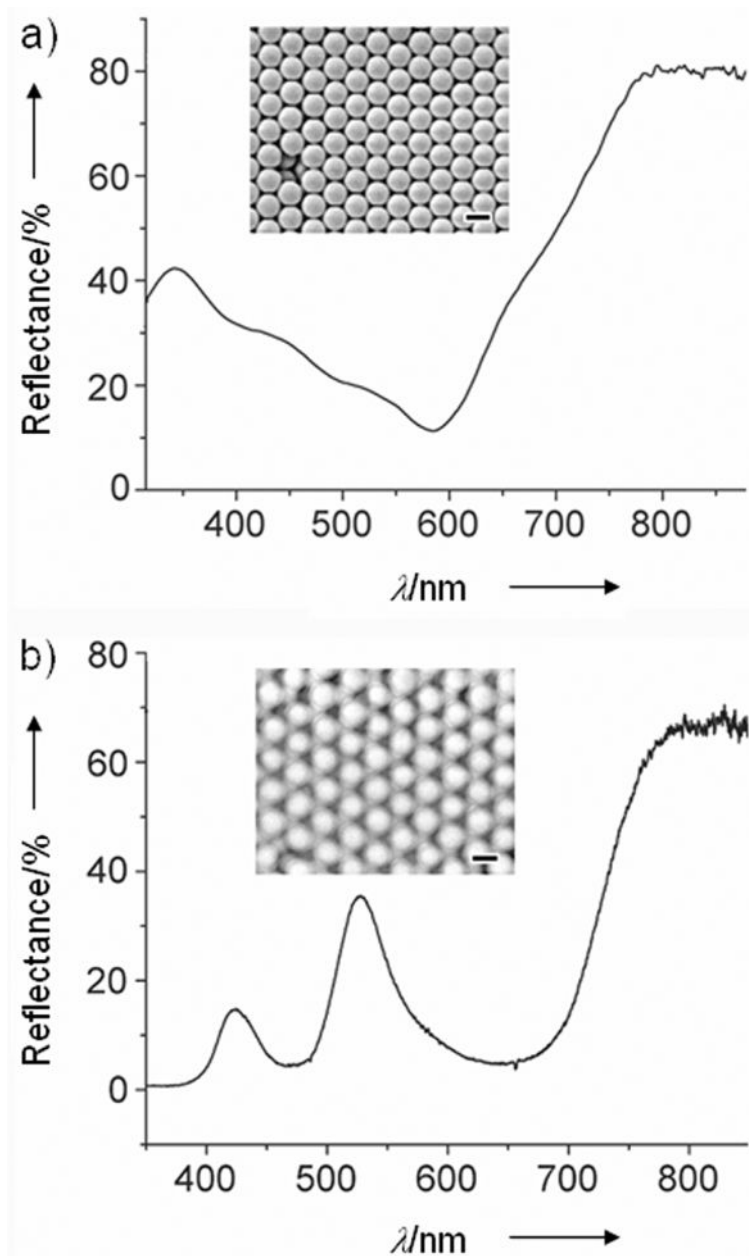


Figure 34. Reflectance spectra obtained from crystalline lattices of a) Pb and b) Pb@SiO₂ nanospheres with the incident light oriented perpendicular to their (111) planes. The insets in both figures show the corresponding top-view SEM images for the two crystalline lattices. Both scale bars in the insets are 200 nm (modified with permission from [178d], copyright 2006 Wiley-VCH).

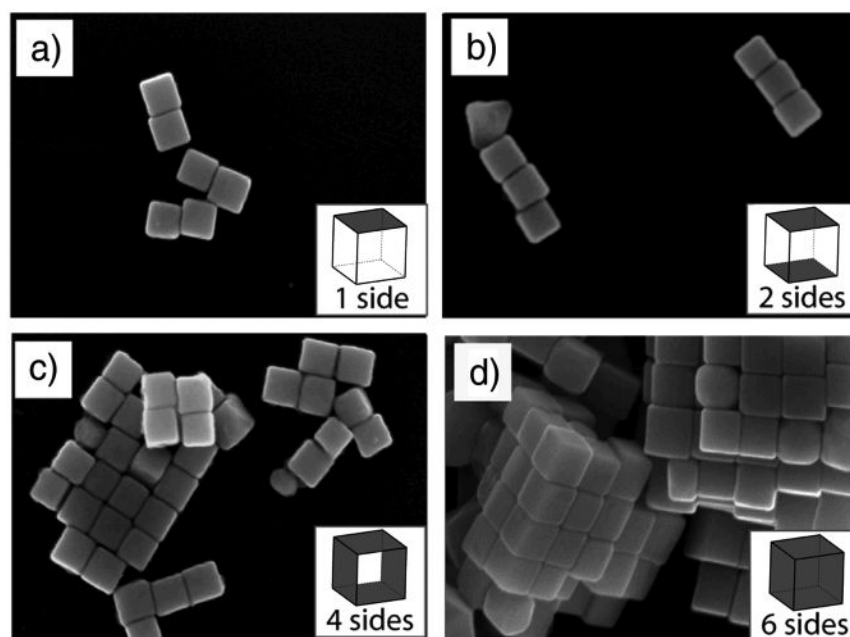
















Figure 35. SEM images of structures self-assembled from Ag nanocubes. The nanocubes were selectively functionalized with hydrophilic and hydrophobic thiolate SAMs and then allowed to assemble in water. The number of faces on each nanocube that were rendered hydrophobic is indicated in grey color in the bottom right corner of each panel, the remaining faces on the nanocube were hydrophilic. All nanocubes used in this study had a mean edge length of 97 ± 6 nm, as determined from 123 cubes (modified with permission from [226], copyright 2008 Wiley-VCH).

Table 1

A summary of different shapes that have been achieved for various metal nanocrystals.

structures	shapes	schematic drawings	metals
single-crystal	perfect/truncated cube ^[a]		Pd, Ag, Au, Pt, Cu, Rh, Bi, Fe
	perfect/truncated octahedron ^[a]		Pd, Ag, Au, Pt
	perfect/truncated tetrahedron ^[a]		Ag, Au, Pt, Rh
	rectangular bar		Pd, Ag, Pt
	octagonal rod		Pd, Au, Fe, Co, Ni
	rectangular or octagonal wire		Pb, In, Sn, Sb, Fe, Co
singly twinned	right bipyramid		Pd, Ag
	beam		Ag
multiply twinned	decahedron ^[a]		Pd, Ag, Au
	icosahedron ^[a]		Pd, Au
	five-fold twinned pentagonal rod		Pd, Ag, Au, Cu
	five-fold twinned pentagonal wire		Ag, Cu
	triangular/hexagonal plate		Pd, Ag, Au, Cu, Pb, Bi, Co, Ni
	disc		Sn, Co

^[a]Platonic solid.

Table 2

Crossover sizes for different types of nanocrystals of various metals (modified with permission from [54b], copyright 2002 American Institute of Physics).

Metal	$N_{\text{Ih} \rightarrow \text{Dh}}^{[a]}$	$N_{\text{Dh} \rightarrow \text{TO}}^{[b]}$
Cu	1000	> 30000
Ag	< 300	20000
Pd	< 100	6500
Pt	< 100	6500
Au	< 100	500

^[a]The transition from icosahedron (Ih) to decahedron (Dh).

^[b]The transition from decahedron (Dh) to truncated octahedron (TO) or Wulff's polyhedron.